

SYNTHESIS OF ZINC PHTHALOCYANINE DERIVATIVES  
FOR POSSIBLE USE IN PHOTODYNAMIC THERAPY

THESIS

Submitted to Rhodes University  
in fulfillment of the requirements for the degree of

MASTERS OF SCIENCE

by

PULANE MASELEKA MATLABA

May 2002

Department of Chemistry

Rhodes University

Grahamstown

## ACKNOWLEDGEMENTS

Many thanks to my supervisor, Professor T. Nyokong, for her guidance, constant encouragement and support throughout the duration of this project.

And a very big thanks to my family, especially my mother, mama-Nkgethi Tlholoe and my sister Lebogang Matlaba, for financial assistance and encouragement throughout the course of my studied.

Thank you to the staff and post graduate students of the chemistry department at Rhodes University for their assistance in so many different ways. Thank you also to NRF for financial assistance.

## Abstract

The synthesis of symmetrically and unsymmetrically substituted zinc phthalocyanines (ZnPc) derivatives is done according to reported procedures. The unsymmetrical ZnPc derivatives are synthesized by ring expansion of sub-phthalocyanine complexes. Ring substitution is effected with *tert*-butyl phenol, naphthol, and hydroxybenzoic acid. Comparison of the redox potentials for the complexes substituted with varying numbers of *tert*-butyl phenol: 1, 2, 3, 6 and 8 show that the complex with the highest number of substituents are more difficult to oxidize and easier to reduce.

Water soluble sulphonated ZnPc (ZnPcS<sub>n</sub>) was prepared. The possibility of using axial ligation to increase the solubility and the photochemical activity of sulphotnated ZnPc in aqueous solutions was investigated. Pyridine, aminopyridyl and bipyridyl were used as axial ligands. When bipyridyl was used as the axial ligand, solubility of the ZnPcS<sub>n</sub> increased, shown by the increase in the Q-band of the monomer species in solution and the singlet oxygen quantum yields was relatively higher than that of the unligated ZnPcS<sub>n</sub>.

The singlet oxygen quantum yields by the various complexes in DMF using diphenylisobenzofuran as a chemical quencher for organic solvent were determined. Singlet oxygen quantum yields for the unsymmetrically ring substituted complexes range from 0.22 to 0.68. Photobleaching quantum yields are in the order of 10<sup>-5</sup>, which means that the complexes are relatively photostable.

# Table of Contents

	Page
Title page.....	i
Acknowledgements.....	ii
Abstract.....	iii
Table of contents.....	iv
List of abbreviations.....	v
List of symbols.....	vi
List of Figures.....	vii
List of Schemes.....	viii
List of Tables.....	viii

# Table of Contents

## 1. INTRODUCTION

1.1 Photodynamic therapy	1
1.1.1 A general overview on photodynamic therapy	1
1.1.2 Mechanism of photodynamic therapy	4
1.1.3 Sensitizers in use for photodynamic therapy	5
1.2 Aims of the project	11
1.3 Phthalocyanines	14
1.3.1 Structure and history of phthalocyanines	14
1.3.2 General preparation methods of phthalocyanines	15
1.3.3 Synthesis of unsymmetrically substituted phthalocyanines	19
1.3.3.1 Synthesis of sub-phthalocyanines	20
1.3.3.2 Ring expansion of sub-phthalocyanines to form phthalocyanines	21
1.3.4 Preparation of axially ligated metallophthalocyanines	25
1.3.5 Aggregation in phthalocyanines	27
1.3.6 Spectral properties of metallophthalocyanines	28
1.4 Photochemical methods	30
1.4.1 Singlet oxygen determination	31
1.4.2 Quantum yields of photobleaching	37
1.4.3 Determination of triplet lifetimes and triplet quantum yields	38

1.4.4	Determination of fluorescence quantum yields and fluorescence lifetimes	41
1.5	Electrochemistry	44
1.5.1	Background on cyclic voltammetry	44
1.5.2	Square wave voltammetry	48
1.5.3	Electrochemical properties of MPcs	48
<b>2.</b>	<b>EXPERIMENTAL</b>	
2.1	Materials	52
2.2	Instrumentation	53
2.3	Synthesis	54
2.3.1	Synthesis of 4-nitrophthalonitrile	54
2.3.2	Preparation of mono-substituted phthalonitriles	56
2.3.3	Synthesis of 4,5-dichlorophthalonitrile	59
2.3.4	Preparation of di-substituted phthalonitriles	61
2.3.5	Synthesis of dicyanonaphthalene	64
2.3.6	Synthesis of sub-phthalocyanine	66
2.3.7	Preparation of substituted sub-phthalocyanines	67
2.3.8	Preparation of sub-naphthalocyanine	68
2.3.9	Synthesis of symmetrically substituted zinc phthalocyanines	69
2.3.10	Synthesis of unsymmetrically substituted zinc phthalocyanines	70

2.3.11 Synthesis of zinc sulphonatedphthalocyanines	77
2.4 Photochemical and photophysical methods	80
2.5 Electrochemical methods	83
<b>3. RESULTS AND DISCUSSION</b>	
3.1 Characterization of phthalocyanine precursors	84
3.1.1 Substituted phthalonitrile derivation	84
3.1.2 Sub-phthalocyanine	87
3.2 Characterization of zinc phthalocyanine derivatives	87
3.2.1 Synthesis	87
3.2.2 Spectroscopic characterization	90
3.2.3 Voltammetry characterization	103
3.3 Photochemical studies	108
3.3.1 Photobleaching	108
3.3.2 Singlet oxygen studies	111
3.4 Photophysical studies	112
3.5 Studies of the interaction of ZnPcS <sub>n</sub> with pyridine ligands	116
<b>CONCLUSION AND FUTURE STUDIES</b>	124
<b>REFERENCES</b>	126

## List of abbreviations

ADMA	=	$\alpha,\alpha'$ -(anthracene-9,10-diyl)bimethylmalonate
AlTsPc	=	Tetrasulphonated aluminium phthalocyanine
BAS	=	Bio-Analytical System
bipyr	=	Bipyridine
CPh	=	Carboxy phenoxy
CV	=	Cyclic Voltammogram
DABCO	=	Diazabicyclo-(2.2.2)-octane
DBU	=	1,8-Diazabicyclo[5.4.0]undec-7-ene
DMF	=	N,N-dimethylformamide
DMSO	=	Dimethylsulphoxide
DPBF	=	Diphenylisobenzofuran
GCE	=	Glassy Carbon Electrode
$^1\text{H NMR}$	=	Proton nuclear magnetic resonance
HpD	=	Heamatoporphyrin Derivative
HOMO	=	Highest Occupied Molecular Orbital
I	=	Intensity of light
$I_{\text{abs}}$	=	Absorbed light
IR	=	Infrared
L	=	Ligand
LUMO	=	Lowest Occupied Molecular Orbital
MPc	=	Metallophthalocyanine

MTsPc	=	Metallotetrasulphonatedphthalocyanine
OSWV	=	Osteryoung square wave voltammogram
Pc	=	Phthalocyanine
Ph	=	Phenoxy
PDT	=	Photodynamic Therapy
py	=	pyridine
SCE	=	Standard calomel electrode
Sen	=	Sensitizer
Sub-Pc	=	Sub-phthalocyanine
TBAP	=	Tetrabutyl ammonium perchlorate
TbPh	=	Tertbutyl phenoxy
TLC	=	Thin layer chromatography
UV-visible	=	Ultra-violet and visible
ZnPc	=	Zinc phthalocyanone
ZnTsPc	=	Tetrasulphonated zinc phthalocyanine
(bipyr)ZnPcS <sub>n</sub>	=	Sulphonated zinc phthalocyanine containing bipyridyl axial ligand
(pyr)ZnPcS <sub>n</sub>	=	Sulphonated zinc phthalocyanine containing pyridyl axial ligand
(aminopyr)ZnPcS <sub>n</sub>	=	Sulphonated zinc phthalocyanine containing aminopyridyl axial ligand

## List of symbols

$\alpha$	=	fraction of light absorbed
$\Delta E$	=	separation between peak potentials
$\lambda_{\max}$	=	wavelength
$\nu$	=	stretching vibrations (IR)
$\pi$	=	pi
$\pi^*$	=	pi antibonding orbital
$\sigma$	=	sigma
$\tau_p$	=	excited state phosphorescence lifetime
$\tau_f$	=	excited state fluorescence lifetime
$\Phi_{\Delta}$	=	quantum yield of singlet oxygen
$\Phi_{\tau}$	=	triplet state quantum yield
$\Phi_{\text{DPBF}}$	=	quantum yield of DPBF
$\Phi_f$	=	fluorescence quantum yield
$\Phi_{\text{photobleaching}}$	=	photobleaching quantum yield
$\Phi_{\text{DPBF}}^{\text{MPc}}$	=	quantum yield of DPBF in the presence of MPc
$\Phi_{\text{DPBF}}^{\text{ZnPc}}$	=	quantum yield of DPBF in the presence of ZnPc
$\tau_f$	=	fluorescence lifetimes
$\tau_T$	=	triplet lifetimes
$\varepsilon$	=	extinction coefficient

$^1\text{O}_2$	=	singlet oxygen
C	=	concentration of the electroactive species
D	=	diffusion coefficient
$D_o$	=	diffusion coefficient of oxidized species
$D_R$	=	diffusion coefficient of reduced species
$e_g$	=	gerade
$E^{\circ}$	=	half wave potential
$E_f$	=	final potential
$E_i$	=	initial potential
$E_o$	=	oxidation potential
$E^{\circ}$	=	formal reduction potential
$E_{pa}$	=	anodic peak potential
$E_{pc}$	=	cathodic peak potential
F	=	Faraday's constant
hv	=	light energy
$i_p$	=	peak current
$i_{pa}$	=	anodic peak current
$i_{pc}$	=	cathodic peak potential
n	=	number of electrons transferred during a redox process
$N_a$	=	Avogadro's constant
nm	=	nanometer
$\text{O}_2(^1\Delta_g)$	=	singlet state oxygen
$\text{O}_2(^3\Sigma_g)$	=	triplet state oxygen

Q	=	charge in coulombs
R	=	gas constant
$^1S^*$	=	excited singlet state
$S_0$	=	ground state
$^3S^*$	=	excited triplet state
$\nu$	=	scan rate
V	=	volts

## List of Figures

<b>Figure 1.1:</b>	Structure of haematoporphyrin	6
<b>Figure 1.2:</b>	Structure of dihaematoporphyrin	6
<b>Figure 1.3:</b>	Structures of (I) photosens and (II) disulphonated AlPc	7
<b>Figure 1.4:</b>	Structure of silicon phthalocyanine Pc-4	10
<b>Figure 1.5:</b>	Structure of zinc dinaphthodi(4-sulphobenzo)-porphyrazine	11
<b>Figure 1.6:</b>	Structures of (MP) and (MPc)	14
<b>Figure 1.7:</b>	Octasubstituted metallophthalocyanine	26
<b>Figure 1.8:</b>	Axial ligation in MPc and symmetry of the molecules	27
<b>Figure 1.9:</b>	Stacked polymeric MPc	28
<b>Figure 1.10:</b>	Electronic energy levels for phthalocyanines	29
<b>Figure 1.11:</b>	A typical absorption spectra of a MPc complex	30
<b>Figure 1.12:</b>	ADMA before and after reacting with singlet oxygen	36
<b>Figure 1.13:</b>	Cyclic voltammogram for a reversible system	46
<b>Figure 1.14:</b>	Cyclic voltammogram of Octaphenoxyphthalocyanato (bis(dimethylaminoxy))	50
<b>Figure 2.1:</b>	Set-up for triplet lifetime and quantum yield determination	54
<b>Figure 2.2:</b>	A representation of zinc phthalocyanine complexes synthesized	72
<b>Figure 2.3:</b>	Photolysis set-up	80
<b>Figure 3.1:</b>	Electronic absorption spectra of an unsubstituted sub-phthalocyanine	87
<b>Figure 3.2:</b>	Changes in the UV/vis spectra during the formation of a ZnPc derivative from a sub-phthalocyanine.	90
<b>Figure 3.3:</b>	Decrease in the absorbance of the Q-band and soret band with	91

decreasing concentration of ZnPc complex.

<b>Figure 3.4:</b>	Beer's law dependence for ZnPc derivatives in DMF.	91
<b>Figure 3.5:</b>	Electronic absorption spectra of selected ZnPc derivatives.	94
<b>Figure 3.6:</b>	IR spectra of complex <b>44</b> .	97
<b>Figure 3.7:</b>	Numbering of phthalocyanines and naphthalocyanines.	98
<b>Figure 3.8:</b>	$^1\text{H}$ NMR of complex <b>45</b> .	100
<b>Figure 3.9:</b>	Osteryoung square wave and cyclic voltamograms of <b>44</b> .	104
<b>Figure 3.10:</b>	Osteryoung square wave and cyclic voltamograms of <b>47</b> .	105
<b>Figure 3.11:</b>	A plot of current vs square root of scan rate for complex <b>44</b> .	106
<b>Figure 3.12:</b>	Variation of the Q-band with increasing concentration for <b>44</b> .	107
<b>Figure 3.13:</b>	UV/vis spectra of <b>44</b> during the photobleaching process.	109
<b>Figure 3.14:</b>	Kinetics curve for the photobleaching process of <b>44</b> in DMF saturated with oxygen, nitrogen, DABCO.	110
<b>Figure 3.15:</b>	Spectral changes observed during photolysis of complex <b>44</b> in the presence of DABCO.	111
<b>Figure 3.16:</b>	Triplet decay of <b>44</b> showing mono exponential decay.	113
<b>Figure 3.17:</b>	Electronic absorption spectra of $\text{ZnPcS}_n$ and axially ligated $\text{ZnPcS}_n$ showing the enhancement of the Q-band with increasing concentrations of bipyridyl.	118
<b>Figure 3.18:</b>	Electronic absorption spectra of $\text{ZnPcS}_n$ in water and in the presence of Triton x-100.	119
<b>Figure 3.19:</b>	A plot of $[\text{L}]$ vs $\log [\text{ML}_n]/[\text{D}]$ for $\text{ZnPcS}_n$ with bipyridyl, aminopyridyl, pyridine as axial ligands.	121
<b>Figure 3.20:</b>	Electronic absorption spectra of $\text{ZnPcS}_n$ + bipyridyl in the presence of ADMA.	123

## List of Schemes

<b>Scheme 1.1:</b>	Type I mechanism, where S represents the sensitizer (e.g. metallophthalocyanine) Sub represents the substrate.	4
<b>Scheme 1.2:</b>	Type II mechanism, where S represents the sensitizer (e.g. metallophthalocyanine) Sub represents the substrate.	5
<b>Scheme 1.3:</b>	Synthesis of MPc from phthalic anhydride.	16
<b>Scheme 1.4:</b>	Preparation of MPC from o-cyanobenzamide.	16
<b>Scheme 1.5:</b>	Preparation of MPC from phthalonitrile.	17
<b>Scheme 1.6:</b>	Preparation of MPC from 1,3-diiminoisoindoline.	17
<b>Scheme 1.7:</b>	Preparation of MPC from uranyl superphthalocyanine.	19
<b>Scheme 1.8:</b>	Preparation of sub-phthalocyanine.	21
<b>Scheme 1.9:</b>	Synthesis of an unsymmetrical phthalocyanine from sub-phthalocyanine.	22
<b>Scheme 1.10:</b>	Representation of the synthesis of an unsymmetrical MPc using polymer bound diiminoisoindoline, where P = polymer.	23
<b>Scheme 1.11:</b>	Representation of the synthesis of an adjacently substituted MPc.	24
<b>Scheme 1.12:</b>	Preparation of axially ligated metallophthalocyanine.	25
<b>Scheme 2.1:</b>	Synthesis of 4-nitrophthalonitrile .	56
<b>Scheme 2.2:</b>	Synthesis of 4-(4-tert-butylphenoxy)benzene-1,2-dicarbonitrile .	57
<b>Scheme 2.3:</b>	Synthesis of 4-(4-carboxyphenoxy)benzene-1,2-dicarbonitrile.	58
<b>Scheme 2.4:</b>	Synthesis of 4-(3-naphthoxy)benzene-1,2-dicarbonitrile.	59
<b>Scheme 2.5:</b>	Synthesis of dichlorophthalonitrile .	61
<b>Scheme 2.6:</b>	Synthesis of 4,5-di(4-carboxyphenoxy)benzene-1,2-dicarbonitrile.	62

<b>Scheme 2.7:</b>	Synthesis of 4,5-di(4-tert-butylphenoxy)benzene-1,2-dicarbonitrile.	63
<b>Scheme 2.8:</b>	Synthesis of 4,5-di(naphthoxy)benzene-1,2-dicarbonitrile.	63
<b>Scheme 2.9:</b>	Preparation of dicyanonaphthalene from dicarboxynaphthalic acid.	65
<b>Scheme 2.10:</b>	Synthesis of an unsubstituted sub-phthalocyanine.	67
<b>Scheme 2.11:</b>	Synthesis of tri-(tert-butylphenoxy) sub-phthalocyanine.	67
<b>Scheme 2.12:</b>	Synthesis of hexa-(tert-butylphenoxy) sub-phthalocyanine.	68
<b>Scheme 2.13:</b>	Synthesis of sub-naphthalocyanine.	69
<b>Scheme 2.14:</b>	Synthesis of 2,3,9,10,16,17,23,24-octa-(4-tert-butylphenoxy)phthalocyanato zinc (II).	70
<b>Scheme 2.15:</b>	Schematic representation for the synthesis of unsymmetrically substituted ZnPc.	71
<b>Scheme 2.16:</b>	Synthesis of tri-benzophthalocyaninato zinc (II) by ring expansion of sub-phthalocyanine.	77
<b>Scheme 2.17:</b>	Schematic representation of ZnPcS <sub>n</sub> synthesis.	78
<b>Scheme 2.18:</b>	Schematic representation of axially ligated ZnPcS <sub>n</sub> synthesis.	79
<b>Scheme 3.1:</b>	Summary of the synthesis of monophenoxy substituted phthalonitriles.	85
<b>Scheme 3.2:</b>	Summary of the synthesis of di-phenoxy substituted phthalonitriles.	86

## List of Tables

	Page
<b>Table 1:</b> Photobleaching and $^1\text{O}_2$ quantum yields for a selected MPcs.	38
<b>Table 2:</b> Photophysical data for selected MPcs.	44
<b>Table 3:</b> Amounts used for the synthesis of mono-substituted dicyanibenzene.	59
<b>Table 4:</b> Amounts used for the synthesis of mono-substituted dicyanibenzene.	64
<b>Table 5:</b> Precursor combinations for unsymmetrically ring substituted ZnPcs synthesis.	73
<b>Table 6:</b> An illustration of the computation of $\alpha$ coefficient.	81
<b>Table 7:</b> Electronic absorption data for zinc phthalocyanine derivatives.	93
<b>Table 8:</b> Infrared spectral data for zinc phthalocyanine derivatives.	95
<b>Table 9:</b> $^1\text{H}$ NMR spectral data for zinc phthalocyanine derivatives.	102
<b>Table 10:</b> Comparison of redox potentials for complexes <b>44</b> , <b>46-52</b> .	108
<b>Table 11:</b> Quantum yields for singlet oxygen and photobleaching for zinc phthalocyanine derivatives in DMSO.	114
<b>Table 12:</b> Quantum yield of fluorescence, fluorescence lifetimes and triplet halftimes for complexes <b>44</b> , <b>46</b> and <b>47</b> in DMF.	115
<b>Table 13:</b> $\lambda_{\text{max}}$ (nm) and absorbance values for different concentrations of 4,4'-bipyridyl.	120
<b>Table 14:</b> K and n values calculated for ZnPcSn with bipyridyl, aminopyridyl and pyridine as axial ligands.	122
<b>Table 15:</b> $\Phi\Delta$ for ZnPc and AlPc derivatives in water, using ADMA as a singlet oxygen quencher.	123

## **1. INTRODUCTION**

### **1.1 Photodynamic therapy**

#### **1.1.1 A general overview on photodynamic therapy**

Photomedicine is the application of the principle of photobiology, photochemistry and photophysics to the diagnosis and therapy of disease. This subject first gained attention in the nineteenth century with the discovery by Niel Finsen that facial lesions resulting from tuberculosis could be cured by irradiation with ultraviolet light [1]. This was further reinforced by the discovery that certain microorganisms were killed by ultraviolet light, also sunlight and artificial light were found to cure vitamin D deficiency [1]. The advent of lasers and fibre optics laid a base for further research in photomedicine.

In the past ten years one of the most sought out research field in photochemistry has been the exploration of the use of photosensitizers that can be retained by malignant tumours. Upon irradiation with a red light of a wavelength between 600 nm and 800 nm (delivered from a laser via an optic fibre) selective tumour destruction can be achieved. This treatment is called photodynamic therapy (PDT). Photodynamic therapy combines the effect of light, oxygen and photosensitizer drug to destroy only the tumour tissue. Steps involved in PDT for cancer treatment involve the photosensitizer drug being administered intravenously, followed by an incubation period [2,3]. During the incubation period the sensitizer is distributed to the tissue cells and accumulates mostly in malignant cells. Photoexcitation of the sensitizer is carried out by introducing laser light via optical fibres. The presence of light activates the sensitizer to convert oxygen into its toxic excited state, which causes chemical

damage and biological damage in the cells, followed by tumour necrosis. The sensitizer is only active when irradiated with light of the correct wavelength and is totally inactive in the dark.

The two major techniques used in the treatment of cancer are chemotherapy and radiotherapy. Both these techniques have been successful to some degree, but they also induce side effects which could be life threatening by destroying normal tissue. Thus PDT has an advantage over these therapies due to the fact that the recovery period is short, it can be coupled with other therapies and allows in-vivo detection of the sensitizer (via fluorescence of sensitizer) [4-7]. Also the therapy depends on selective cell destruction, thus the drug has to be totally selective, if not additional selectivity can be attained by spatial localisation of the illumination to the target tissue. The major thrust of research in this field is towards the development of better photosensitizing drugs with the following properties:

1. Red or near infrared light absorbing.
2. Non toxic, with low skin photosensitizing potency.
3. Selectively retained in tumours relative to normal adjacent tissue.
4. An efficient generator of cytotoxic species, usually singlet oxygen.
5. Fluorescent for visualization.
6. Defined chemical composition.
7. Preferably water soluble, for easy administration.

The ideal properties can be easily acquired but the heterogeneous nature of biological systems can extremely affect the properties.

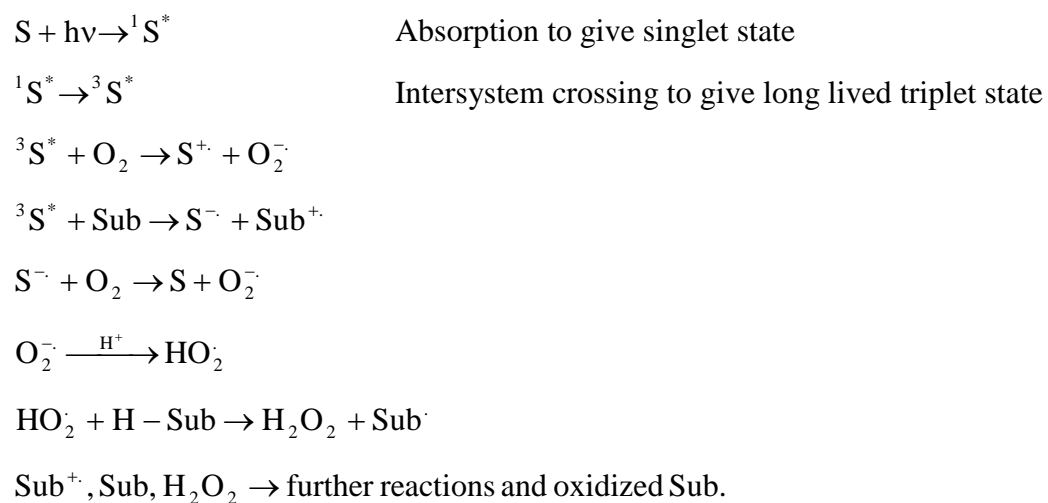
In photodynamic therapy molecular oxygen is required and it is generally assumed that singlet oxygen is the active species responsible for tissue destruction. Other reactive species such as superoxides, hydroperoxyl and hydroxyl radicals may be involved in tissue necrosis. The sensitizer in photodynamic therapy acts in a catalytic way because it generally does not react with the tissue directly. On light absorption of appropriate wavelength, the sensitizer is converted to from a stable electron structure (the ground electronic state) to an excited singlet state ( $^1S^*$ ) which is short lived. The excited singlet state may undergo conversion to a long lived excited state known as the triplet state ( $^3S^*$ ) responsible for the photochemical generation of cytotoxic singlet oxygen species [8].

The ability of sensitizers to target tissues in photodynamic therapy is assisted by the fact that the sensitizers have the property of localising in tumour tissue relative to the surrounding healthy tissues. The extent of this in humans has not been studied extensively. The high reactivity and short lifetime of the activated oxygen restricts the cytotoxicity to a specific region of the tissue absorbing the light. This means that the cytotoxic species will not be released from their point of action to the neighbouring tissue cells. The ongoing developments in lasers and fibre optics, whereby a beam of intense light can be directed to a specific location in the body have led to photodynamic therapy being a successful therapy for cancer.

It is important to note that neither the light nor the sensitizer, have any independent biological effect. Only when the three component (oxygen, sensitizer and light) come together in the tissue at the same time, is there a cytotoxic effect.

### 1.1.2 Mechanisms of Photodynamic therapy

The cytotoxic agent in photodynamic therapy is produced by one of the two processes, referred to as Type I and Type II processes. These processes are mediated by the excited triplet state of the photosensitizer. Type I mechanism results from electron transfer reactions between the excited sensitizer and substrate or oxygen to yield radicals and/or radical ions [9,10,11]. These radicals and/or radical ions can further react with oxygen to yield superoxide radical anion [12]. The Type I process can be very complex and generally involves electron transfer steps illustrated in **Scheme 1.1**.

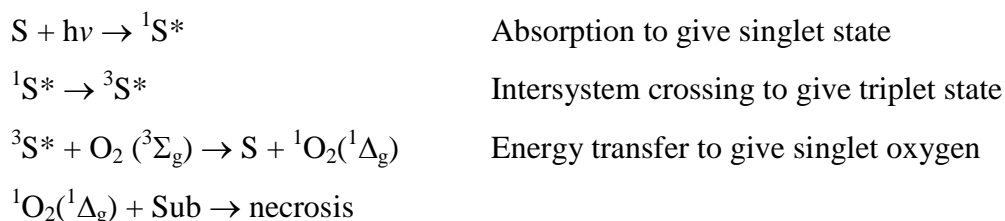


**Scheme 1.1:** Type I mechanism where S represents the sensitizer

(e.g. metallophthalocyanine) and Sub represents the substrate.

Type II process involves energy transfer from the sensitizer, S to the ground state oxygen. Which is then converted to singlet state oxygen, **Scheme 1.2**. Both singlet

oxygen (Type II) and superoxide (Type I) are cytotoxic species and constitute the basis of PDT [10,13].



**Scheme 1.2:** Type II mechanism where S represents the sensitizer (e.g. metallophthalocyanine) and Sub represents the substrate.

### 1.1.3 Sensitizers in use for photodynamic therapy

The most commonly used sensitizers are haematoporphyrin derivative (HpD) and its purified form marketed as Photofrin. HpD is formed from treating haematoporphyrin, **Figure 1.1** with acetic and sulphuric acids to give a mixture of dimers and oligomers. The active component in HpD is believed to be the dihaematoporphyrin, **Figure 1.2** [10]. HpD has disadvantages in that it is a mixture of compounds, some of which are PDT inactive and it is difficult to reproduce the same properties from batch to batch. HpD localises in both healthy in addition to tumour cells and is cleared slowly from the body and thus patients have to be kept in the dark for long periods of time. HpD also has its light absorption at 400 nm, which is not efficient for PDT.

In the USA, Photofrin is being used as a PDT sensitizer for the treatment of early and late stage of lung cancer, bladder, advanced oesophageal cancer. Trials are on in the USA for brain, skin, breast, gastrointestinal tract, head and neck and gynaecological cancers [11]. The photosensitizing ability of Photofrin is also used in the treatment of

non-malignant conditions like plagues that occur in arterial disease, blood purging (for viral deactivation).

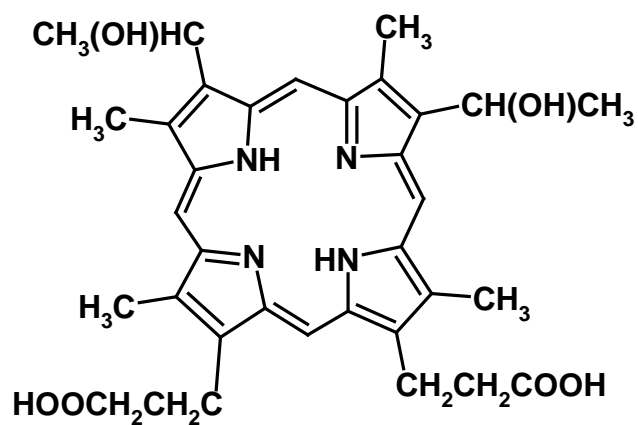


**Figure 1.1:** Structure of heamatoporphyrin

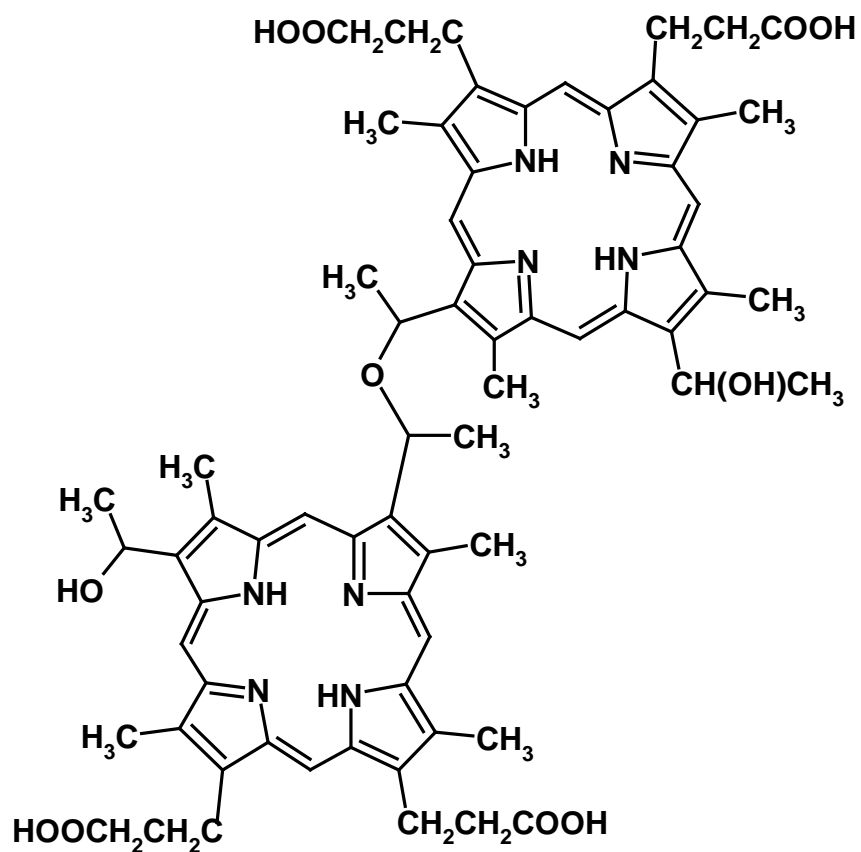


**Figure 1.2:** Structure of diheamatoporphyrin.

Photofrin however only partially fulfils the ideal PDT requirements, it exhibits poor chemical and photophysical properties, with low absorption coefficient in the red part of the spectrum, where the transparency of biological tissue is higher, and as stated above has low cancer cell selectivity [13,14]. The phthalocyanines (Pcs) demonstrate a much stronger absorption of red light at 650-700 nm than Photofrin, allowing more effective light penetration into tissues and are essentially transparent at wavelengths between 400 and 600 nm.

Remarkable progress has been made over the years in the use of metallophthalocyanines (MPc) as sensitizers for PDT.

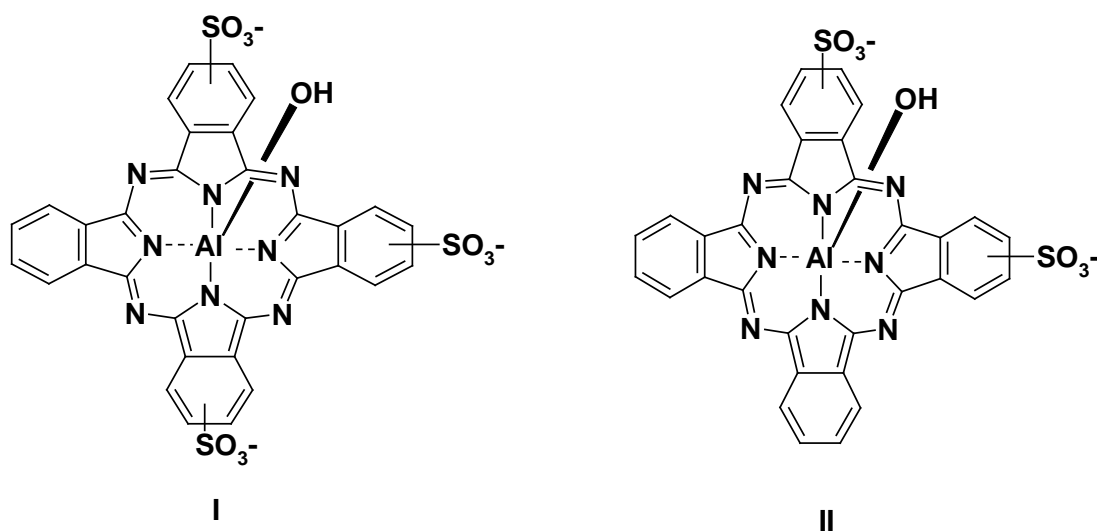


**Figure 1.3:** Structures of **(I)** photosens and **(II)** disulphonated aluminium Pc.

Photosens, **Figure 1.3(I)** a sulpho-substituted aluminium phthalocyanine has no doubt advantages over porphyrin derivatives and is used routinely in Russia and disulphonated AlPc used in the UK, **Figure 1.3(II)** [7,15,16]. Photosens is a mixture of sulpho-substituted AlPc, containing mono, di and tri sulpho-substituted AlPcs.

Properties of sulphonated aluminium Pcs have been extensively studied. It has been shown that the efficiency of the photosensitizer depends on the degree of sulphonation. Which in turn determines lipophilicity of the complex and its propensity to aggregate in water. The degree of sulphonation also affects the extent of localization of sensitizer in the cells, and its efficiency in photogeneration of singlet oxygen. Water soluble phthalocyanines have a tendency to aggregate in solution. Aggregation diminishes the photosensitizing ability of these complexes.

Changing either the central metal or the substituents on the phthalocyanine ring alters the properties of these compounds. Placing diamagnetic metals such as aluminium or zinc at the centre of the phthalocyanine ring as opposed to paramagnetic metals such as copper or iron, improves the photosensitisation of the compounds for use in PDT. Paramagnetic metal ions shorten the triplet lifetime and make the sensitizer inactive. Phthalocyanines are usually not soluble in water, but incorporating substituents such as sulphonic acids and carboxylic acids into the phthalocyanine ring improves solubility in water. Tetrasulpho complexes are readily soluble and thus released readily from the body, hence not retained long enough for PDT action. Disulfonated zinc and aluminium phthalocyanines, **Figure 1.3(II)**, are less soluble than tetrasulphonated zinc and aluminium phthalocyanines and have proven to be potent photosensitizers and are currently undergoing clinical trials in Russia [7]. Also aluminium sulphophthalocyanine species are usually preferred since they do not dimerize due to the presence of chloride or hydroxide as an axial ligand.

It has been shown that cell uptake is optimal for sulphonated aluminium phthalocyanine preparations consisting of various regioisomers or different

substituted compounds. Therefore mixed isomeric preparations may be more efficient as photodynamic therapy agents than isomerically pure compounds.

Zinc phthalocyanine is a lipophilic sensitizer with a wavelength of 671 nm, a high extinction coefficient, long triplet lifetime, high singlet oxygen quantum yields and good fluorescent properties [17]. To make it injectable it is incorporated into small liposomes. It has been shown that binding of insoluble ZnPc sensitizers to proteins, albumin and liposomes leads to significant increase in monomeric form of the sensitizer and improved tumour localisation [18,19]. Tetrasulphonated zinc Pc shows good selectivity and cytotoxic effects and could thus be an effective drug for PDT.

The efficiency of the injected photosensitizer depends on its efficiency to accumulate preferentially in malignant tissue, its light absorbance and its quantum yield for singlet oxygen production.

For Pcs to accumulate preferentially in cancerous tissue, it is important to get the correct balance between hydrophilicity and lipophilicity of its substituents [17]. For example silicon phthalocyanines are mainly insoluble in water, but a variety of axial ligands are used to improve their solubility and transport by body fluids. Also the use of axially ligated, but ring unsubstituted Pcs in PDT studies rather than peripherally substituted Pcs offers advantages, ring unsubstituted Pcs do not form isomers [20]. A variety of axially substituted aluminium and silicon Pcs have been researched extensively for possible use as photosensitizers for photodynamic therapy. One of these complexes is Pc-4, a silicon Pc, **Figure 1.4**, which is being tested for PDT and now approved in the USA [21]. Pc-4 has low dark toxicity and absorbs at 668 nm, and

is being used for PDT as a sensitizer, in viral blood purging and as a therapeutic agent against some parasites. A cleaner and efficient synthesis has been developed for this drug [22].

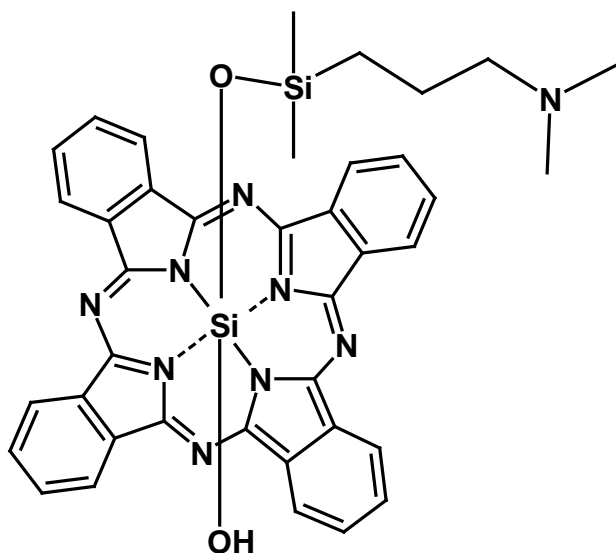


**Figure 1.4:** Structure of silicon phthalocyanine, Pc-4.

Organo soluble octa-alkyl-phthalocyanine zinc compounds with absorption at 700 nm have been proposed for the use in PDT [7,23], while hydroxyphthalocyanines have been tested as photosensitizers with positive results [7]. Mono-hydroxy ring substituted ZnPc and di-hydroxy ring substituted ZnPc have been tested and it was found that in vitro, mono-hydroxy ring substituted ZnPc was the most active, while in vivo the dihydroxy ring substituted ZnPc was the most efficient [7]. Unsymmetrically substituted Pcs are reported to have enhanced efficiency as photosensitizers and are more stable than symmetrically substituted Pcs or unsubstituted Pcs. Unsymmetrically ring substituted ZnPc have not been extensively studied as photosensitisers for PDT. Zinc dinaphthodi(4-sulphobenzo)porphyrazine, **Figure 1.5**, is one of the few

complexes studied. This complex has photoactivity at low concentrations ( $10^{-8}$  M), which is related to the amphiphilic nature of the complex and the improved cell-penetrating properties [7,23].

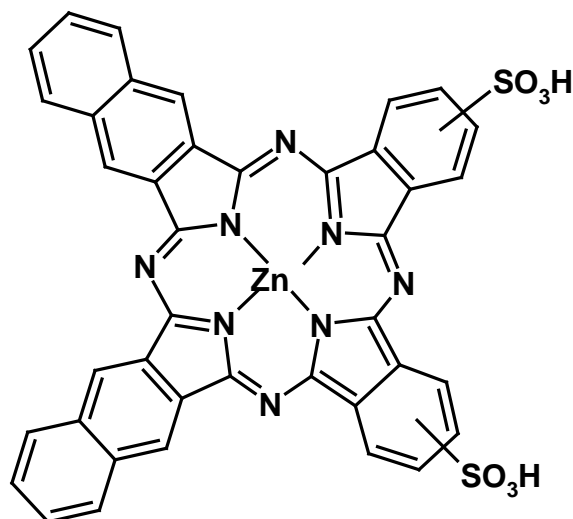


**Figure 1.5:** Structure of zinc dinaphthodi(4-sulphobenzo)-porphyrazine.

## 1.2 Aims of the project

Ring substituted or unsubstituted zinc phthalocyanines produce sufficient amount of singlet oxygen required for tumour cell destruction making them highly suitable for photodynamic cancer therapy. As mentioned above disulfonated phthalocyanine complexes of zinc are currently being tested as sensitizers for PDT [25-27]. These type of complexes aggregate in water solution [28-30]. It has been shown that the photosensitizing effect of the Pcs is mainly due to the monomer fraction. It is known that axial ligation prevents stacking of Pc rings in solution and may be used as an approach to monomerization. This approach was successful with aluminium and silicon phthalocyanines. The aim of the thesis is to study the possibility of using axial

ligation to increase the solubility and activity of zinc sulphophthalocyanine in water solutions, using bipyridyl and its derivatives as axial ligands. Also to study the effect of axial ligation on the spectroscopic and photochemical properties of zinc sulphophthalocyanine.

The major limitation of phthalocyanines for use in PDT is the lack of selectivity. All sensitizers show only relative selectivity towards some tumours. Amphiphilic photosensitizers seem to have some advantage over hydrophobic ones. Amphiphilic unsymmetrically substituted phthalocyanines have been shown to have cell penetrating powers [30,31].

Unsymmetrically substituted phthalocyanines are interesting compounds because of features such as improved solubility in both non-aqueous and aqueous solvents. Much effort has gone into the synthesis of unsymmetrically substituted phthalocyanines. Despite the variety of synthesis methods developed for the preparation of these macrocycles, mixtures of different Pcs are usually obtained which make the purification procedures difficult, thus the isolation of the desired product difficult.

The most widely used method for the synthesis of unsymmetrically substituted Pcs, is the statistical condensation method. This method is based on the statistical reaction of two differently substituted phthalonitriles or 1,3-diiminoisoindolines. The stoichiometry can play an important role, and one of the reactants is usually in excess, typically in a 3:1 molar ratio. The major compound is usually the symmetrically substituted Pc derived from the most abundant precursor. The desired

unsymmetrically substituted compound must therefore be separated from the mixture by standard chromatographic techniques.

Within this context it is worth noting that the preparation of unsymmetrically substituted Pc's through ring enlargement of sub-phthalocyanines by reaction with substituted phthalonitriles has an advantage over the mixed condensation methods because of good yields, easy purification, it is possible to form only one product [32-35]. In this thesis ring enlargement reactions were carried out in the presence of zinc (II) acetate dihydrate as a template in order to provide selectivity for the formation of metallated Pc's in one step.

Unsymmetrically substituted zinc phthalocyanines offer a possibility of improving selectivity since groups with different properties may be attached to the ring, making it possible to synthesize complexes which may have both lipophilic and amphiphilic properties.

The aim of this thesis is (i) to synthesize unsymmetrically substituted phthalocyanines and (ii) to study the effects of the substituents on the singlet oxygen quantum yield and (iii) to study the effects of substituents on photobleaching quantum yield.

## 1.3 Phthalocyanines

### 1.3.1 Structure and history of phthalocyanines

Phthalocyanines are synthetic substances related to naturally occurring porphyrins, **Figure 1.6**. They consist of a macrocycle made up of four isoindole units linked by aza nitrogen atoms [27]. Phthalocyanines are stable compounds both chemically and photochemically. They are typically blue or green in colour and are used as pigments in printing inks, paints and plastics [27]. Metallated phthalocyanines have a  $D_{4h}$  symmetry and show strong absorption in the visible and near infrared region called Q-band near 670 nm and a weaker absorption in the UV region called B-band or Soret band 330 nm.

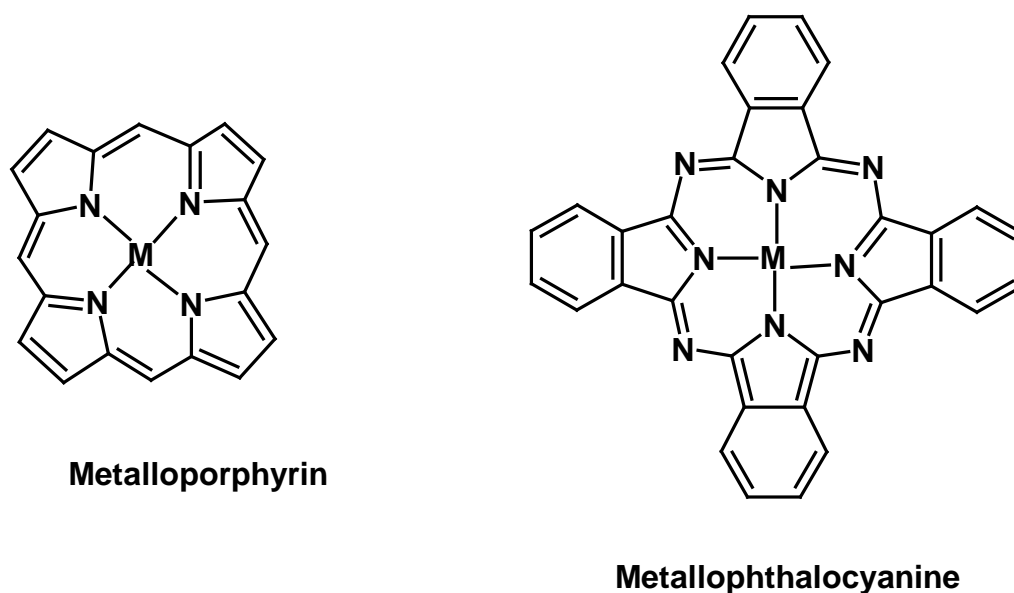


**Figure 1.6:** Structures of metalloporphyrin (MP) and metallophthalocyanine (MPc).

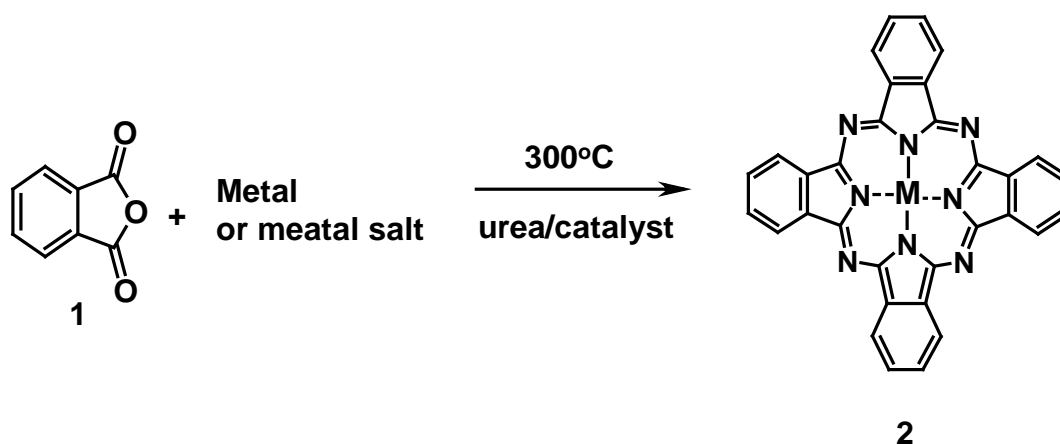
They are an interesting class of compounds with increasingly diverse industrial and biomedical applications, photosensitization [26], non-linear optics [36], catalysis [37], liquid crystals [38], and gas sensing [39]. Phthalocyanines can coordinate with most metals and can be substituted at the periphery with a variety of substituents. Axial ligands can also be introduced to the central metal ion depending on the efficiency of the ion to coordinate. These modifications promote specificity of the complexes in their applications.

Phthalocyanines were first discovered in 1928 during the preparation of phthalamide at Messrs Scottish Dyes Ltd [17]. Phthalamide was prepared from phthalic anhydride and ammonia and the product had traces of dark blue particles, which were later discovered to be iron phthalocyanine, the iron originates from the iron vessel used for the production process [17]. The geometric structure of metallophthalocyanine was later elucidated by Robertson using x-ray diffraction [40].

### **1.3.2 General methods of preparation of metallophthalocyanines (2)**

There are many methods that can be used for the preparation of metallophthalocyanines. The choice of a method usually depends on the availability of the precursors involved, the cost of the synthesis and the substituents on the starting materials. The first synthesis of iron phthalocyanine described above pioneered the synthesis for other metallophthalocyanines which involves heating phthalic anhydride (**1**) with urea and the metal salt or metal, with catalytic amounts of ammonium molybdate or aluminium oxide, **Scheme 1.3** [41,42]. This method is

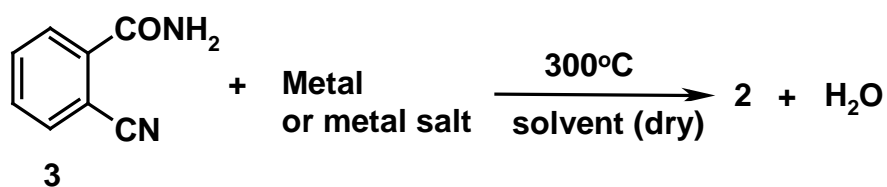
relatively cheap compared to the other methods, thus making it, the industry's first choice.



**Scheme 1.3:** Synthesis of MPc from phthalic anhydride (1).

The metal free phthalocyanine may be formed by treatment of the MPc with concentrated sulphuric acid [41-43]. The metal free phthalocyanine will react with the metal salt or metal if the product is more soluble.

Condensation of o-cyanobenzamide (3) in the presence of a metal salt or metal in a dry solvent gives a metallophthalocyanine (2), **Scheme 1.4** [45].



**Scheme 1.4:** Preparation of MPc from o-cyanobenzamide (3).

The cleanest laboratory scale synthesis is achieved using phthalonitrile (**4**) [42] as the precursor, **Scheme 1.5**, although industrially cheaper phthalic anhydride (**1**) [41] may also be used instead, **Scheme 1.3**. Most substituted phthalocyanines are derived from the cyclotetramerisation of the appropriate phthalonitrile derivative. The phthalonitrile method, allows for the preparation of substituted metallophthalocyanines from substituted phthalonitrile which are readily available and most are easy to synthesise. This method usually requires the use of strong bases such as 1,8-diazabicyclo[5.4.0]undec-7-ene (DBU) to catalyse the reaction and thus increase the yields [45].



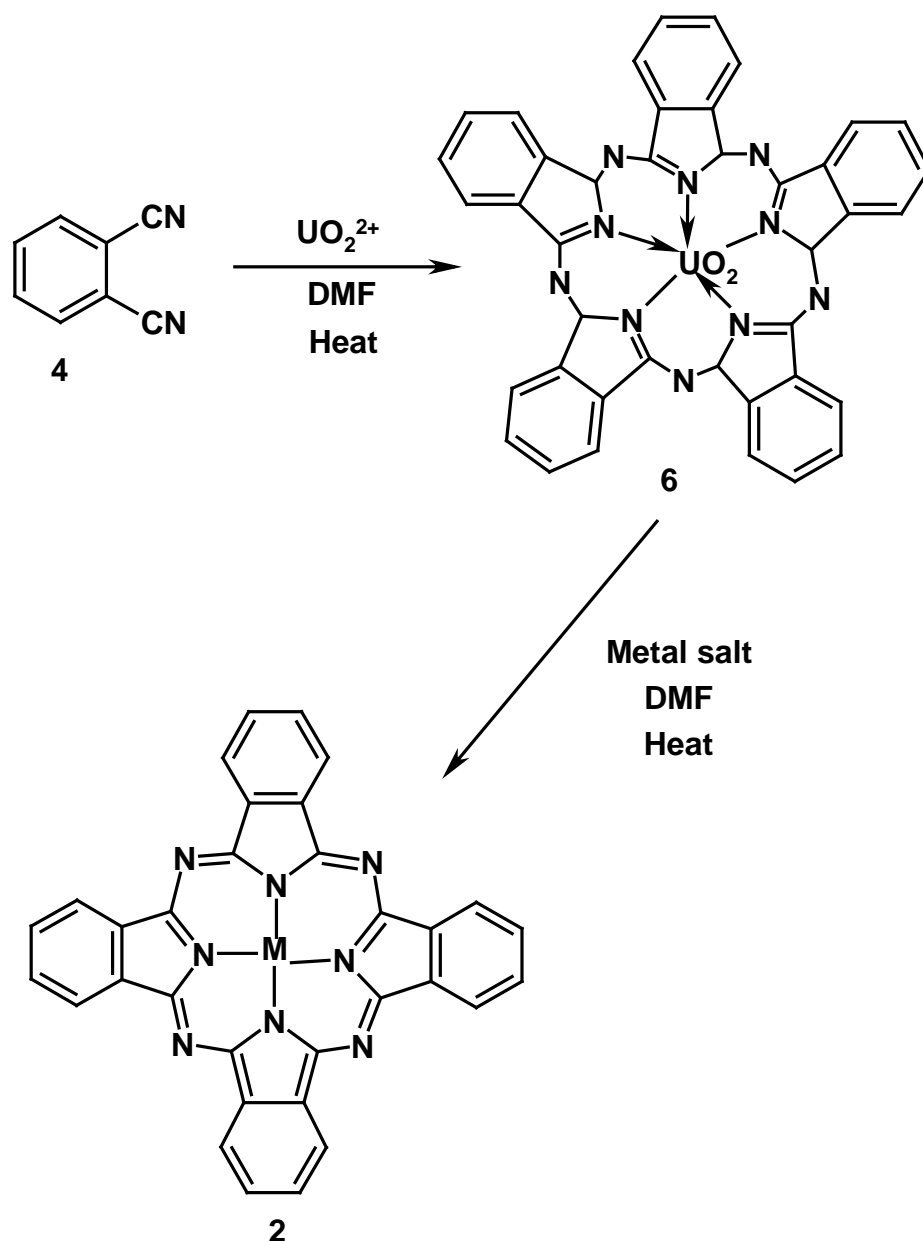
**Scheme 1.5:** Preparation of MPC from phthalonitrile (**4**).

Using 1,3-diiminoisoindoline (**5**) with a metal salt in a hydrophilic solvent is also one of the most popular methods of preparing metallophthalocyanines, **Scheme 1.6** [46]. 1,3-Diiminoisoindoline (**5**) is more reactive and thus requires milder reaction conditions compared to phthalonitriles [46].



**Scheme 1.6:** Preparation of MPC from 1,3-diiminoisoindoline (**5**).

Superphthalocyanine (SPc) (**6**) molecules comprise of a uranium oxide, which serves as a nucleus and five phthalonitrile moieties around it to produce a five subunit uranyl superphthalocyanine (**6**). The molecule is prepared by heating phthalonitrile (**4**) in the presence of anhydrous uranyl chloride in DMF at 170°C for one hour, **Scheme 1.7** [47]. Ring substituted superphthalocyanine complexes are also prepared using the same method [48]. Due to inherent instability of superphthalocyanine complexes, symmetrical phthalocyanines may be obtained by reacting the corresponding superphthalocyanine complex with a metal salt in DMF [47,48]. The reaction is illustrated in **Scheme 1.7**.



**Scheme 1.7:** Preparation of phthalocyanines from uranyl superphthalocyanines (6).

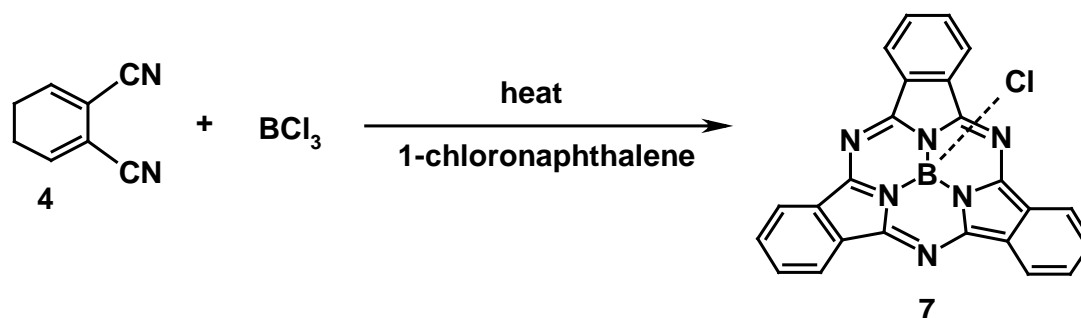
### 1.3.3 Synthesis of unsymmetrically substituted phthalocyanines

The aim of the thesis is to synthesize unsymmetrically substituted zinc phthalocyanines from ring expansion of unsubstituted and ring substituted Sub-phthalocyanines.

### 1.3.3.1 Synthesis of sub-phthalocyanines

Sub-phthalocyanines (**7**) were first synthesized in 1972 by reacting phthalonitrile (**4**) with boron trichloride or boron trifluoride at 240°C in 1-chloronaphthalene, the synthesis is shown in **Scheme 1.8**. X-ray crystallographic structure of this compound was only known a year later [32]. Sub-phthalocyanines (**7**) have gained tremendous popularity due to their non-linear optical properties and their use as intermediates for the synthesis of unsymmetrically substituted phthalocyanines [24,25,49-51].

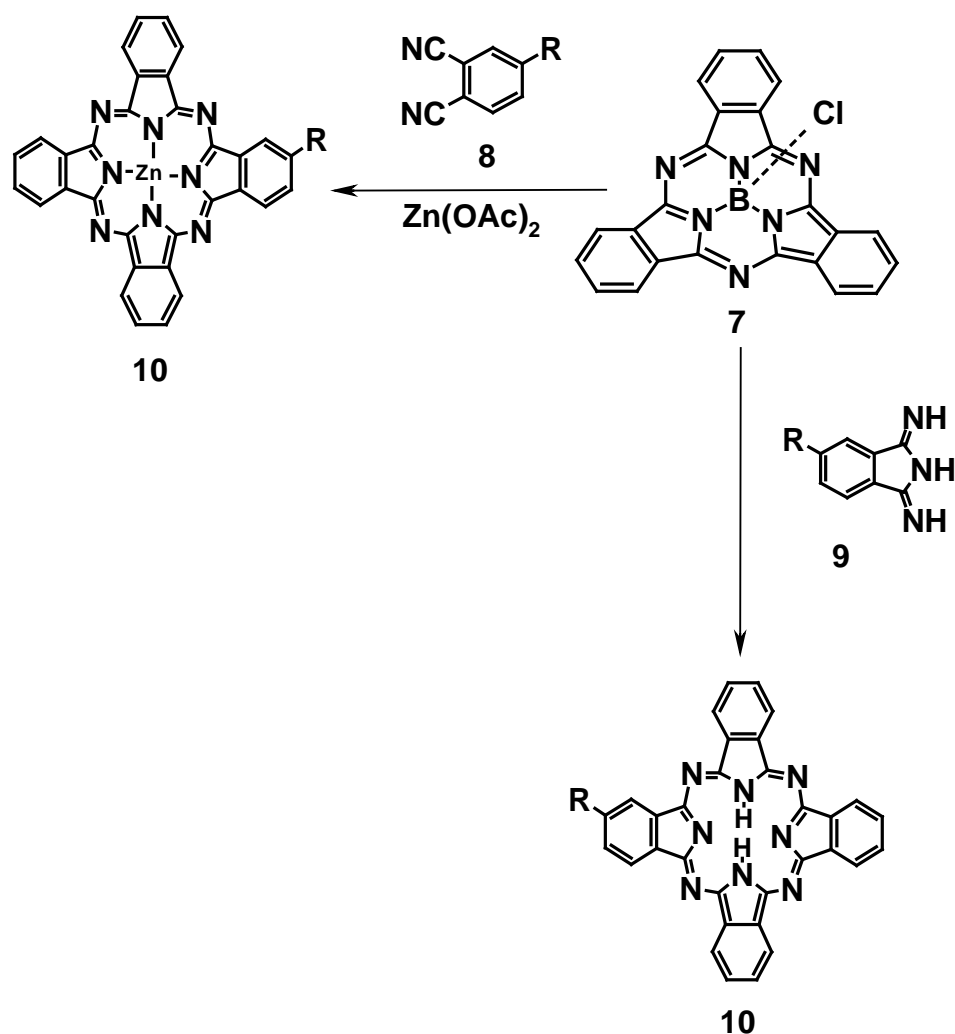
Sub-phthalocyanines are composed of three isoindoline units containing boron as the central atom with a  $C_{3v}$  symmetry and a Huckel aromatic delocalised 14  $\pi$ -electron system. They are non planar, and their cone shaped structure provides them with distinct properties [34,50]. The structure appears to be strained and unstable, this enables ring expansion reaction to occur. Thus they are by far much more soluble than phthalocyanines and aggregate to a lesser extent. Sub-phthalocyanines are soluble in most organic solvents like acetone, dimethylformamide (DMF),  $CH_2Cl_2$  and chloroform ( $CHCl_3$ ), but are not soluble in non-polar organic solvents like hexane and methanol. These properties assist in their purification processes [33]. The ultra-violet/visible (UV/vis) spectrum of sub-phthalocyanines is similar to that of phthalocyanines, except that the Q-band is located at lower wavelengths, near 570 nm and the Soret band near 300 nm for unsubstituted derivatives [51]. The position of the bands can be shifted towards the red region of the spectrum by introducing electron withdrawing substituents on the ring [31]. Hence sub-phthalocyanines with absorption spectra extended into the red region could meet both the photophysical and photochemical requirements for PDT [34].



**Scheme 1.8:** Synthesis of sub-phthalocyanine

### 1.3.3.2 Ring expansion of sub-phthalocyanines to form phthalocyanines

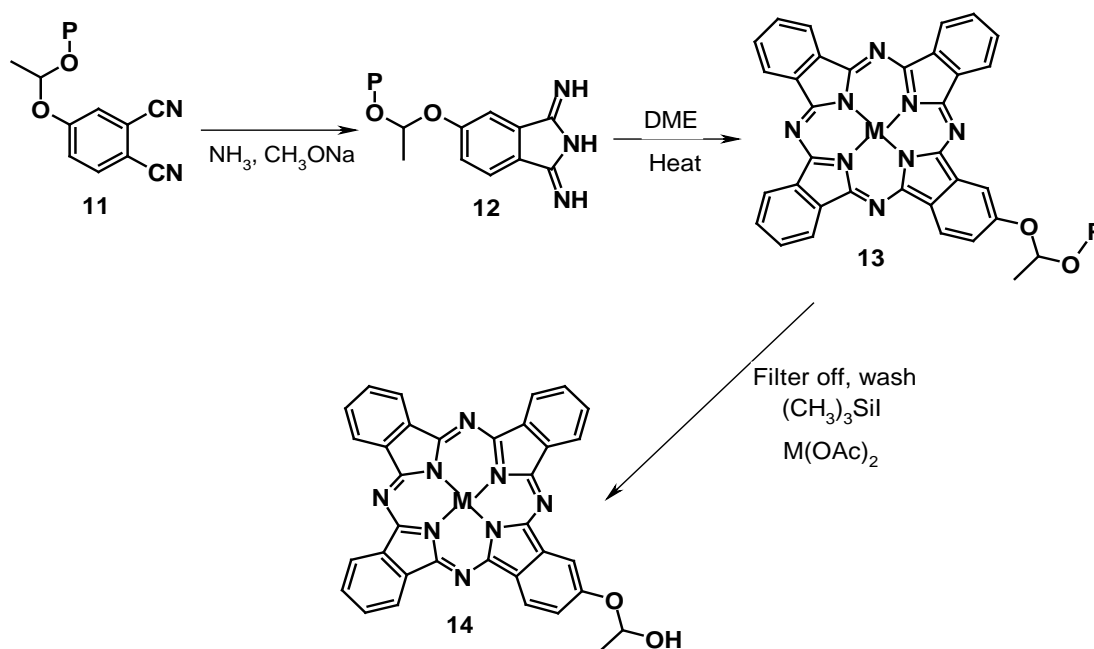
As discussed in Section 1.2 the most commonly used routes for synthesizing unsymmetrically ring substituted phthalocyanines are statistical condensation and ring enlargement of sub-phthalocyanines [34,35]. As also discussed in Section 1.2 the statistical condensation method suffers from the formation of different products that are difficult to separate. Ring enlargement method can be carried out using substituted phthalonitrile (**8**) or 1,3-diiminoisoindoline (**9**). Zinc metallation can not be done when diiminoisoindoline is employed due to its tendency to cyclotetramerise with zinc salts [35]. The less reactive substituted phthalonitrile (**8**) can be used instead to effect direct zinc metallation, **Scheme 1.9**. Since the metallation of the sub-phthalocyanines is required in most cases, a single step procedure for the preparation is advantageous. The ring enlargement of sub-phthalocyanines has been found to result not only in the desired ring substituted products but also in unsubstituted and differently substituted phthalocyanines [30,32]. Ring chlorinated phthalocyanines are also included in the product mixture, which are difficult to separate. In spite of the relatively easy synthesis of sub-phthalocyanines (**7**), only a few reports have been published about their purification.



**Scheme 1.9:** Synthesis of an unsymmetrically substituted phthalocyanine (**10**) from sub-phthalocyanine (**7**).

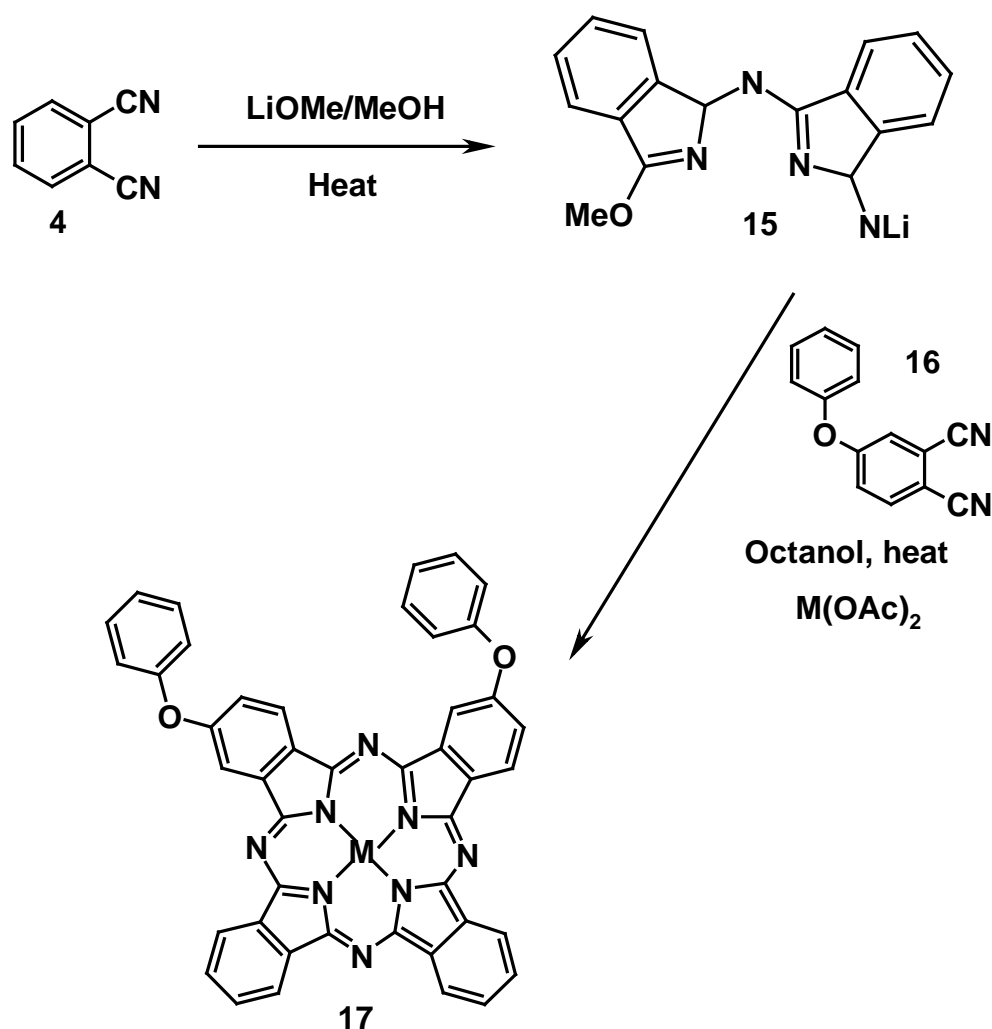
The ring enlargement method has several advantages over the mixed condensation methods because the yields are generally higher, but the separation of different Pcs is still a problem. Separation of the Pc from the sub-phthalocyanine is easy as thin layer chromatography (TLC) exhibits two separable coloured bands due to sub-phthalocyanine and Pc, but still the mixture of differently ring substituted Pcs remain.

Synthesis of unsymmetrically substituted phthalocyanines using immobilised phthalonitriles (**11**) has also received considerable attention as an alternative method. Usually polymer bound diiminoisoindoline (**12**) is reacted with an excess of unbound diiminoisoindoline (**5**) to give an unsymmetrically substituted polymer bound Pc (**13**), **Scheme 1.10** [52,53]. Filtration and Soxhlet extraction of the polymer with iodomethylsilane ( $(\text{CH}_3)_3\text{SiI}$ ) removes the bound polymer from the Pc, giving (**14**). This method also results in differently substituted Pcs. The separation of these products from each other by any method including extensive chromatography is usually difficult. Aggregation is believed to be the main problem in that it inhibits clean separation and even a single spot on TLC can actually be a mixture of compounds.



**Scheme 1.10:** Representation of the synthesis of an unsymmetrical MPc using polymer bound diiminoisoindoline, where P = polymer.

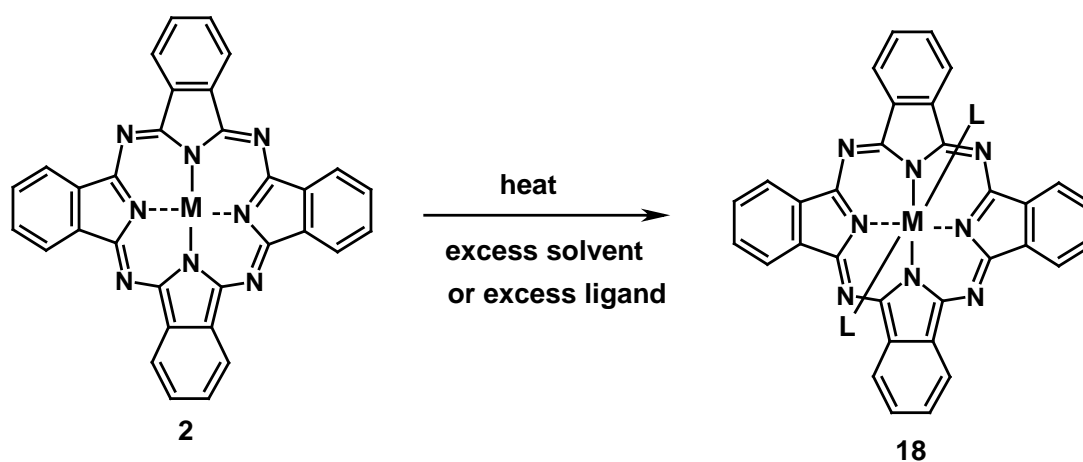
Azabenzopyrromethene (half-phthalocyanines) (**15**) are also widely used for synthesizing phthalocyanines lacking  $D_{4h}$  symmetry of peripheral substitution, **Scheme 1.11**. Half-phthalocyanines (**15**) can be synthesized by reacting phthalonitrile (**4**) with lithium methoxide in methanol [53,54]. Subsequent condensation of with a substituted phthalonitrile (**16**) results in ring closure reactions, which cyclize to give a conjugated macrocycle [53], mainly the adjacently di-substituted Pc (**17**), **Scheme 1.11**.



**Scheme 1.11:** Representation of the synthesis of an adjacently di-substituted MPc.

### 1.3.4 Preparation of axially ligated metallophthalocyanines

MPC complex with axial ligands can be synthesised directly by reacting the precursors with a metal salt containing an anion that can ligate to the central metal. Chlorides are usually used for this purpose and can be substituted by the ligand of choice. Axially ligated phthalocyanines are also prepared by refluxing MPC in coordinating solvents, like dimethylsulfoxide (DMSO) and pyridine or in the presence of the axial ligand, **Scheme 1.12**. Solvent-free axial ligand substitution of MPC using microwave is also possible [55].



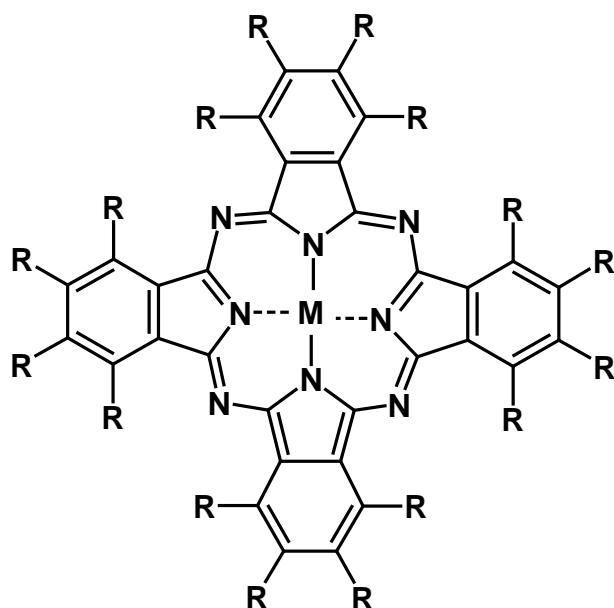
**Scheme 1.12:** Preparation of axially ligated metallophthalocyanine.

### 1.3.5 Aggregation in phthalocyanines

Aggregation is defined as a coplanar association of rings and is usually enhanced by van der Waals attractive forces between large planar molecules like phthalocyanine rings and the propensity of the molecules to avoid contact with water molecules [8]. Aggregation prevents easy purification, lowers solubility and suppresses photochemistry. Aggregation results in the broadening and splitting of the Q band and

blue shifting of Q band with increasing Pc concentration. These properties indicate addition of electronic levels from the aggregates. The high overlap of electron levels lead to rapid radiationless decay of the triplet excited state of the aggregate and thus low singlet oxygen quantum yields [8].

It is possible though to prevent aggregation by introducing bulky substituents on the phthalocyanine ring, **Figure 1.7 (19)**. For example, to obtain non-aggregating Pcs, large substituents can be placed on each one of the 16 possible site for substitution on the Pc ring as in **Figure 1.7** [36].



**R** could be any bulky molecule like  $C_{12}H_{25}$ .

**Figure 1.7:** Octasubstituted metallophthalocyanine (**19**), containing bulky ligands to prevent aggregation.

The steric crowding of the side chains make them non-planar, by forcing them out of the plane of the macrocycle, thus preventing aggregation of the molecules [36].

Axial ligation, **Figure 1.8** is also another method of preventing aggregation of phthalocyanines and improving solubility. Solubility can also be improved in several other ways such as incorporating sulphonic acid groups on the anellated benzene rings of the phthalocyanines [56]. Other functionalities which may be employed in water solubilization of phthalocyanines are carboxylic acid, phosphonic acid and butyl chains terminating in diesterified phosphate groups [57]. Considerable research has been undertaken on the axial ligation of phthalocyanines with central metals such as silicon, iron, ruthenium cobalt and many others [58,59].

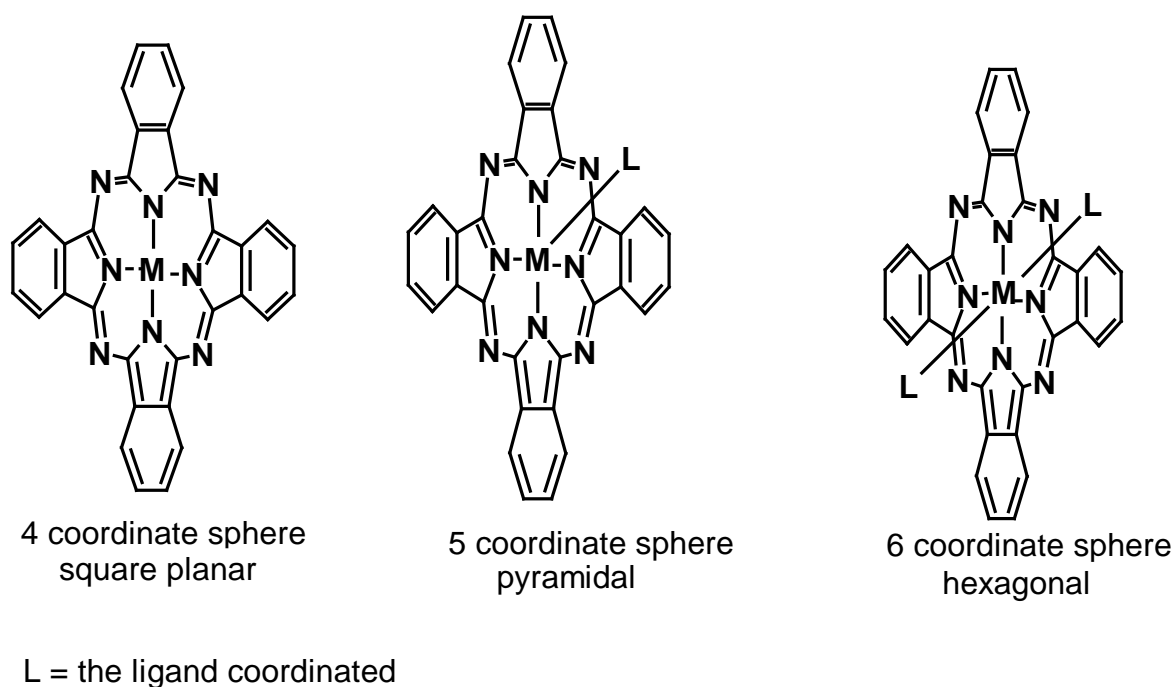


**Figure 1.8:** Axial ligation in MPC and symmetry of the molecules, L = ligand.

N-donor ligands like pyrazine, substituted pyrazines, 4,4'-bipyridine, pyridine, pyridazine and pyrimidine have been extensively used to coordinate axially to various

metallophthalocyanines to give coordinated monomeric Pc derivatives indicated in **Figure 1.8** [58,59]. Pyrazine and 4,4'-bipyridine are bidentate and can lead to bridged polymer chain structures, as shown in **Figure 1.9** [55,59]. If the ligands are monodentate, monomeric compounds such as structures illustrated in **Figure 1.8** are obtained.

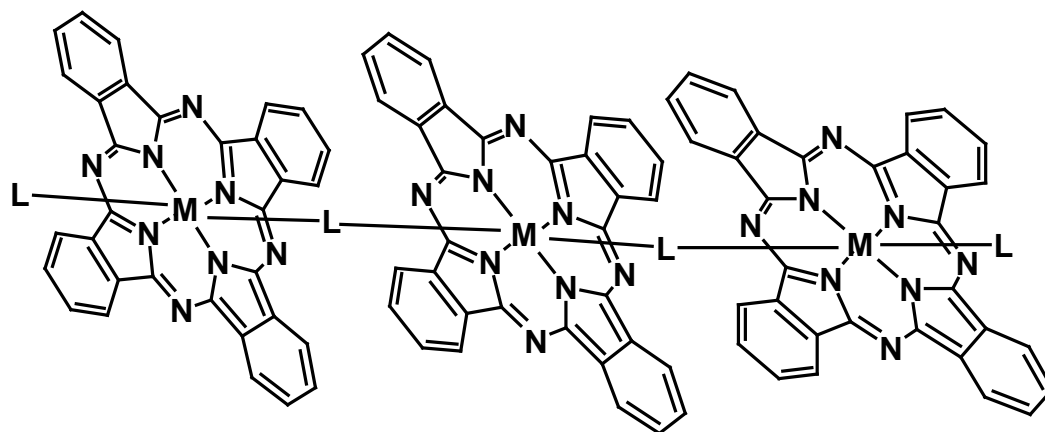


**Figure 1.9:** Stacked polymeric MPc.

### 1.3.6 Spectral properties of metallophthalocyanines

The strong colour of the MPc arise from the strong band in the far red of the visible spectrum near 670 nm (Q band). The most energetic set of transitions are less intense, lying to the blue of the electromagnetic spectrum near 340 nm (B or Soret band). The intense features are due to transitions from bonding to anti-bonding orbitals,  $\pi \rightarrow \pi^*$  states. Similar electron transitions are observed in macromolecules like porphyrins.

In phthalocyanines the highest occupied molecular orbital (HOMO) of the phthalocyanine ring is  $a_{1u}$  ( $\pi$ ) and the next low lying orbital is  $a_{2u}$  ( $\pi$ ) [60]. The lowest unoccupied molecular orbital (LUMO) is doubly degenerate  $e_g$  ( $\pi^*$ ) and the

one after it is  $b_{1u}$  ( $\pi^*$ ) [60]. The  $\pi$ - $\pi^*$  transition involves  $a_{1u}$  to  $e_g$  transition which results in the intense Q-band near 670 nm, **Figure 1.10**. The  $\pi$ - $\pi^*$  transitions involving  $a_{2u}$  and/ or  $b_{2u}$  to  $e_g$  transition yield the less intense B-band or Soret band which lies near 350 nm, illustrated in **Figure 1.10**. **Figure 1.11** shows the actual spectra of MPc with a Q-band and B-band at 670 nm and 350 nm, respectively.

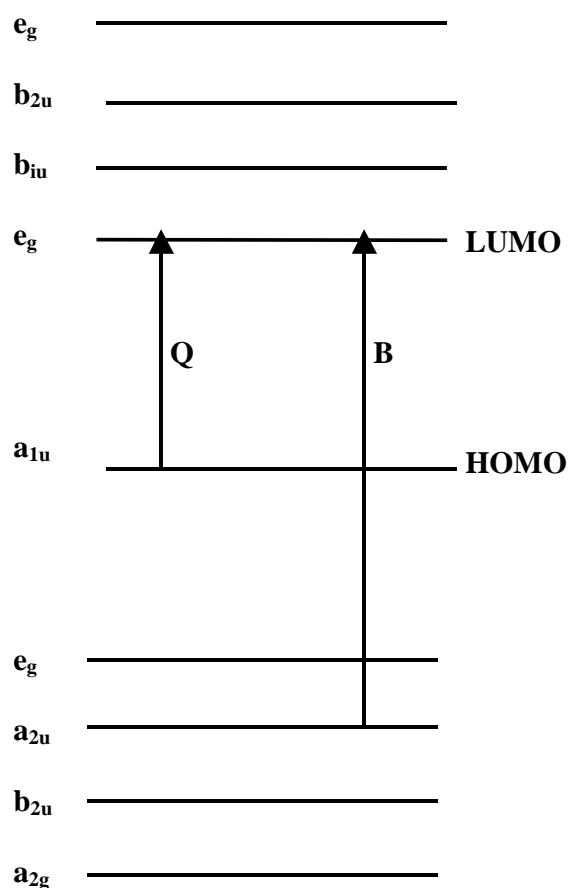


**Figure 1.10:** Electronic energy levels for phthalocyanines.

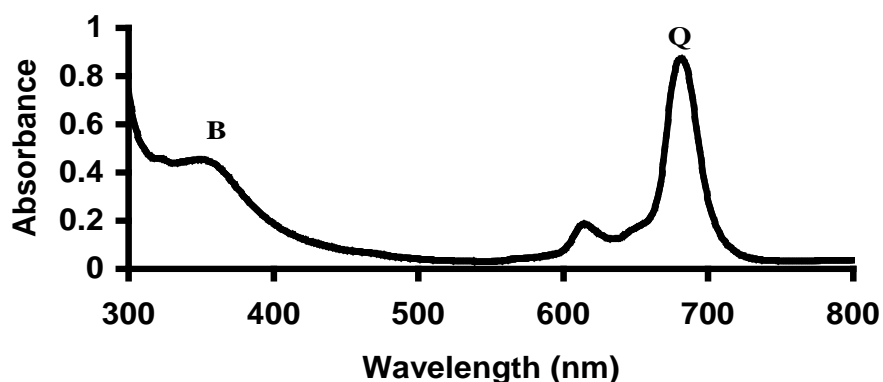


**Figure 1.11:** A typical absorption spectra of a MPc complex.

The Q-band's wavelength is very sensitive to changes in the axial ligand coordinated to the central metal and also to changes in the central metal ion. Thus a shift in the wavelength of the Q-band will be observed in the presence of coordinating solvents or added coordinating ligands [61-63].

Coupling between two or more  $\pi$  systems of aggregated phthalocyanine rings lead to blue shifting of the Q-band. Two absorption bands near 630 nm and 670 nm are usually observed due to dimeric and monomeric species, respectively.

#### 1.4 Photochemical methods

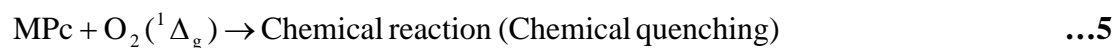
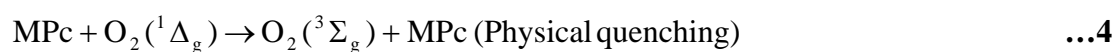
Quantum yields are of great concern in photodynamic therapy research. Photochemical and photophysical properties of complexes synthesized for use as potential sensitizers in PDT are determined as a measure of the efficiency of various photo-induced pathways. This means quantifying the yield of products formed with

relation to the amount of light used for the reaction. For PDT the sensitizer's triplet excited state is the reactive species which can result in any number of products including the ones that take part in PDT, such as radicals and singlet oxygen. In a photochemical process there are other de-excitation processes like internal conversion, fluorescence and phosphorescence. For PDT these processes have to be minimal for efficient production of singlet oxygen which is known to play a key role in PDT. The efficiency of photochemical processes is quantified by quantum yields. Quantum yields of fluorescence ( $\Phi_f$ ), phosphorescence ( $\Phi_p$ ), triplet excited states ( $\Phi_t$ ) and singlet oxygen generation ( $\Phi_\Delta$ ) are important in photochemistry [64]. The values of quantum yields are between zero and unity. If the photoexcitation initiates a radical chain reaction process, a variety of products can be formed resulting in quantum yields greater than unity [65].

#### **1.4.1 Singlet oxygen determination**

Since singlet oxygen is involved in photo-induced oxidative processes in biological systems, the determination of singlet oxygen quantum yields is of great interest to PDT research, since Type II mechanism is the most common. The effects of substituents, like halides and phenyl groups, on the photophysical properties of ZnPc complex have been studied. Phenyl substitution increases the efficiency of singlet oxygen photogeneration, due to increased solubility of the sensitizer. The number or position of the phenyl substituents on the ring only has negligible influence on the efficiency of singlet oxygen generation. Different methods can be used in determining singlet oxygen quantum yields, for this work a singlet oxygen chemical quencher 1,3-

diphenylisobenzofuran (DPBF) was used. DPBF was employed because it reacts quickly with the singlet oxygen in organic solvents without any side reactions. Also the decomposition products do not affect the detection of the quencher or react with either the singlet oxygen produced or the sensitizer. DPBF has absorption bands at 415 nm and 437 nm which can be monitored spectroscopically. The fate of singlet oxygen in the presence of DPBF may be represented by the following equations 1-5.



Physical quenching by DPBF is negligible in equation 2, because the quencher acts exclusively as a chemical quencher in organic solvents.  $\text{O}_2(^1\Delta_g)$  quantum yield does not depend on the concentration of MPc, thus physical quenching by MPc is ignored, thus making equation 4 not important. Equation 5 is also ignored because the pathway for the decay involving chemical reactions with MPc is negligible compared to the rate of reaction with DPBF. Only equations 1 and 3 are important in the decay of  $\text{O}_2(^1\Delta_g)$ . The rate of disappearance of DPBF in the presence of  $\text{O}_2(^1\Delta_g)$  is given by equation 6.

$$\frac{-[\text{DPBF}]}{dt} = k_q [\text{DPBF}][\text{O}_2(^1\Delta_g)] \quad \dots 6$$

Applying the steady state approximation for  $\text{O}_2(^1\Delta_g)$  and rearranging gives equation 7:

$$\text{O}_2(^1\Delta_g) = \frac{\Phi_{\Delta} I_{\text{abs}}}{k_q [\text{DPBF}] + k_d} \quad \dots 7$$

Substituting equation 7 into equation 6 gives equation 8: Where  $I_{\text{abs}}$  is the amount of light absorbed by the sensitizer, and  $\Phi_{\Delta}$  is the singlet oxygen quantum yield.

$$\frac{-[\text{DPBF}]}{dt} = \frac{k_q \Phi_{\Delta} I_{\text{abs}} [\text{DPBF}]}{k_q [\text{DPBF}] + k_d} \quad \dots 8$$

The change in the rate of disappearance of DPBF can be expressed as equation 9,

$$\Phi_{\text{DPBF}} I_{\text{abs}} = \frac{-d[\text{DPBF}]}{dt} \quad \dots 9$$

Substituting equation 9 into equation 8 gives equation 10:

$$\Phi_{\text{DPBF}} = \frac{k_q \Phi_{\Delta} [\text{DPBF}]}{k_q [\text{DPBF}] + k_d} \quad \dots 10$$

At low  $[\text{DPBF}]$  concentration,  $k_d \gg k_q [\text{DPBF}]$ , and the equation 10 becomes:

$$\Phi_{\text{DPBF}} = \frac{k_q \Phi_{\Delta} [\text{DPBF}]}{k_d} \quad \dots 11$$

Thus the reaction kinetics is first order at low [DPBF], whereas at high [DPBF],  $k_q [\text{DPBF}]$  is large and  $k_q [\text{DPBF}] \gg k_d$  and the reaction kinetics become zero order, which is undesirable in the present case. For MPc, equation 11 becomes equation 12:

$$\Phi_{\text{DPBF}}^{\text{MPc}} = \Phi_{\Delta}^{\text{MPc}} \frac{k_q}{k_d} [\text{DPBF}]^{\text{MPc}} \quad \dots 12$$

Where  $\Phi_{\text{DPBF}}^{\text{MPc}}$  represents the quantum yield of DPBF in the presence of the metallophthalocyanine (MPc),  $\Phi_{\Delta}^{\text{MPc}}$  is the singlet oxygen quantum yield in the presence of MPc and  $[\text{DPBF}]^{\text{MPc}}$  is the concentration of DPBF in the presence of MPc. Equation 12 can also be written for the standard with known  $\Phi_{\Delta}$  (eg. ZnPc). The ratio of the  $\Phi_{\text{DPBF}}$  for MPc and ZnPc can be used to obtain the  $\Phi_{\Delta}$  of the MPc using equation 13.

$$\Phi_{\Delta}^{\text{MPc}} = \Phi_{\Delta}^{\text{ZnPc}} \times \frac{\Phi_{\text{DPBF}}^{\text{MPc}}}{\Phi_{\text{DPBF}}^{\text{ZnPc}}} \times \frac{[\text{DPBF}]^{\text{ZnPc}}}{[\text{DPBF}]^{\text{MPc}}} \quad \dots 13$$

Knowing that

$$\Phi_{\text{DPBF}} = \frac{(C_0 - C_t)V}{I_{\text{abs}} \times t} \quad \dots 14$$

Where  $C_0$  and  $C_t$  are the concentration of DPBF before and after photolysis for time  $t$ , and  $v$  is the volume of the sample in the cell.  $I_{\text{abs}}$ , the light absorbed is determined by equation 15:

$$I_{\text{abs}} = \frac{\alpha \times S \times I}{N_a} \quad \dots 15$$

Where  $S$  is the cell area irradiated,  $I$  is the intensity of the light and  $N_a$  is Avogadro's constant.  $\alpha$  is the fraction of light absorbed and  $I_{\text{abs}}$  is the light absorbed. Substituting equation 15 into equation 14, and replacing  $\Phi_{\text{DPBF}}^{\text{MPc}}$  and  $\Phi_{\text{DPBF}}^{\text{ZnPc}}$  in equation 13 with the equation resulting from the substitution, gives equation 16.

$$\Phi_{\Delta}^{\text{MPc}} = \Phi_{\Delta}^{\text{ZnPc}} \times \frac{(C_0 - C_t)^{\text{MPc}}}{(C_0 - C_t)^{\text{ZnPc}}} \times \frac{(\alpha t)^{\text{ZnPc}}}{(\alpha t)^{\text{MPc}}} \times \frac{[\text{DPBF}]^{\text{ZnPc}}}{[\text{DPBF}]^{\text{MPc}}} \quad \dots 16$$

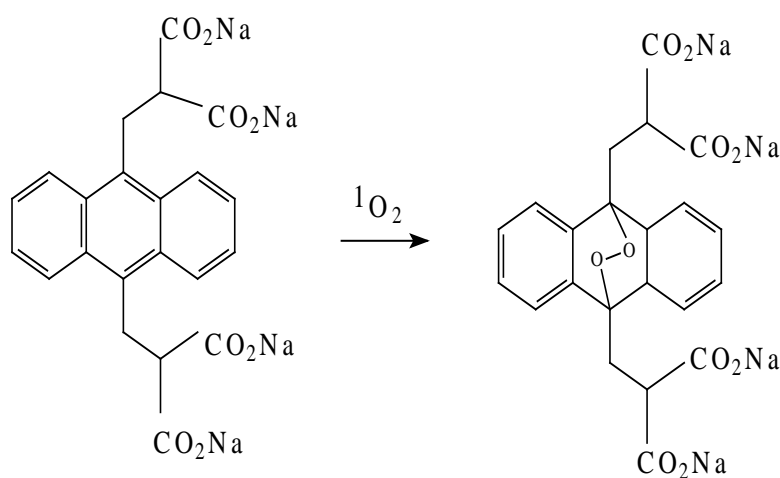
Where  $(C_0 - C_t)^{\text{MPc}}$ ,  $(C_0 - C_t)^{\text{ZnPc}}$  are changes in DPBF concentration in the presence of MPc (unknown) and ZnPc (standard), respectively.  $t^{\text{ZnPc}}$  and  $t^{\text{MPc}}$  represent the photolysis times in the presence of ZnPc and MPc, respectively.  $S$ ,  $v$  and  $N_a$  are the same in the presence of both the standard and unknown, hence cancel out. The light intensity was the same for both MPc and ZnPc, hence cancel out in equation 16.

$\alpha$  is determined using equation 17:

$$\alpha = \frac{\sum T_{\text{filter}} (1 - T_{\text{dye}})}{\sum T_{\text{filter}}} \quad \dots 17$$

Where  $\alpha$  is the fraction of the overlap intergral of light used,  $T_{\text{dye}}$  is the transmittance of the dye (MPc) and  $T_{\text{filter}}$  the transmittance of the filter used. The values of  $\alpha$ , usually range  $\sim 0.3-0.8$  for good overlap.  $\alpha$  is not constant and thus has to be calculated for every solution used. Details for the calculation are provided in the experimental section.

DPBF is a singlet oxygen quencher in non-aqueous media. Determination of  $\Phi_{\Delta}$  in aqueous media was carried out using  $\alpha, \alpha'$ -(anthracene-9, 10-diyl) bimethylmalonate (ADMA), shown in **Figure 1.12**. ADMA has several peaks in the UV region of the spectra but the one at 380 nm is of interest for this purpose. Equation 16 was also employed when ADMA was a quencher.



2,2'- [(9,9'-anthracenediyl)  
dimethyl] bimalic acid, tetrasodium salt

**Figure 1.12:** The structure of ADMA before and after reacting with singlet oxygen.

### 1.4.2 Quantum yield of photobleaching

Photobleaching of MPcs is characterised by the disappearance of the UV/vis spectra due to the degradation of the Pc ring, in the presence of light. Photostability is important both to the shelf life of the sensitizers, as well as their behaviour inside living tissue. Upon localisation in tissue cells, a small fraction of the sensitizer may locate in the neighbouring healthy cells. If irradiated with light, photodegradation of the sensitizer at low concentration may occur before damage is done to the healthy cells.

As already mentioned quantum yields for photobleaching can be determined using the same method as for singlet oxygen quantum yield, except that DPBF is not added. Quantum yield of photobleaching is represented by  $\Phi_{\text{photobleaching}}$ , and equation 14 is employed the determination where  $C_0$  and  $C_t$  represent the concentrations of the sensitizer before and after irradiation respectively. The concentrations of the sensitizer are obtained using their Q-band extinction coefficients.

Aggregation plays an important role in the properties of MPcs. It lowers the quantum yields of singlet oxygen through dissipation of energy by aggregates. In **Table 1**, selected MPcs are given with their respective singlet oxygen quantum yields. ZnPc(CPh) has a relatively low singlet oxygen quantum yield as a result of aggregation, this causes broad spectra, and deviation from Beer-Lambert law.

**Table 1:** Photobleaching and singlet oxygen quantum yields for a selected MPcs. Where TbPh = tertbutyl phenoxy, Ph = phenoxy and CPh = carboxy phenoxy.

Sensitizer	$\Phi_{\Delta}$	$\Phi_{\text{photobleaching}}$	References
ZnPc	0.55		66
ZnTsPc	0.43		4,5
AlTsPc	0.36		4,5
SiTsPc	0.35		4,5
ZnPc(TbPh) <sub>8</sub>	0.73	$4.6 \times 10^{-3}$	88
ZnPc(Ph) <sub>8</sub>	0.60	$2.5 \times 10^{-5}$	88
ZnPc(CPh) <sub>8</sub>	0.23	$2.3 \times 10^{-6}$	88

ZnPc(CPh) has COOH groups as peripheral substituents and these may form hydrogen bonds with neighbouring molecules and in this manner cause aggregation of the molecule. Low singlet oxygen quantum yield could reflect the aggregated of species used for the photochemical study. Other factors such as the yield and lifetime of excited states of the complexes affect the singlet oxygen quantum yield values.

#### 1.4.3 Determination of triplet lifetimes, triplet quantum yields

Values of triplet quantum yield ( $\Phi_{\tau}$ ) and triplet state lifetimes ( $\tau_{\tau}$ ) are important for PDT, since these values have to be reasonably high for PDT action.

*Triplet lifetimes*

Deactivation of the triplet state,  $M^*$ , to the ground state,  $S_0$ , can be described by the equation 18:

$$\frac{-d[M^*]}{dt} = k_1[M^*] + k_2[M^*][S_0] + 2k_3[M^*]^2 \quad \dots 18$$

Where  $k_1$  is the measured first order rate constant and is the sum of the radiative and non-radiative unimolecular decay processes. In most cases for molecules in solution, the radiative process from the triplet state like phosphorescence, is negligible. The second term in the equation is due to quenching of the excited triplet state by ground state molecules, i.e. self-quenching and the final term is due to quenching of the triplet by another triplet state, ie. Triplet-triplet annihilation. At low sensitizer concentrations and low laser powers, only the first term in the equation is important and the rate constant  $k_1$  is obtained from a first order-plot i.e.  $\ln [M^*]_0/[M^*]_t$  vs  $t$  from  $\ln [M^*]_0/[M^*]_t = k_1 t$  where  $[M^*]_0$  and  $[M^*]_t$  are the triplet concentrations at zero and time  $t$ , and are directly proportional to the transmittance and thus the voltage change measured on the oscilloscope (see experimental section). Thus the change in absorbance,  $\Delta A$ , can be calculated using Beer-Lambert law, equation 19:

$$\Delta A = \epsilon \Delta c l = \ln \frac{I_0}{I} = \ln \frac{V_\infty}{V_\infty - \Delta V} \quad \dots 19$$

Where  $l = 1\text{cm}$  pathlength,  $V_\infty$  is the 0 – 100% voltage and  $\Delta V$  is the change in voltage observed. A linear plot of  $\ln(A)$  vs  $t$  thus gives a gradient  $k_1$  and its reciprocal the triplet lifetime,  $\tau_t = 1/k_1$

### *Triplet quantum yields*

Triplet extinction coefficients,  $\varepsilon_t$ , were determined by the singlet depletion method [64,65]. The phthalocyanine triplet state (max ~ 490 nm) does not absorb in the same region as the ground state (max ~ 680 nm) and thus equation 20 applies:

$$\varepsilon_t = \frac{(\Delta A)_{490} \varepsilon_s}{(\Delta A)_{680}} \quad \dots 20$$

Triplet quantum yields were determined by the relative method [68], using zinc phthalocyanine as a standard ( $\text{ZnPc} = 0.25$  in DMSO) with equation 21:

$$\Phi_x = \frac{\Phi_{st} (\Delta A)_x \varepsilon_{st}}{(\Delta A)_{st} \varepsilon_x} \quad \dots 21$$

Where  $\Phi_x$  and  $\Phi_{st}$  are the triplet quantum yields for the sample and the standard respectively.  $\Delta A_x$  and  $\Delta A_{st}$ , and  $\varepsilon_x$  and  $\varepsilon_{st}$  are the triplet absorbance and the triplet extinction coefficients of the unknown and standard, respectively.

#### 1.4.4 Determination of fluorescence quantum yields and fluorescence lifetimes

Since phthalocyanines and other related compounds with potential use in PDT are to some extent selective towards tumours, their  $\Phi_f$  and the lifetime of fluorescence have become important in imaging and locating tumours. Fluorescence lifetimes for phthalocyanines range between 1 and 7 ns [69].

##### *Fluorescence lifetimes*

If a first order radiative process is experimentally observed, it may be assumed that no other process exists but only that which is being studied. The electronically excited species will decay radiatively to the ground state and the process may therefore be formulated as in equation 22 and 23:

$$\frac{d[M^*]}{dt} = -A_{ul}[M^*] \quad \dots 22$$

Where

$$\therefore [M^*] = M_0 * e^{-A_{ul}t} \quad \dots 23$$

Where  $A_{ul}$  is the Einstein coefficient, which is the number of times per second that an excited state emits a photon. The radiative lifetime is defined by, equation 24:

$$\tau_0 = \frac{1}{A_{ul}} \quad \dots 24$$

Which is the time taken to diminish the population to 1/e of its initial concentration. This first order exponential decay may be recorded by a pulsed laser able to pulse at picosecond (ps) intervals. The lifetime is important because it determines the time available for the fluorophore to interact with the diffuse environment.

### *Fluorescence quantum yields*

Fluorescence quantum yields, that is, the number of emitted photons from singlet state relative to the number of absorbed photons, may be determined by a relative method using a reference material. Compounds that have known fluorescence quantum yields in specific solvents such as ZnPc in DMSO ( $\Phi_F = 0.18$ ) [70] may be used for comparative determinations. These measurements involve the absorption spectra as well as the emission spectra of a sample wherein the optical density is less than 0.1. Low concentrations are essential to avoid quenching. The fluorescence quantum yields may thus be determined using equation 25 (derived in the same manner as for the singlet oxygen quantum yields):

$$\Phi_F = \Phi_{F(st)} \frac{\text{Area}_x \cdot A_{st} \cdot \eta_x^2}{\text{Area}_{st} \cdot A_x \cdot \eta_{st}^2} \quad \dots 25$$

Where  $\text{Area}_x$  and  $\text{Area}_{st}$  are the respective areas of the unknown sample and standard (determined by simply adding up the relative emission of the Q-band and its vibrational bands).  $A_s$  and  $A_{st}$  are the absorptions at the respective excitation wavelengths of the sample and standard. Different excitation wavelengths may be

used for excitation.  $\eta_x$  and  $\eta_{st}$  are the refractive indexes of the solvents used for the sample and standard respectively.

The next important factor of photochemistry is the energy of excitation. Under illumination into the Soret band, the high lying orbitals are populated. The high lying electronic states have higher energy and are consequently reactive. Besides this, under Soret band excitation we obtain excited states with charge transfer between metal and axial ligand and  $n\pi^*$  excited states. Charge transfer between metal and axial ligand may lead to ligand photodissociation followed by its loss or change.

In general the photophysical properties of symmetrical ZnPc complexes have been studied extensively. The quantum yield of any photo-induced process is very important as it gives an idea of what to expect in vivo. In PDT terms, the quantum yield of fluorescence has to be efficiently low as to result in high quantum yields of the triplet state of the sensitizer. High production of the excited triplet state, results in reasonably high singlet oxygen quantum yields, though competing processes like phosphorescence and non-radiative decay may lower the yield for singlet oxygen production, **Table 2**, shows that unsubstituted ZnPc has a relatively high triplet lifetime of 300  $\mu$ s and a higher singlet oxygen quantum yield as compared to the other complexes.

**Table 2:** Photophysical data of selected MPcs.  $\Phi_F$ ,  $\Phi_\tau$  and  $\Phi_\Delta$  represents quantum yield for fluorescence, triplet state and singlet oxygen of the sensitizer respectively in DMF.

Sensitizer	$\Phi_F$	$\tau_F$ (ns)	$\tau_T$ ( $\mu$ s)	$\Phi_\Delta$
ZnPc	0.55 [66]	3.9	300	0.40
ZnTsPc <sup>1</sup>	0.36 [4,5]	2.9	245	0.30
AlTsPc <sup>1</sup>	0.35 [4,5]	2.9	245	0.36

<sup>1</sup>TsPc represents tetra-sulphonated phthalocyanine in **Table 2**.

## 1.5 Electrochemistry

### 1.5.1 Background on cyclic voltammetry

Cyclic voltammetry is the most commonly used electrochemical technique for characterisation of metal complexes. This method locates the redox potentials of complexes by scanning the potential on a stationary solid working electrode, in this case a glassy carbon electrode was used. The technique is also popular for determining the reversibility of redox systems. Cyclic voltammetry is employed in this work for characterization of MPcs, hence it is discussed below.

In cyclic voltammetry, the potential is scanned from an initial value  $E_i$  to a final value  $E_f$  back to  $E_i$  and the current is recorded. This gives a complete cycle, thus the name

cyclic voltammetry. In the forward scan reduction/oxidation occurs as indicated by the cathodic/anodic current, and in the reverse scan the reduced/oxidized species are oxidised/reduced back to the original species, indicated by the anodic/cathodic current. This technique is capable of generating a new species during the forward scan and then monitoring its fate on the reverse scan. Cyclic voltammetry scans can either be classified as reversible, quasi-reversible or irreversible.

i) Reversible process

A reversible process is one in which species formed on the forward scan are reduced on the reverse scan. Measuring the potential difference between the two peak potentials can identify reversible systems.

Equation 26 applies to a system that is reversible both electrochemically and chemically.

$$\Delta E = E_a - E_c = \frac{RT}{nF} \approx \frac{0.059V}{n} \text{ at } 25^\circ\text{C} \quad \dots 26$$

Where  $\Delta E$  is the difference between the anodic and cathodic peak potentials.  $E_a$  and  $E_c$  are the anodic and cathodic peak potentials, respectively, in volts.  $n$  is the number of electrons transferred,  $F$  the Faraday constant,  $R$  the gas constant and  $T$  is the temperature in Kelvin.

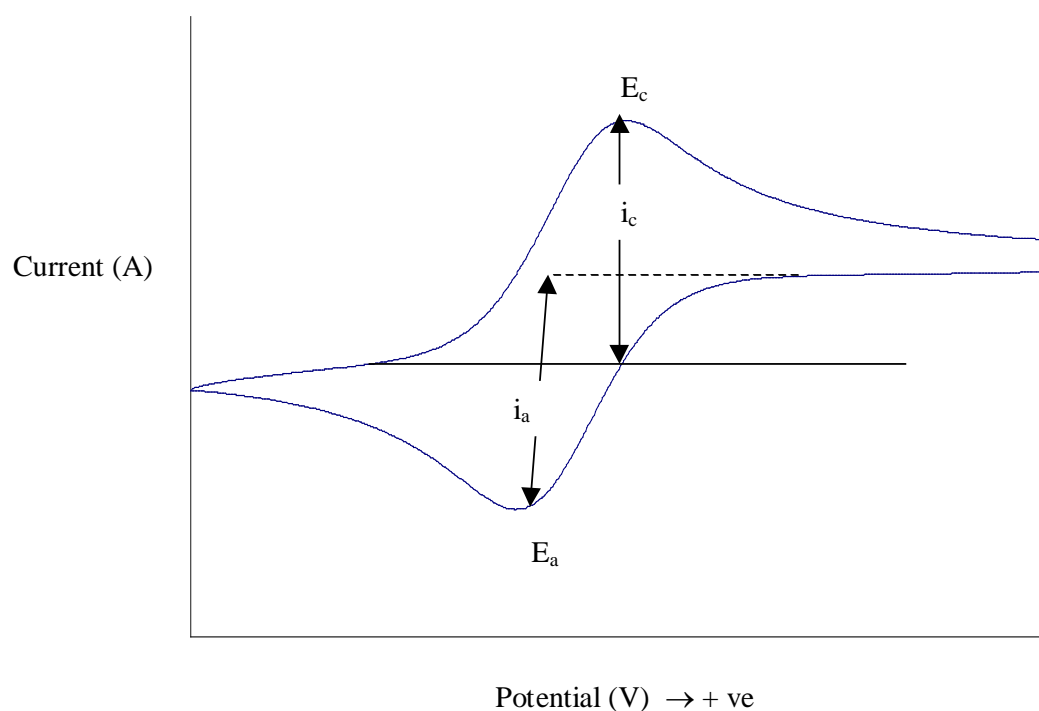


**Figure 1.13:** Cyclic voltammogram for a reversible system.

The peak potential separation is independent of the scan rate for a reversible couple.

The potential midway between the two peak potentials is known as the formal potential  $E^{0'}$  [71,72], and is approximately equal to the half wave potential ( $E_{1/2}$ ).

$$E^{0'} = \frac{1}{2} (E_a + E_c) \sim E_{1/2}$$

...27

The peak current is related to other parameters by the Randles –Sevcik equation:

$$i_p = (2.69 \times 10^{-5}) n^{3/2} A D^{1/2} C v^{1/2} \quad \dots 28$$

Where  $i_p$  = peak current in Amperes

$n$  = is the number of electrons transferred

$A$  = the surface area of the electrode ( $\text{cm}^2$ )

$D$  = the diffusion coefficient ( $\text{cm}^2/\text{s}$ )

$C$  = concentration ( $\text{mol}/\text{cm}^3$ )

$v$  = scan rate ( $\text{V}/\text{s}$ )

For reversible systems, the peak current is directly proportional to the concentration,  $C$  and increases with increase in the square root of scan rate,  $v^{1/2}$ . Thus plots of peak current against  $v^{1/2}$  are linear. The ratio of the forward and reverse peak currents are similar and thus their ratio is close to unity, and is independent of the scan rate.

$$\frac{i_a}{i_c} \approx 1 \quad \dots 29$$

Where  $i_a$  and  $i_c$  are the anodic and cathodic currents in amperes, respectively.

ii) Quasi reversible process

Peaks are more drawn out and exhibit larger separation in peak potentials compared to reversible systems.

iii) Irreversible process

Characterized by slow electron exchange of the redox species at the electrode. In an irreversible process, the voltammogram usually has one oxidation or reduction wave

indicative of non-regeneration of the starting species. This may result from the formation of electroinactive reduction or oxidation products. If both waves are present the separation between them is much greater than  $0.059/n$  and is dependent on the scan rate.

### **1.5.2 Square wave voltammetry**

Square wave voltammetry (SWV) is composed of a square wave superimposed on a staircase, a full square wave cycle corresponding to the duration of one step in the square waveform [72-74]. The current is sampled twice, both in the positive and negative directions. The positive and negative going pulses correspond to the oxidation or reduction peaks of the electroactive species at the electrode surface and can be obtained in the same scan by subtraction of their differences [73,74].

Cyclic voltammetry was complemented in this work by Osteryoung square wave voltammetry (OSWV), which is a more sensitive technique with optimal peak separation. Since the difference in current is plotted hence the effects of changing currents are minimized.

### **1.5.3 Electrochemical properties of MPcs**

The electrochemistry of metallophthalocyanines has been researched extensively. These complexes have rich electrochemical properties with many redox processes. Differences in the central metal ions and variations in the substituents on the

periphery of the ring result in varied electrochemical properties of the phthalocyanine complexes [75]. Redox process of the MPc complexes may be centred at the phthalocyanine ring or at the central metal ion [75]. Changes in the oxidation states usually result in reversible and dramatic colour changes because of redox processes taking place mainly on the ring [75], especially for zinc phthalocyanines. The phthalocyanine ring exists as a dianion (Pc<sup>2-</sup>) and may be reduced by up to four successive electron transfer processes, which may or may not be reversible.

To illustrate ring based redox processes a cyclic voltammogram of octaphenoxypthalocyanato (bis(dimethylaminoxy)) silicon in DMF containing tetrabutylammonium hexafluorophosphate (TBAHP) is shown in **Figure 1.14**.

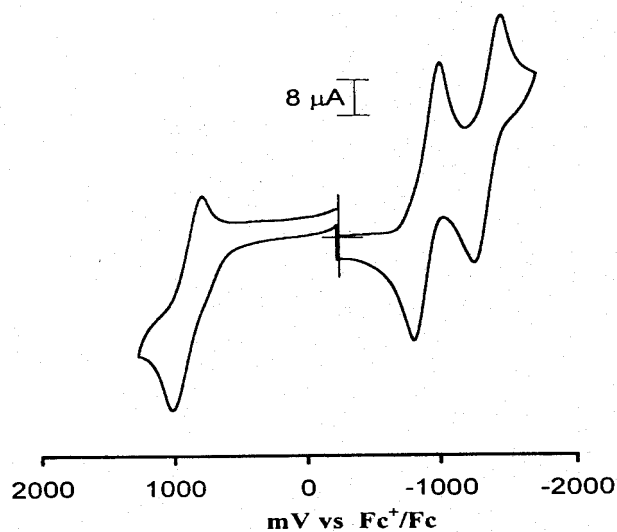


**Figure 1.14:** Cyclic voltammogram of octaphenoxyphthalocyanato (bis(dimethylaminoxy)) silicon in DMF at  $100 \text{ mVs}^{-1}$  scan rate [76].

Up to four successive ring reductions can occur by addition of electrons into the LUMO of the ring. These are  $\text{Pc}^{-2} \rightarrow \text{Pc}^{-3}$ ,  $\text{Pc}^{-3} \rightarrow \text{Pc}^{-4}$ ,  $\text{Pc}^{-4} \rightarrow \text{Pc}^{-5}$ ,  $\text{Pc}^{-5} \rightarrow \text{Pc}^{-6}$ . Two oxidations are possible by removing electrons from  $a_{iu}$  (HOMO),  $\text{Pc}^{-2} \rightarrow \text{Pc}^{-1} \rightarrow \text{Pc}^0$ .

Oxidation and/or reduction of the central metal can only occur when the metal orbitals lie at energies within the HOMO-LUMO gap of the ring [73], and also depending on the conditions such as the solvent used, etc. For example phthalocyanines containing central metals such as FePc and CoPc show redox properties at the metal.

**SUMMARY OF AIMS**

1. Synthesis of unsymmetrically ring substituted zinc phthalocyanines.
2. Characterization of the unsymmetrically ring substituted zinc phthalocyanines.
3. Study of photochemical and photophysical properties of these complexes.
4. Effects of axial ligation on the photochemical properties of water-soluble zinc phthalocyanine.

## 2. EXPERIMENTAL

### 2.1 Materials

N,N'-dimethylformamide (DMF) used for electrochemical studies was dried over aluminium oxide and distilled before use. Dimethylsulphoxide (DMSO) was dried in alumina before use. Thionyl chloride, potassium carbonate, nitrophthalimide, dichlorophthalic anhydride, 4-*tert*-butylphenol, 4-hydroxybenzoic acid, 4-hydroxybenzenesulfonic acid, 3-naphthol, 1,8-diazabicyclo[5.4.0]undec-7-ene (DBU), 1,3-diphenylisobenzofuran (DPBF), diazabicyclooctane (DABCO) bipyridine, pyridine and aminopyridyl were obtained from Sigma or Aldrich and used as received. Ferrocene was recrystallized from ethanol before use as an internal standard for electrochemical studies. Distilled deionised water was used for studies in aqueous media. Tetrabutylammonium perchlorate (TBAP) was prepared and used as an electrolyte for electrochemical studies. 2,2'-[(9,9'-anthracenediyl)dimethyl]bimalic salt (ADMA) was a gift from the Organic Intermediates and Dyes Institute in Moscow. ZnPc used as an internal standard for photochemical studies was also a gift from Organic Intermediates and Dyes Institute.

#### *Preparation of tetrabutylammonium perchlorate (TBAP)*

Hot solutions of sodium perchlorate and tetrabutylammonium chloride (Sigma) were mixed and the mixture was cooled in ice. The precipitate formed was filtered, washed with cold ethanol and TBAP was recrystallised from ethanol. TBAP was left in the open to dry overnight and used as an electrolyte in non-aqueous solvents. The yield

was 86%.

## 2.2 Instrumentation

UV/vis spectra were recorded on a Varian 500 UV/visible/NIR spectrophotometer. IR spectra (KBr pellets) were recorded with the Perkin Elmer Spectrum 2000 FTIR spectrometre. Electrochemical data were collected with the BioAnalytical System (BAS) model 100 B/W electrochemical workstation.  $^1\text{H}$ -nuclear magnetic resonance (NMR) spectra were obtained in deuterated DMSO, using the Bruker EMX 400 NMR spectrometer. Triplet state life times and quantum yields were determined at Imperial college (London) using a flash photolysis system. The excitation pulse was provided by a Nd-Yag (in frequency-doubled mode, providing 160 mJ, 8 ns pulses of laser light at 0-10 Hz), pumping a Lambda-Phsik FL2002 dye laser, **Figure 2.1**. Single laser pulse energies used ranged from 0.001 to 2 mJ. A 75 W xenon arc lamp provided the analysing light.

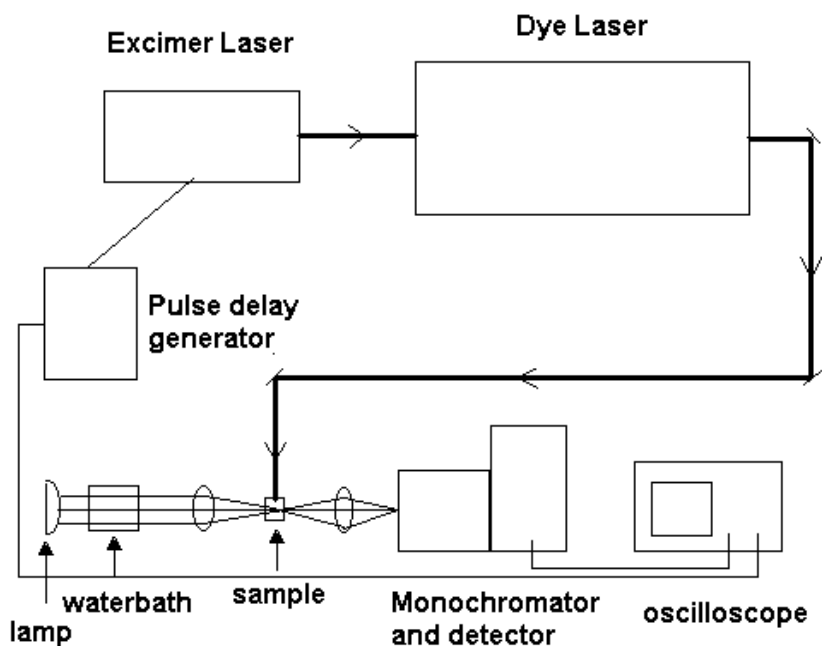


**Figure 2.1:** Set-up for triplet lifetime and quantum yield determinations.

## 2.3 Synthesis

### 2.3.1 Synthesis of 4-nitrophthalonitrile (**24**)

4-Nitrophthalonitrile was synthesized starting with 4-nitrophthalic acid using reported procedures [43,77], as follows:

#### *4-Nitrophthalic anhydride* [77] (**21**, Scheme 2.1)

A mixture of 4-nitrophthalic acid **20** (13,5 g, 54,4 mmol) and acetic anhydride (23 ml) were refluxed for 5 hours. After cooling, the product was filtered, washed with

petroleum ether until all acetic anhydride was removed and air dried to yield 11.6 g of a white crystalline product **21** (93%).

IR (KBr,  $\text{cm}^{-1}$ ):  $\nu = 1736$  and  $1699$  (anhydride),  $1544$  ( $\text{NO}_2$  asym),  $1349$  ( $\text{NO}_2$  sym).

*4-Nitrophthalimide* [77] (**22**, Scheme 2.1)

A suspension of 4-nitrophthalic anhydride **21** (11.6 g, 51.5 mmol) in formamide (15 ml) was refluxed for 3 hours. After cooling, the product was filtered, washed with water and dried at  $60^\circ\text{C}$  to yield 11.0 g of a cream white crystalline product **22** (90%).

IR (KBr,  $\text{cm}^{-1}$ ):  $\nu = 3466$  (N-H),  $1775$  and  $1728$  (imide),  $1550$  ( $\text{NO}_2$  asym),  $1357$  ( $\text{NO}_2$  sym).

*4-Nitrophthalamide* [77] (**23**, Scheme 2.1)

A suspension of 4-nitrophthalimide **22** (11.0 g, 50.9 mmol) in 25%  $\text{NH}_4\text{OH}$  (150 ml) was stirred for 24 hours and then 33%  $\text{NH}_4\text{OH}$  (50 ml) was added and stirring was continued for an additional 24 hours. The product was filtered off, washed with water and dried at  $60^\circ\text{C}$  to yield 8.3 g of a yellow crystalline product **23** (71%).

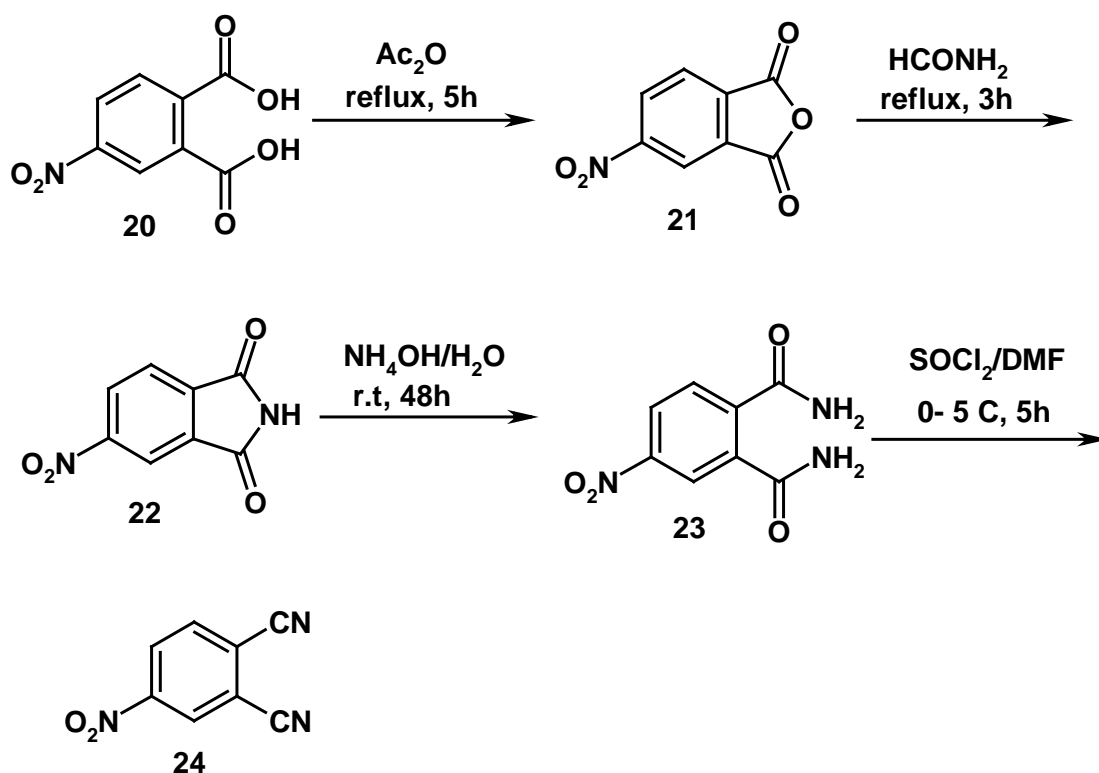
IR (KBr,  $\text{cm}^{-1}$ ):  $\nu = 3420$ ,  $3335$  and  $3252$  (N-H),  $2794$  (C-H),  $1677$  (C=O),  $1551$  ( $\text{NO}_2$  asym),  $1350$  ( $\text{NO}_2$  sym).

*4-Nitrophthalonitrile* [77] (**24**, Scheme 2.1)

Distilled  $\text{SOCl}_2$  (29 ml) was added under stirring and nitrogen to dry dimethylformamide (42 ml) at  $0^\circ\text{C}$ . after 2 hours dry 4,5-dichlorophthalamide **23** (8.3

g, 35.6 mmol) was added and the mixture stirred at 0-5°C for 5 hours and then at room temperature for 24 hours. The product **24** was added to ice water, filtered, washed with water and recrystallised from methanol to yield 4.9 g of a yellow crystalline product (72%).

IR (KBr,  $\text{cm}^{-1}$ ):  $\nu = 3081$  (C-H), 2239 (C $\equiv$ N), 1549 (NO<sub>2</sub> asym), 1349 (NO<sub>2</sub> sym).



**Scheme 2.1:** Synthesis of 4-nitrophthalonitrile (**24**).

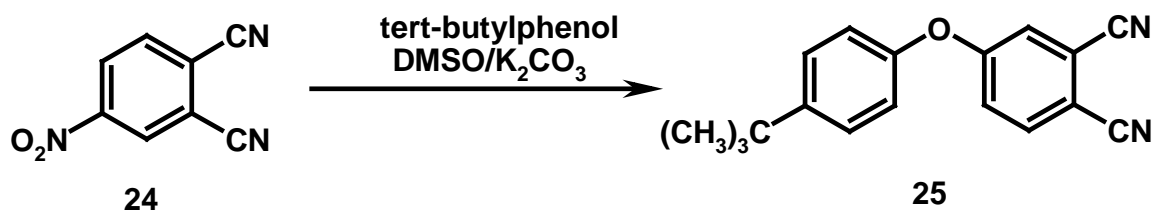
### 2.3.2 Preparation of mono-substituted phthalonitriles

The method was adopted from Wohrle et al. [77] and used for the synthesis of mono-substituted phthalonitriles as follows:

*4-(4-Tert-butylphenoxy)benzene-1,2-dicarbonitrile (25, Scheme 2.2)*

4-*tert*-butylphenol (4.4g, 0.03 mol) and 4-nitrophthalonitrile **24** (3.4g, 0.02 mol) were dissolved in dry DMSO (40 ml) under nitrogen. To this suspension dry potassium carbonate (5.5g, 0.04 mol) was added and the mixture stirred at room temperature. Further aliquots of potassium carbonate were added after 4h and 24h of stirring. After 48h total reaction time the mixture was poured into 1M HCl (200 ml) thereby precipitating a brownish yellow product which was then filtered. The product was recrystallised from acetone to yield light brown crystals of the *tert*-butyl compound **25** (2.3g, 48%).

IR (KBr,  $\text{cm}^{-1}$ ):  $\nu = 3085, 3015, 2238(\text{CN}), 1694, 1634, 1562, 1505, 1488, 1468, 1428, 1385, 1350, 1276(\text{C-O-C}), 1258, 1222, 1165, 1142, 1015, 938, 917$ .



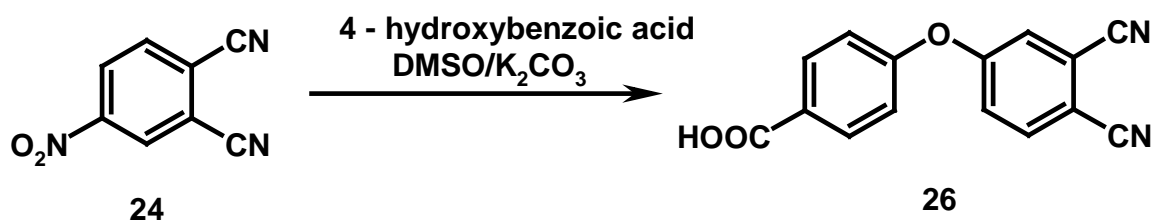
**Scheme 2.2:** Synthesis of 4-(4-*tert*-butylphenoxy)benzene-1,2-dicarbonitrile (**25**).

*4-(4-carboxyphenoxy)benzene-1,2-dicarbonitrile (26, Scheme 2.3)*

Dry potassium carbonate (0.64g, 0.0046 mol) was suspended in dry DMSO (6 ml) under nitrogen. To this suspension 4-hydroxybenzoic acid (0.43g, 0.0031 mol) and 4-nitrophthalonitrile **24** (0.36g, 0.0021 mol) was added. Further aliquots of potassium carbonate were added after 4 hours and 24 hours of stirring at room temperature. The

suspension turned milky yellow and was then stirred at room temperature for a further 5 days under nitrogen atmosphere. The precipitate was dissolved in water (50 ml) and concentrated HCl added to adjust the pH to 1. The filtered product **26** (0.24g, 55%) was recrystallized from methanol. IR spectra showed intense bands corresponding to C=N and C-O-C bond stretches.

IR (KBr,  $\text{cm}^{-1}$ ):  $\nu = 3085, 3015, 2238$  (CN), 1816, 1545, 1547, 1467, 1384, 1350, 1274 (C-O-C), 1258, 1222, 1142, 954, 938, 917, 731, 684, 554, 541, 489, 431.

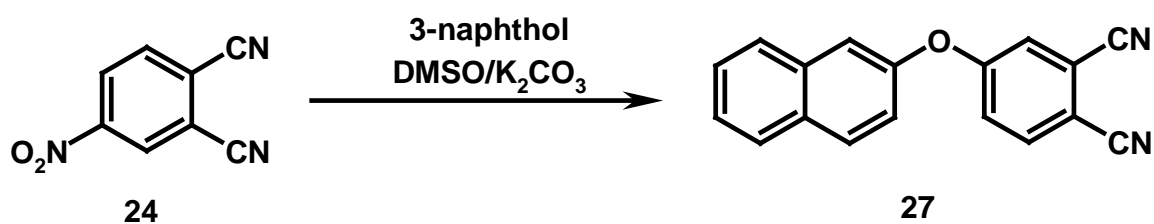


**Scheme 2.3:** Synthesis of 4-(4-carboxyphenoxy)benzene-1,2-dicarbonitrile (**27**).

*Synthesis of 4-(naphthoxy)benzene-1,2-dicarbonitrile (**27**, Scheme 2.4)*

The same method was used for preparing 4-(naphthoxy)benzene-1,2-dicarbonitrile as for the other mono-substituted phthalonitriles (**25** and **26**).

IR (KBr,  $\text{cm}^{-1}$ ):  $\nu = 2238$  (C=N), 1582, 1548, 1390, 1234 (C-O-C), 917, 820, 688, 554, 489, 431.



**Scheme 2.4:** Synthesis of 4-(naphthoxy)benzene-1,2-dicarbonitrile (**27**).

Synthesis of MPc by ring expansion using **27** was however not successful.

**Table 3:** Amounts used for the synthesis of mono-substituted phthalonitriles.

Substituent	Amount of substituent added	Nitrophthalonitrile	Total $K_2CO_3$ added	Total stirring time
<b>4-dihydroxy benzoic acid</b>	0.43 g, 0.0031 mol	0.36g, 0.0021 mol	1.92 g, 0.0138 mol	5 days
<b>4-tert-butylphenol</b>	4.4 g, 0.03 mol	3.4 g, 0.02 mol	16.5 g, 0.12 mol	48 hours
<b>2-naphthol</b>	1.3 g, 0.009 mol	1.0 g, 0.0059 mol	5.4 g, 0.039 mol	5 days

### 2.3.3 Synthesis of 4,5-dichlorophthalonitrile (**32**)

#### 4,5-Dichlorophthalic anhydride [77] (**29**, Scheme 2.5)

A mixture of 4,5-dichlorophthalic acid **28** (13,5 g, 54,4 mmol) and acetic anhydride (23 ml) were refluxed for 5 hours. After cooling, the product was filtered, washed with petroleum ether until all acetic anhydride was removed and air dried to yield 11.6 g of a white crystalline product **29** (93%).

IR (KBr,  $cm^{-1}$ ):  $\nu = 3085$  (C-H), 3022 (C-H), 1828 and 1781 (anhydride).

#### 4,5-Dichlorophthalimide [77] (**30**, Scheme 2.5)

A suspension of 4,5-dichlorophthalic anhydride **29** (11.6 g, 51.5 mmol) in formamide (15 ml) was refluxed for 3 hours. After cooling, the product was filtered, washed with water and dried at 60°C to yield 11.0 g of a cream white crystalline product, **30**.

IR (KBr,  $\text{cm}^{-1}$ ):  $\nu = 3464$  (N-H), 1775 and 1722 (imide) (95%).

*4,5-Dichlorophthalamide* [77] (**31**, Scheme 2.5)

A suspension of 4,5-dichlorophthalimide **30** (11.0 g, 50.9 mmol) in 25%  $\text{NH}_4\text{OH}$  (150 ml) was stirred for 24 hours and then 33%  $\text{NH}_4\text{OH}$  (50 ml) was added and stirring was continued for an additional 24 hours. The product was filtered off, washed with water and dried at 60°C to yield 8.3 g of a yellow crystalline product **31** (71%).

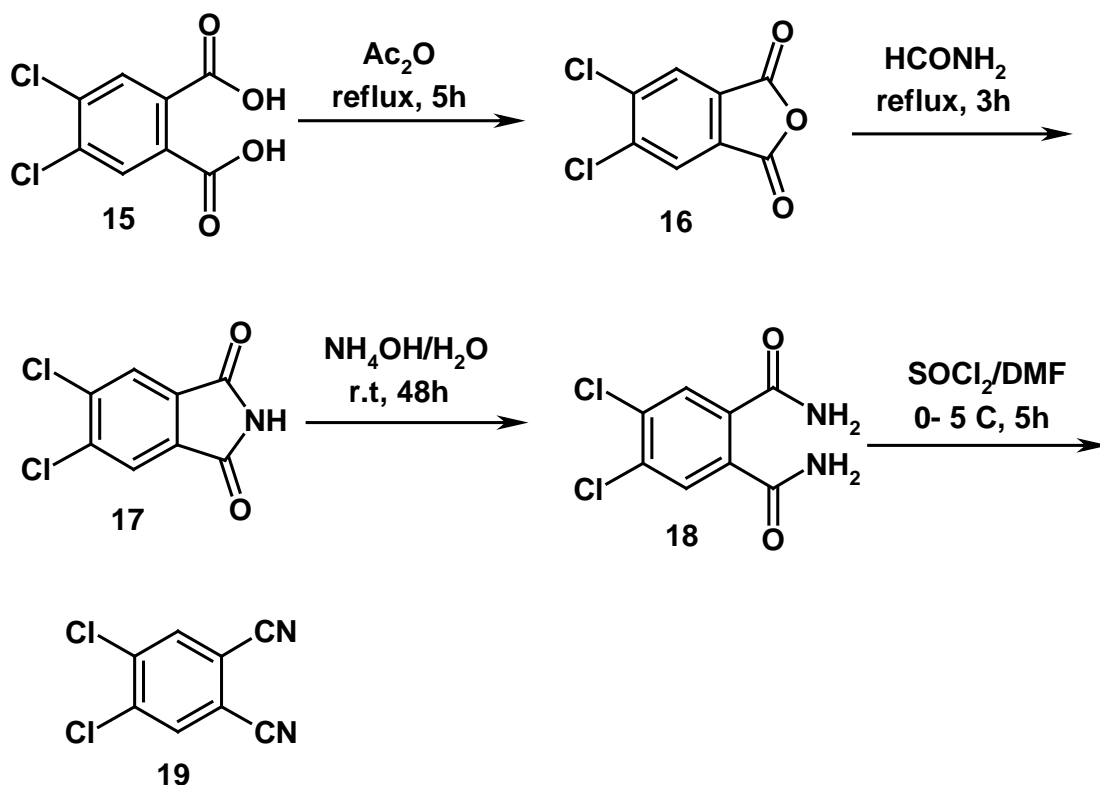
IR (KBr,  $\text{cm}^{-1}$ ):  $\nu = 3420$ , 3305 and 3152 (N-H), 2794 (C-H), 1654 (C=O).

*4,5-Dichlorophthalonitrile* [77] (**32**, Scheme 2.5)

Distilled  $\text{SOCl}_2$  (29 ml) was added under stirring and nitrogen to dry dimethylformamide (42 ml) at 0°C. After 2 hours dry 4,5-dichlorophthalamide **31** (8.3 g, 35.6 mmol) was added and the mixture stirred at 0-5°C for 5 hours and then at room temperature for 24 hours. The product was added to ice water, filtered, washed with water and recrystallised from methanol to yield 4.9 g of a yellow crystalline product, **32** (72%).

IR (KBr,  $\text{cm}^{-1}$ ):  $\nu = 2229$  ( $\text{C}\equiv\text{N}$ ).

$^1\text{H}$  NMR (400 MHz,  $\text{CDCl}_3$ ):  $\delta_{\text{H}} = 7.93$  (s, 2H, CH).



**Scheme 2.5:** Synthesis of dichlorophthalonitrile (**32**).

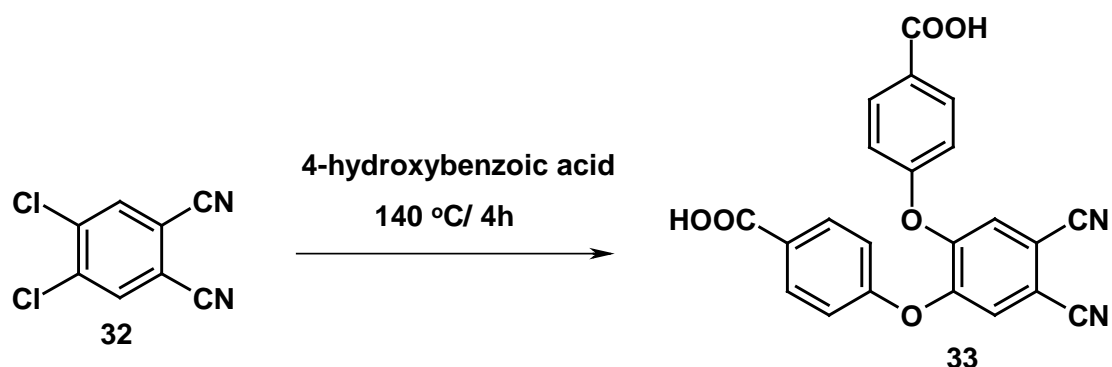
### 2.3.4 Preparation of di-substituted phthalonitriles

#### *4,5-di-(4-carboxyphenoxy)benzene-1,2-dicarbonitrile* [77] (**33**, **Scheme 2.6**)

4,5-dichlorophthalonitrile **32** (0.21g, 0.00021 mol) and 4-hydroxybenzoic acid (0.36g, 0.0021 mol) were dissolved under nitrogen in dry DMSO (0.9 ml). The mixture was heated with stirring at 140 °C. Every 10 minutes, K<sub>2</sub>CO<sub>3</sub> (0.1g, 0.0001 mol) was added in three portions. After 4 hours at 140 °C, water was added to dissolve the precipitate. Then the solution was acidified to pH 1. The solution was concentrated under vacuum until a precipitate was obtained. After cooling, the isolated residue was washed with cold ethanol. The product **33** was obtained in 75% yields.

IR (KBr, cm<sup>-1</sup>):  $\nu = 2229$  (C≡N), 1685 (C=O), 1590, 1498, 1397, 1288, 1212.

$^1\text{H}$  NMR (400 MHz,  $\text{CDCl}_3$ ):  $\delta_{\text{H}}$  = 8.09 (s, 2H, CH), 7.95 (d, 4H, CH-phenoxy), 7.15 (d, 4H-phenoxy).



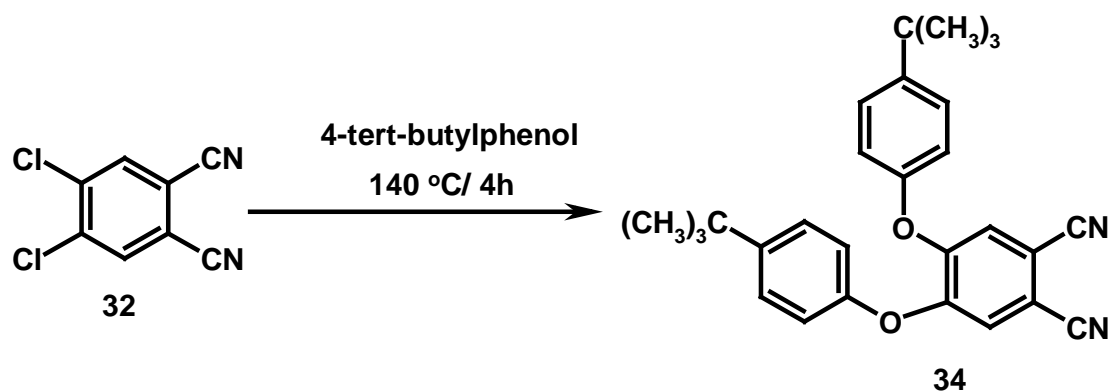
**Scheme 2.6:** Synthesis of 4,5-di-(4-carboxyphenoxy)benzene-1,2-dicarbonitrile (33).

*Preparation of 4,5-di-(4-tert-butylphenoxy)benzene-1,2-dicarbonitrile* [77] (34, Scheme 2.7)

4,5-(4-tert-butylphenoxy)benzene-1,2-dicarbonitrile was prepared using the same method used for synthesizing 4,5-(4-carboxyphenoxy)benzene-1,2-dicarbonitrile and the yield was 68%.

IR (KBr,  $\text{cm}^{-1}$ ):  $\nu$  = 2956, 2870 (C-H), 2223 (C $\equiv$ N), 1581, 1503, 1398, 1295, 1221.

$^1\text{H}$  NMR (400 MHz,  $\text{CDCl}_3$ ):  $\delta_{\text{H}}$  = 7.48 (d, 4H, CH-phenoxy), 7.16 (s, 2H, CH), 7.04 (d, 4H, CH-phenoxy), 1.38 (s, 18H,  $\text{CH}_3$ ).



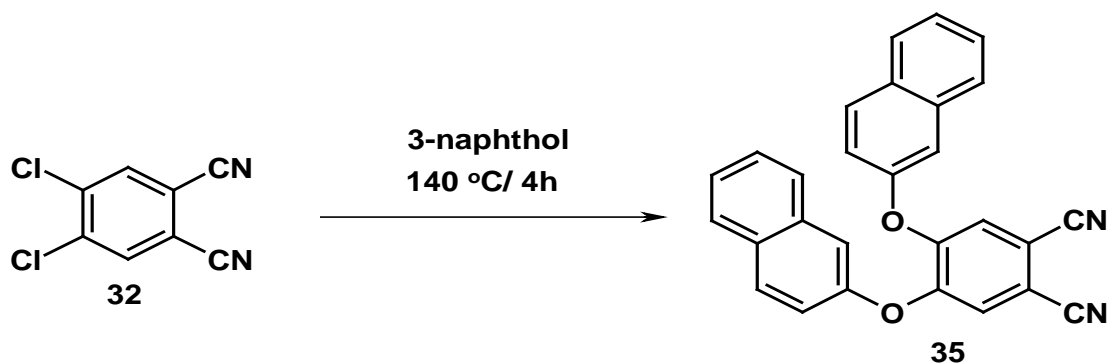
**Scheme 2.7:** Preparation of 4,5-di-(4-tert-butylphenoxy)benzene-1,2-dicarbonitrile (34).

*Preparation of 4,5-di-(3-naphthoxy)benzene-1,2-dicarbonitrile [77] (35, Scheme 2.8)*

4,5-(naphthoxy)benzene-1,2-dicarbonitrile was prepared using the same method used for synthesizing 4,5-(4-tert-butylphenoxy)benzene-1,2-dicarbonitrile and the yield was 52%.

IR (KBr,  $\text{cm}^{-1}$ ):  $\nu = 2952, 2855$  (C-H),  $2224$  ( $\text{C}\equiv\text{N}$ ),  $1595, 1503, 1447, 1295, 1212$ .

$^1\text{H}$  NMR (400 MHz,  $\text{CDCl}_3$ ):  $\delta_{\text{H}} = 7.82$  (m, 4H, CH-naphthoxy),  $7.36$  (m, 6H, CH-naphthoxy),  $7.24$  (d, 4H, CH-naphthoxy).



**Scheme 2.8:** Preparation of 4,5-di-(3-naphthoxy)benzene-1,2-dicarbonitrile (35).

**Table 4:** Amounts used for the synthesis of di-substituted phthalonitriles.

Substituent	Amount of substituent added	4,5-dichloro-dicyanobenzene	Total added	$\text{K}_2\text{CO}_3$	Total stirring time

<b>4-hydroxy benzoic acid</b>	0.21 g, 0.00021 mol	0.36g, 0.0021 mol	1.92 g, 0.0138 mol	4 hours
<b>4-tert-butylphenol</b>	2.2 g, 0.015 mol	1.0 g, 0.005 mol	4.1 g, 0.12 mol	4 hours
<b>3-naphthol</b>	8.6 g, 0.06 mol	2.0 g, 0.0095 mol	8.2 g, 0.24 mol	4 hours

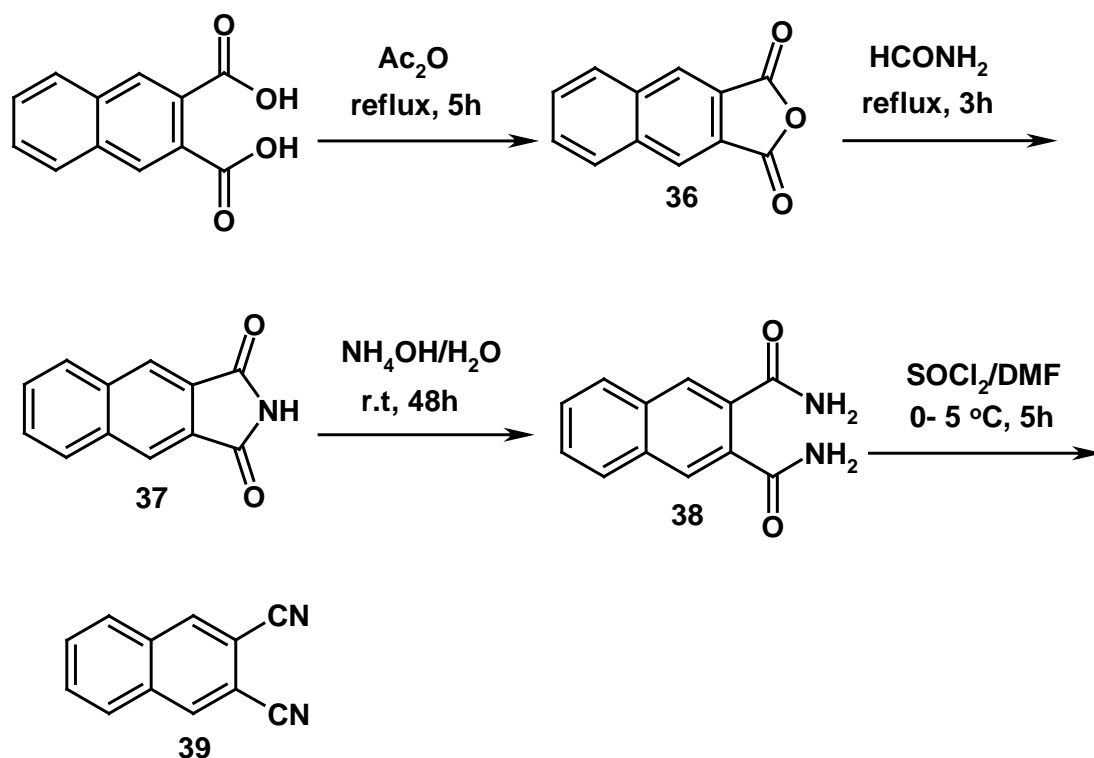
### 2.3.5 Synthesis of dicyanonaphthalene (39, Scheme 2.9).

The same general synthesis procedure as that used for preparing dichlorophthalonitrile, **Scheme 2.5** but starting with dicarboxyphthalic acid, **Scheme 2.9**. The synthesis method was adopted from Worhle et. al [77], but the amounts of reagents were a quarter of those used in **Scheme 2.5**.

#### Compound 36

Yield = 73%

IR (KBr,  $\text{cm}^{-1}$ ):  $\nu = 3037, 1836$  (anhydride),  $1761$  (anhydride),  $1629, 1601, 1514, 1455, 1419, 1367, 1338, 1245, 1278, 1196, 1075, 928, 888, 771, 733, 633, 622, 605, 546, 471$ .



**Scheme 2.9:** Preparation of dicyanonaphthalene (**39**) from dicarboxynaphthalic acid (**35**).

*Compound 37*

Yield = 78%

IR (KBr,  $\text{cm}^{-1}$ ):  $\nu = 3233, 3060, 1769$  (imide),  $1709$ (imide),  $1650, 1514, 1445, 1422, 1320, 1202, 1147, 1110, 1012, 963, 921, 897, 798, 763, 709, 640, 617, 546, 469, 475$ .

*Compound 38*

Yield = 52%

IR (KBr,  $\text{cm}^{-1}$ ):  $\nu = 3347, 3195, 1672$ (amide),  $1614$ (amide),  $1547, 1464, 1400, 1350, 1315, 1126, 952, 910, 897, 838, 812, 778, 747, 638, 602, 477$ .

*Dicyanonaphthalene (39)*

Yield = 55%

IR (KBr,  $\text{cm}^{-1}$ ):  $\nu = 3110, 3050, 2241(\text{nitrile}), 1856, 1743, 1609, 1587, 1480, 1355, 1297, 1214, 1177, 1075, 929, 856, 801, 744, 744, 717, 647, 599, 524, 490, 426.$

$^1\text{H NMR}$  (400 MHz,  $\text{CDCl}_3$ ):  $\delta_{\text{H}} = 7.94$  (d, 2H, CH),  $7.90$  (d, 2H, CH),  $7.23$  (s, 2H, CH).

### 2.3.6 Synthesis of sub-phthalocyanines

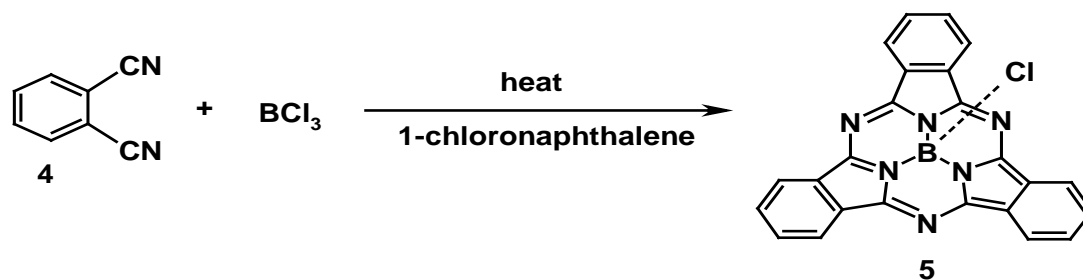
The unsubstituted sub-phthalocyanine (**5**) was synthesized by following reported procedures [25,26,79]. Dicyanobenzene (**3**, 0.4 g, 0.003 mol) was suspended in 1-chloronaphthalene (6 ml), stirred at room temperature in the presence of  $\text{BCl}_3$  (0.12 g, 0.001 mol), and under nitrogen. The reaction mixture was heated to  $220\text{ }^\circ\text{C}$  for 0.5 hours. The product was purified by TLC using toluene: DMF (5:1) to give a purple sub-phthalocyanine (**5**). A schematic representation of the synthesis is given in

#### Scheme 2.10.

Yield = 58%

UV/vis (nm, chloroform):  $\lambda_{\text{max}} = 575, 558, 526, 310, 272.$

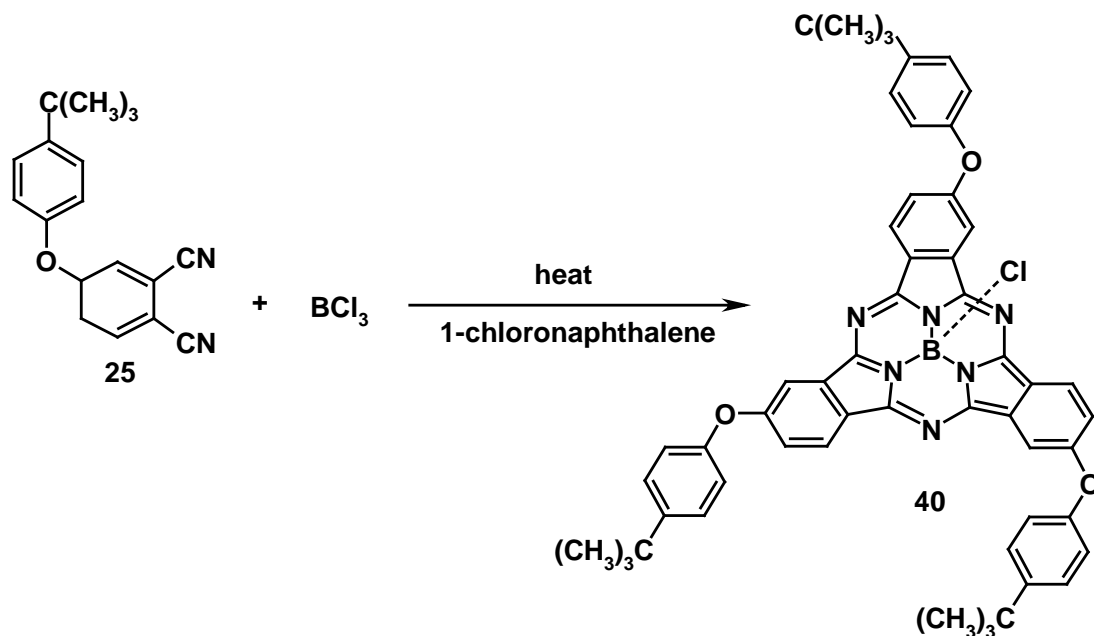
$^1\text{H NMR}$  (400 MHz,  $\text{CDCl}_3$ ):  $\delta_{\text{H}} = 8.9$  (m, 6H, 1,4-Sub-phthalocyanine),  $7.43$  (m, 6H, 2,3-Sub-phthalocyanine).



**Scheme 2.9:** Synthesis of an unsubstituted sub-phthalocyanine (**5**).

### 2.3.7 Preparation of substituted sub-phthalocyanines

Tri-substituted (**40**), **Scheme 2.11** and hexa-substituted (**41**), **Scheme 2.12** tertbutylphenoxy sub-phthalocyanines were synthesized using the same method and same amounts as used for the synthesis of sub-phthalocyanine. Hence mono- (**25**) and di-substituted (**34**) phthalonitriles respectively, were reacted with boron trichloride under nitrogen to give violet products, which were purified by TLC to yield purple to brown products in good yields.



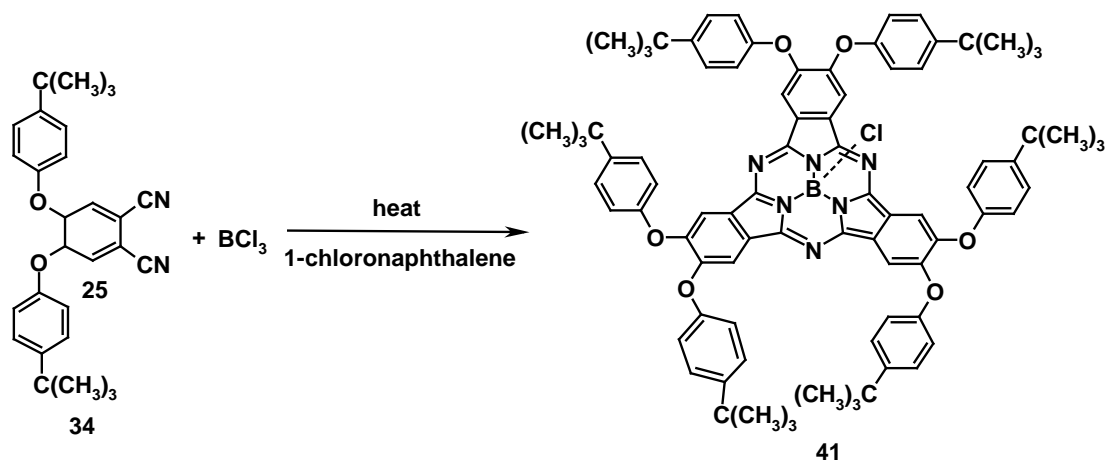
**Scheme 2.11:** Synthesis of tri-(4-*tert*-butylphenoxy) sub-phthalocyanine (**40**).

*Tri-(4-tert-butylphenoxy)sub-phthalocyanine* [25] (**40**, **Scheme 2.11**)

Yield = 42%

UV/vis (nm, chloroform):  $\lambda_{\text{max}} = 545, 542, 495, 315$

$^1\text{H}$  NMR (400 MHz,  $\text{CDCl}_3$ ):  $\delta_{\text{H}} = 8.7\text{-}8.6$  (d, 6H, 1,4-CH-Sub-phthalocyanine), 8.8 (d, 6H, 1',5'-CH-phenoxy), 7.8 (d, 6H, 2',4'-CH-phenoxy), 1.69 (s, 27H,  $\text{CH}_3$ ).



**Scheme 2.12:** Synthesis of hexa-(4-*tert*-butylphenoxy)sub-phthalocyanine (**41**).

*Hexa-(4-tert-butylphenoxy)sub-phthalocyanine* [25] (**41**, **Scheme 2.12**)

Yield = 36%

UV/vis (nm, chloroform):  $\lambda_{\text{max}} = 549, 565, 540, 320$ .

$^1\text{H}$  NMR (400 MHz,  $\text{CDCl}_3$ ):  $\delta_{\text{H}} = 8.12$  (s, 6H, 1,4-Sub-phthalocyanine), 7.88 (d, 12H, 1',5'CH-phenoxy), 7.46 (d, 12H, 2',4'CH-phenoxy), 2.92 (s, 55H,  $\text{CH}_3$ ).

### 2.3.8 Preparation of sub-naphthalocyanine (**42**)

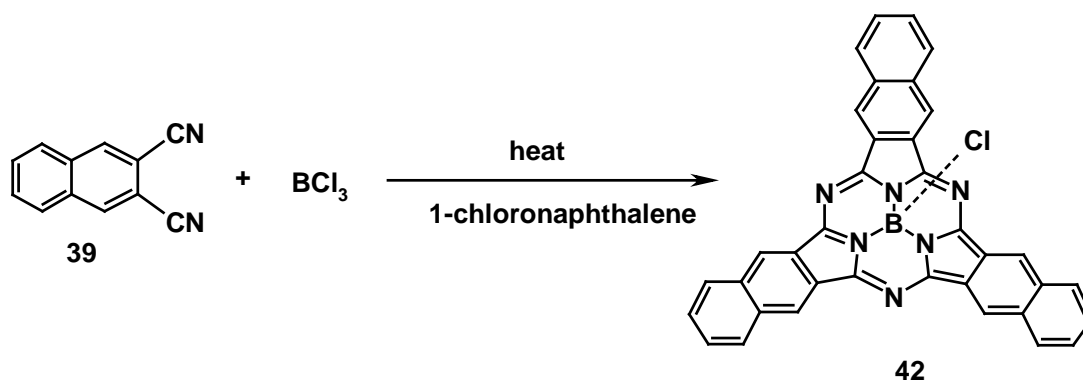
Sub-naphthalocyanine was synthesized from dicyanonaphthalocyanine (**39**) following the procedure already outlined for sub-phthalocyanine, by replacing dicyanophthalonitrile with dicyanonaphthalonitrile, **Scheme 2.13**. Similar ratio of amounts of reagents and reaction times were employed.

Yield = 40%

UV/vis (dichlorobenzene):  $\lambda_{\text{max}}$  (nm) ( $\log \epsilon$ ) = 667 (6.26), 608 (2.06), 328 (2.09), 3.02 (3.62).

IR (KBr,  $\text{cm}^{-1}$ ):  $\nu = 3399, 3183, 3050, 1720, 1440, 1250, 1141, 1100, 796$ .

$^1\text{H}$  NMR (400 MHz, toluene- $d_6$ ):  $\delta_{\text{H}} = 9.4$  (s, 6H, 1,4-H), 8.6 (d, 6H, 6,7-H), 8.1 (d, 6H, 2,3-H).



**Scheme 2.13:** Synthesis of sub-naphthalocyanine (**42**).

### 2.3.9 Synthesis of symmetrically substituted zinc phthalocyanine

*Synthesis of 2,3,9,10,16,17,23,24-octa-(4-tert-butylphenoxy)phthalocyanato zinc (II)*

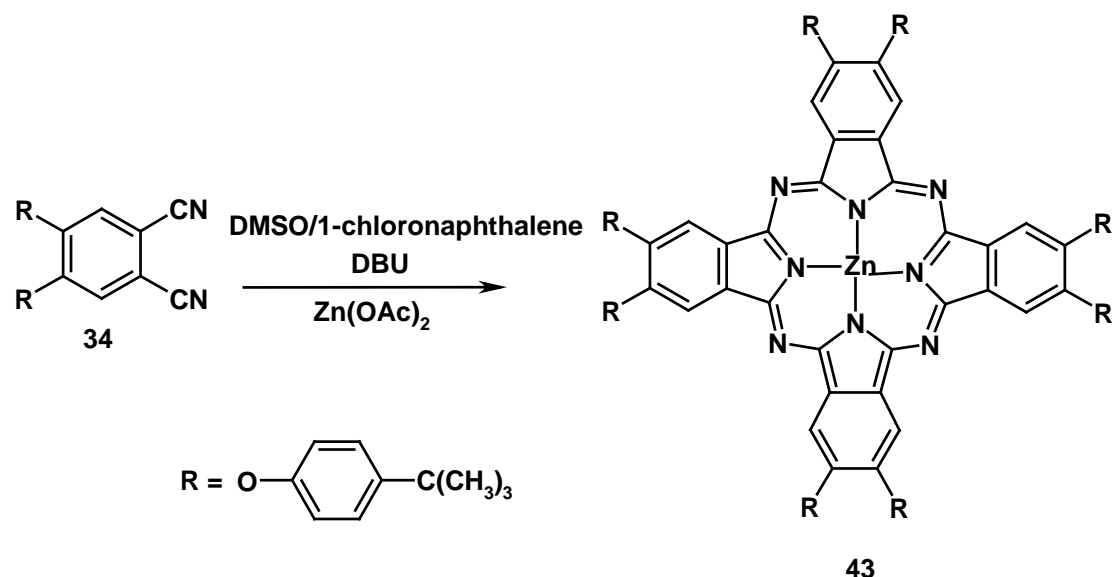
[76] (**43**, **Scheme 2.14**)

4-(4-tert-butylphenoxy)benzene-1,2-dicarbonitrile (**34**, 0.25g, 0.00090 mol) was heated in the presence of a strong base 1,8-diazabicyclo[5.4.0]undec-7-ene (DBU) and zinc (II) acetate dihydrate in a distilled DMSO/1-chloronaphthalene solvent mixture. After cooling methanol was added and the product was separated by centrifugation. The product was washed 5 times with methanol and further purified by thin layer chromatography (TLC) to yield a blue crystalline complex **43** (38%).

$\lambda_{\text{max}}$  (log  $\epsilon$ ): 670 (4.73), 605 (4.20), 335 (4.48) in DMF.

IR (KBr,  $\text{cm}^{-1}$ ):  $\nu = 3057, 2959$  (C-H), 2622, 2560, 2433, 1955, 1719, 1607, 1506, 1484, 1457, 1407, 1331, 1283 (C-O-C), 1244, 1209, 1164, 1114, 1092, 1059, 950, 886, 829, 794, 774, 751, 728, 634, 540, 499, 435.

$^1\text{H NMR}$  [ $\text{d}_6\text{-DMSO}$ , 400Hz]: 9.5 (s, 8H, 1,4-Pc), 7.5 (d, 16H, 1',5'-H), 7.0 (d, 16H, 2',4'-H), 1.2 (s, 72H,  $\text{CH}_3$ ).



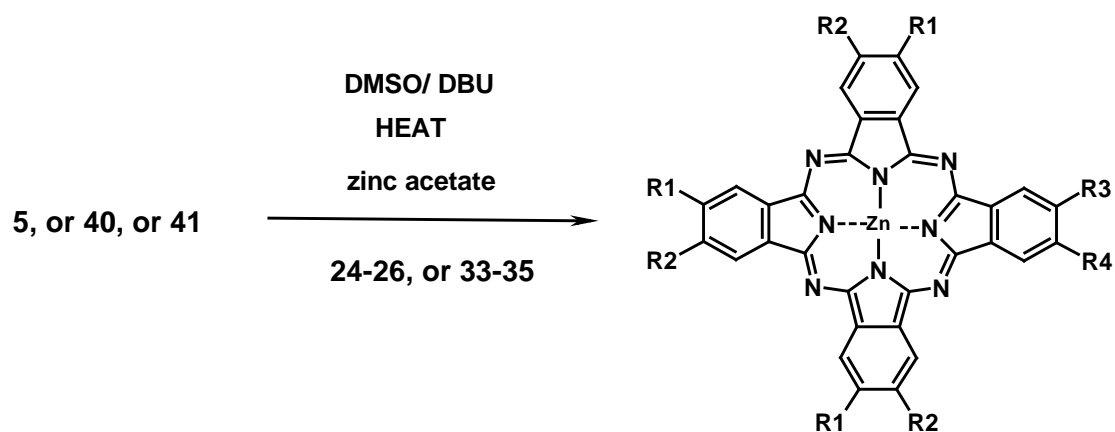
**Scheme 2.14:** Synthesis of 2,3,9,10,16,17,23,24-octa-(*tert*-butylphenoxy)phthalocyanato zinc(II) (**43**).

### 2.3.10 Synthesis of unsymmetrically substituted zinc phthalocyanines (**44-51**), Scheme 2.15 and Figure 2.2)

These complexes were synthesized according to literature methods [78] by dissolving 0.25 g, 0.00092 mol) of the mono- (**25-27**) or di- (**33-35**) substituted dicyanobenzene to be used for ring expansion in a mixture of freshly distilled DMSO/1-chloronaphthalene (4ml/2ml) in the presence of DBU (0.1 g, 0.00065 mol). The reaction mixture was heated to 130  $^{\circ}\text{C}$ , then a suspension of the appropriate substituted (**40**, **41**) or unsubstituted (**5**) sub-phthalocyanine (**5**, 0.2g, 0.00046 mol) and zinc(II) acetate dihydrate (0.11 g, 0.0005 mol) in the DMSO/1-chloronaphthalene solvent mixture was added drop-wise to the heated mixture over a

period of 1 to 4 hours depending on the complex, see section 3.2.1 for discussion. After cooling, glacial acetic acid (0.04g, 0.65 mol) was added and the solvents evaporated. Methanol was added and the respective products were separated by centrifugation. The products were further purified by thin layer chromatography (TLC).

Elemental analysis was obtained for only some complexes. There is difficulty in obtaining reliable elemental analysis due to the presence of a mixture of differently ring substituted isomers.



**Scheme 2.15:** Schematic representation for the synthesis of unsymmetrically substituted ZnPcs.

Not all the combinations were synthesized, see **Figure 2.17** for the complexes synthesized.

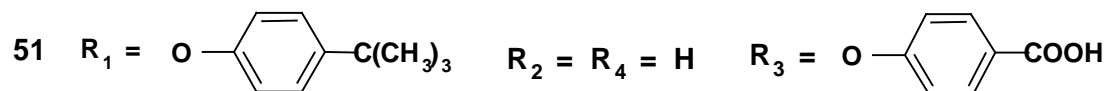
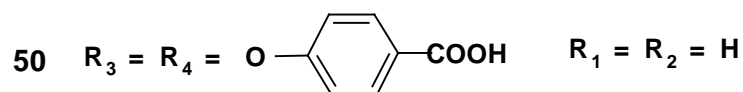
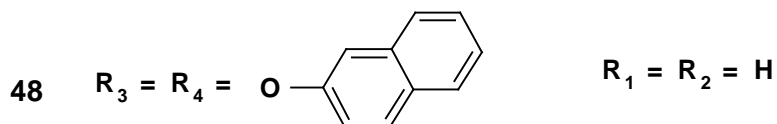
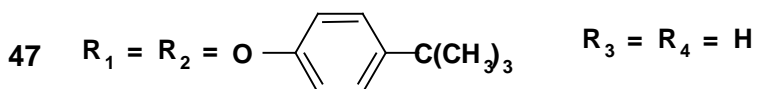
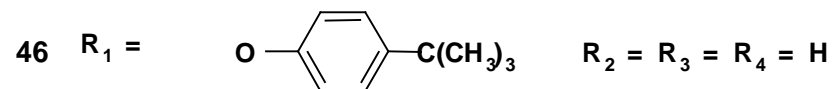
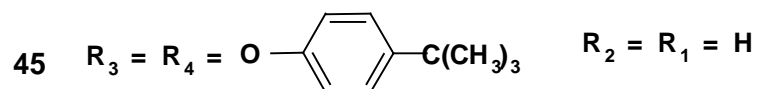
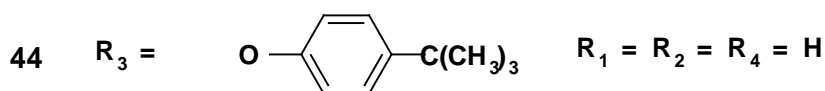
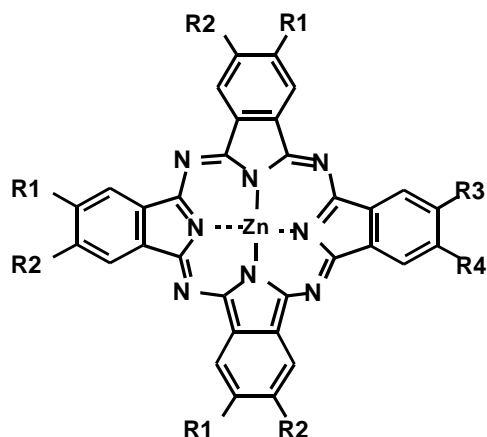


**Figure 2.2:** A representation of zinc phthalocyanine complexes synthesized.

**Table 5** shows the combinations of substituted (**40** or **41**) or unsubstituted sub-phthalocyanines (**5**), with unsubstituted (**4**), mono- (**25**, **26**), or di- (**33-35**) substituted

phthalonitrile used for synthesizing the unsymmetrically ring substituted zinc phthalocyanines.

**Table 5:** Precursor combinations for unsymmetrically zinc phthalocyanines synthesis.

Complex formed	Sub-phthalocyanine	Phthalonitrile for ring expansion
44	5	25
45	5	34
46	40	4
47	41	4
48	5	35
49	5	24
50	5	33
51	40	26

**2-Mono(*tert*-butylphenoxy) phthalocyanato zinc (44):** Yield 35%. Anal: Calcd. For  $C_{42}H_{28}N_8O_1Zn \cdot 6(C_4H_8O_2)$ : C,63.16, H,6.06, N,8.93. Found: C,63.99, H,6.24, N,8.14. IR (KBr),  $\nu/cm^{-1}$ . 3057, 2959, 2622, 2560, 2433, 2230, 1955, 1719, 1607, 1506 (C-H), 1484, 1456, 1407, 1331, 1283 (C-O-C), 1244, 1163, 1114, 1092, 1059, 950, 886, 829, 794, 774, 750, 727, 634, 540, 499, 434.  $^1H$ NMR [d-DMSO, 400Hz]: 8.90(s, 8H, 1,4-Pc), 8.85 (s, 7H, 2,3-Pc), 8.10 (d, 2H, 1',5'-H), 7.40 (d, 2H, 2',4'-H), 1.30 (s, 9H, CH<sub>3</sub>).  $\lambda_{max}/nm$  (log  $\epsilon$ ) in DMF: 675 (5.09), 609 (3.71), 348 (3.96).

**2,3-Bis(*tert*-butylphenoxy) phthalocyanato zinc (45):** Yield 40%. Anal: Calcd. For  $C_{52}H_{40}N_8O_2Zn \cdot 6H_2O$ : C,63.58, H,5.30, N,11.41. Found: C,61.55, H,3.55, N,13.41. IR

(KBr),  $\nu/\text{cm}^{-1}$  : 3403, 2964 (C-H), 1601, 1508 (C-H), 1392, 1247, 1106, 994, 895 (C-O-C), 831, 745, 726, 477.  $^1\text{HNMR}$  [ $\text{CDCl}_3$ , 400Hz]: 8.57-9.40 (14H, 1,4-Pc, 2,3-Pc), 8.21-8.17 (d, 4H, 1',5'-H), 8.12-8.07 (d, 4H, 2',4'-H), 1.82-1.78 (s, 18H,  $\text{CH}_3$ ).  $\lambda_{\text{max}}/\text{nm}$  (log  $\epsilon$ ) in DMF: 678 (4.47), 611 (3.74), 359 (4.00).

**2, 9, 16-Tri(*tert*-butylphenoxy) phthalocyanato zinc (46):** Yield 43%.  $\text{C}_{62}\text{H}_{52}\text{N}_8\text{O}_3\text{Zn}$ . IR (KBr),  $\nu/\text{cm}^{-1}$  : 3385, 2931 (C-H), 1709, 1625, 1485, 1331, 1250 (C-O-C), 1185, 1092, 887, 776, 751, 725, 467.  $^1\text{HNMR}$  [d-DMSO, 400Hz]: 9.48 (s, 8H, 1,4-Pc), 8.55 (m, 2H, 2,3-Pc), 8.10 (m, 3H, 2,3-Pc), 7.60 (d, 6H, 1', 5'-H), 7.30 (d, 6H, 2', 4'-H), 1.3 (s, 27H,  $\text{CH}_3$ ).  $\lambda_{\text{max}}/\text{nm}$  (log  $\epsilon$ ) in DMF: 669 (4.54), 604 (3.82), 335 (4.24).

**2,3,9,10,16,17-Hexa(*tert*-butylphenoxy) phthalocyanato zinc (47):** Yield 30%.  $\text{C}_{92}\text{H}_{88}\text{N}_8\text{O}_6\text{Zn}$ . IR (KBr),  $\nu/\text{cm}^{-1}$ : 2946 (C-H), 1699, 1486, 1409, 1332, 1273 (C-O-C), 1091, 889, 774, 752, 467.  $^1\text{HNMR}$  [d-DMSO, 400Hz]: 9.80 (s, 8H, 1,4-Pc), 8.75 (s, 2H, 2,3-Pc), 8.00 (d, 12H, 1',5'-H), 7.70 (d, 12H, 2',4'-H), 1.3 (s, 55H,  $\text{CH}_3$ ).  $\lambda_{\text{max}}/\text{nm}$  (log  $\epsilon$ ) in DMF: 670 (4.75), 605 (3.91), 342 (4.09).

**2,3-Bis(naphthoxy) phthalocyanato zinc(II) (48):** Yield 20%. Anal: Calcd. For  $\text{C}_{42}\text{H}_{28}\text{N}_8\text{O}_1\text{Zn} \cdot 2(\text{H}_2\text{O})$ : C,69.60, H,3.54, N,12.50. Found: C,68.78, H,2.70, N,14.17. IR (KBr),  $\nu/\text{cm}^{-1}$  : 3054, 2930 (C-H),2859, 2625, 2557, 1954, 1713, 1600, 1484, 1408, 1334, 1285 (C-O-C), 1210, 1165, 1059, 962, 913, 887, 809, 771, 752, 721, 634, 541, 500, 471, 433.  $^1\text{HNMR}$  [d-DMSO, 400Hz]: 9.25 (s, 8H, 1,4-Pc), 8.25 (s, 6H, 2,3-Pc), 8.8-7.5 (m, 16H, naphthoxy).  $\lambda_{\text{max}}/\text{nm}$  (log  $\epsilon$ ) in DMF: 670 (4.97), 605(4.24), 335 (4.69).

**2-Mono-nitro phthalocyanato zinc(II) (49):** Yield 41%. Anal: Calcd. For  $C_{32}H_{15}N_9O_2Zn \cdot 2(C_4H_8O_2)$ : C,60.15, H,3.88, N,15.79. Found: C,59.67, H,3.18, N,16.28. IR (KBr),  $\nu/cm^{-1}$ : 3931, 3332, 1950, 1702, 1652, 1458, 1322 (NO<sub>2</sub>), 1162, 1056, 885, 724, 632, 577, 495, 433. <sup>1</sup>HNMR [d-DMSO, 400Hz]: 9.70 (s, 8H, 1,4-Pc), 8.60 (s, 7H, 2,3-H).  $\lambda_{max}/nm$  (log  $\epsilon$ ) in DMF: 670 (4.00), 605 (3.50), 343 (4.10).

**2,3-Bis(carboxyphenoxy) phthalocyanato zinc(II) (50):** Yield 48%. Anal: Calcd. For  $C_{46}H_{24}N_8O_6Zn \cdot 5H_2O$ : C,54.68, H,3.76, N,11.70. Found: C,59.76, H,3.58, N,11.85. IR (KBr),  $\nu/cm^{-1}$ : 3437, 3050 (OH),1602, 1502, 1403, 1271 (C-O-C), 1213, 1165, 1013, 951, 889, 858, 782, 745, 699, 618, 495, 433. <sup>1</sup>HNMR [d-DMSO, 400Hz]: 9.4-9.6 (s, 8H, 1,4-Pc), 8.35 (d, 6H, 2,3-Pc), 7.95 (d, 4H, 1',5'-H), 7.50 (d, 4H, 2',4'-H), 2H from COOH are not seen as their peak is too weak compared to that of the Pc ring and the phenoxy ring.  $\lambda_{max}/nm$  (log  $\epsilon$ ) in DMF: 671 (6.05), 606 (4.32), 354 (3.71), 284 4.54).

**2,9,16-Tri(tert-butylphenoxy)-23-mono(carboxyphenoxy) phthalocyanato zinc(II) (51):** Yield 20%. Anal: Calcd. For  $C_{42}H_{28}N_8O_1Zn \cdot 2(H_2O)$ : C,66.19, H,4.20, N,14.71. Found: C,66.54, H,4.21, N,6.36. IR (KBr),  $\nu/cm^{-1}$ : 3057, 2946 (C-H), 1716, 1658, 1597, 1499, 1454, 1270 (C-O-C), 1218, 1162, 1107, 1015, 883, 759, 690, 619, 486. <sup>1</sup>HNMR [d-DMSO, 400Hz]: 9.40 (s, 8H, 1,4-Pc), 9.00 (s, 4H, 2,3-Pc), 7.56 (d, 8H, 2',4'-H), 7.42 (d, 8H, 1',5,-H), 1.28 (t, 27H, CH<sub>3</sub>).  $\lambda_{max}/nm$  (log  $\epsilon$ ) in DMF: 682 (4.97), 614 (4.24), 346 (4.69).

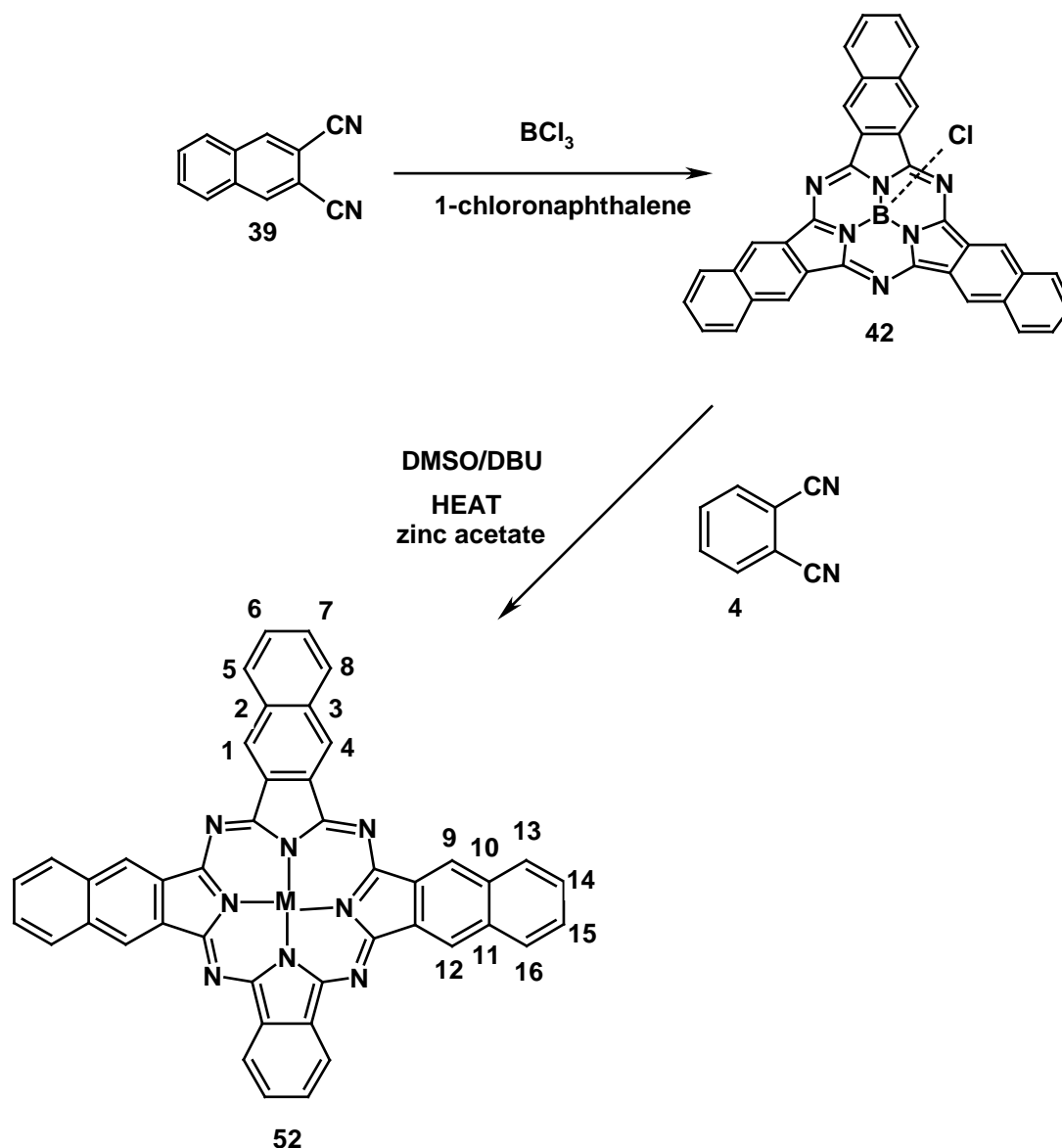
*Synthesis of 2,3-tribenzo phthalocyanato zinc (II) (52, Scheme 2.16)*

Complex (**52**) was synthesized using the same methods used for preparing unsymmetrically ring substituted zinc phthalocyanines. (0.25 g, 0.00092 mol) phthalonitrile (**4**) was stirred in DMSO/1-chloronaphthalene (4ml/2ml) solvent mixture in the presence of DBU (0.1 g, 0.00065 mol). A mixture of sub-naphthalocyanine (**42**, 0.2g, 0.00046 mol) and zinc(II) acetate dihydrate (0.11 g, 0.0005 mol) in the DMSO/1-chloronaphthalene solvent mixture was added drop-wise to the phthalonitrile mixture over a period of 1 hour. After cooling, glacial acetic acid (0.04g, 0.65 mol) was added and the solvents evaporated. Methanol was added and the product was separated by centrifugation. The product (**52**) was further purified by thin layer chromatography (TLC) to give a green product with yield 38%.

$\lambda_{\text{max}}$  (log  $\epsilon$ ): 672 (4.76), 607 (4.07), 344 (4.69) in DMF.

IR (KBr,  $\text{cm}^{-1}$ ):  $\nu = 3389, 3180, 3057$  (C-H), 1720, 1440, 1256, 1009, 797, 752, 615, 468.

$^1\text{H NMR}$  [d-DMSO, 400Hz]: 9.45 (d, 8H, 1,4-Pc), 8.30 (d, 6H,  $\alpha$ -Pc), 7.9 (d, 6H,  $\beta$ -H), 7.8 (d, 2H, 2,3-Pc).



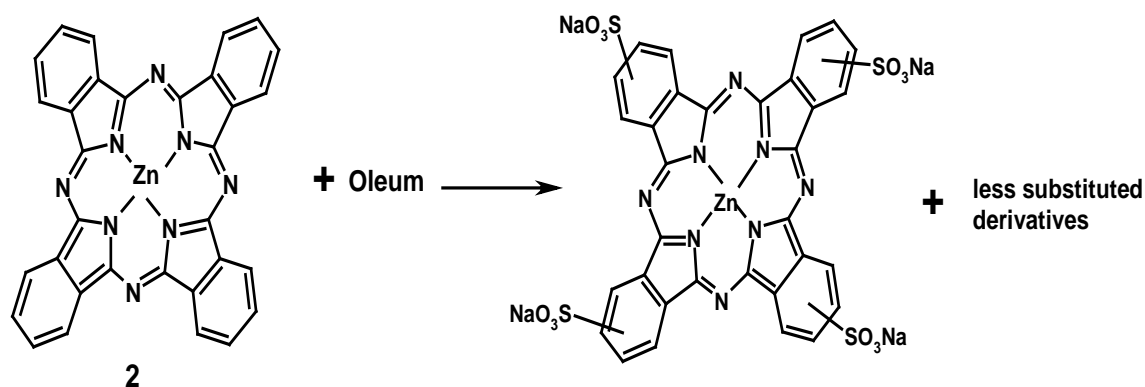
**Scheme 2.16:** Synthesis of tri-benzophthalocyanato zinc (II) (52) by ring expansion of sub-naphthalocyanine.

### 2.3.11 Synthesis of zinc sulphophthalocyanine [16] (Scheme 2.17), $\text{ZnPcS}_n$

The synthesis of zinc sulphophthalocyanine was adopted from Ambroz *et al.* [16].  $\text{ZnPc}$  (0.25g) was heated and stirred to  $100^\circ\text{C}$ , oleum (1.25 ml containing 20%  $\text{SO}_3^-$ ) was added and the mixture was stirred and maintained at  $100^\circ\text{C}$  for 25 minutes. The mixture was quenched by pouring onto 10 g crushed ice. The resulting mixture was

adjusted to pH 7.0 – 7.9 by adding aqueous sodium hydroxide to give a deep blue solution. The solvent was evaporated and the resulting solid was dissolved in water containing sodium hydroxide (0.1 M). HCl (0.1 M) was then added to precipitate the salt of zinc sulphophthalocyanine. The synthesis is illustrated on **Scheme 2.17**. The sodium salt was used as it is without further purification. The spectrum shows that the solid contains a mixture of monomers and dimers.

UV/vis (KBr,  $\text{cm}^{-1}$ ):  $\lambda_{\text{max}}$  (nm) = 335, 630, 668 in water.



**Scheme 2.17:** Schematic representation of zinc sulphophthalocyanine ( $\text{ZnPcS}_n$ ) synthesis where  $n$  represents the number of  $\text{SO}_3^-$  groups on the ring, ranging between 1 and 4.

#### *Synthesis of axially ligated $\text{ZnPcS}_n$ (Scheme 2.18)*

An aqueous solutions of  $\text{ZnPcS}_n$  ( $1 \times 10^{-6}$  to  $1 \times 10^{-3}$  mol  $\text{dm}^{-3}$ ) was refluxed in the presence of (0.25 g) an excess of the ligand (pyridine, bipyridine or aminopyridyl). The mixture was refluxed at  $85^\circ\text{C}$  for 10 minutes, to give axially ligated complexes, which were stable only in solution.

(pyridine) zinc sulphophthalocyanine (pyr)ZnPcS<sub>n</sub>) (**a**)

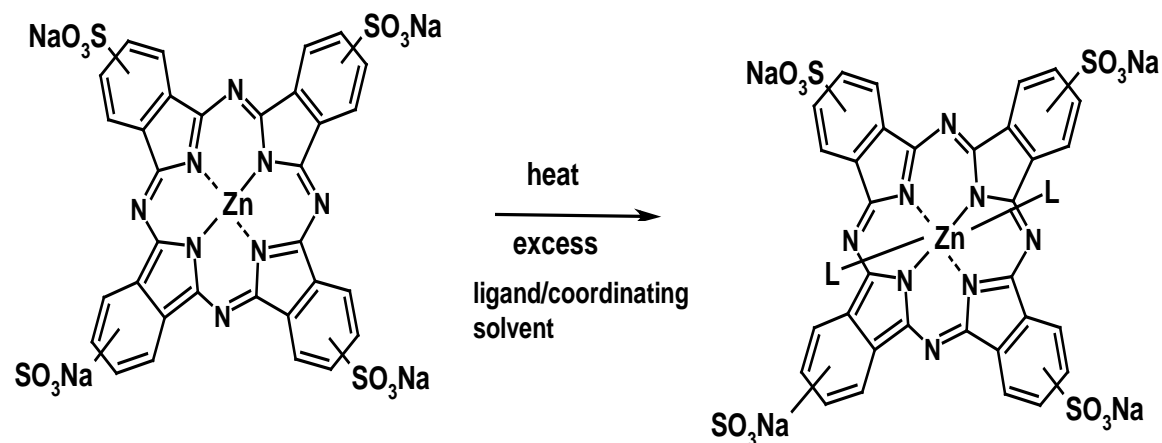
UV/vis (pH 7.4):  $\lambda_{\max}$  (nm) = 674, 629, 335.

(bipyridine) zinc sulphophthalocyanine (bipyr)ZnPcS<sub>n</sub>) (**b**)

UV/vis (pH 7.4):  $\lambda_{\max}$  (nm) = 674, 607, 335.

(aminopyridyl) zinc sulphophthalocyanine (aminopyr)ZnPcS<sub>n</sub>) (**c**)

UV/vis (pH 7.4):  $\lambda_{\max}$  (nm) = 674, 630, 335.



**Scheme 2.18:** Schematic representation of axially ligated ZnPcSn synthesis. Where

(**a**) L = pyridine (pyr), (**b**) L = Bipyridyl (bipyr), (**c**) L = Aminopyridyl (aminopyr). Only one ligand was confirmed (see **Table 13**) to be coordinated.

## 2.4 Photochemical and photophysical methods

Both photobleaching and singlet oxygen quantum yields were determined for the ZnPc derivatives.  $\Phi_T$ ,  $\tau_T$  and  $\tau_f$  were determined for a selected number of complexes. The later studies were done in Imperial College (London). For photobleaching and  $\Phi_\Delta$  studies, the photochemical experiments were carried out in a spectrophotometric cell of 1 cm pathlength. A 2 ml solution in DMF of the ZnPc derivatives in the presence or absence of DPBF was introduced to the cell and photolysed in the Q-band region of the dye, with an Electric Quartz line lamp (300W) in the presence of air. A 600 nm glass cut off filter (Schott) and a water bath filter were used to filter off ultraviolet light and far infrared radiation. An interference filter (Intor, 670 nm with band width of 20 nm) was placed in the light path before the sample, illustrated in **Figure 2.3**. The wavelength of the interference filter was chosen so that it could be close to that of the

MPCs.

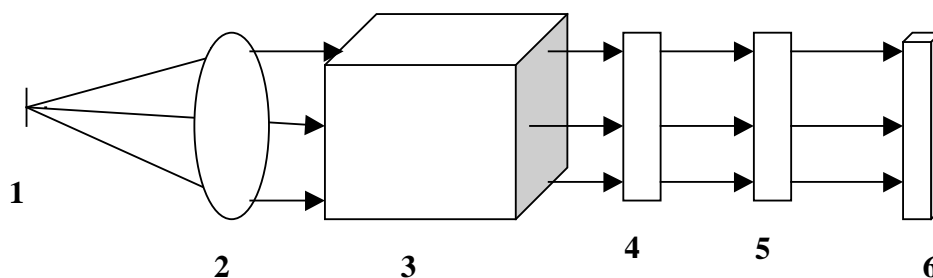


**Figure 2.3:** Photolysis set-up, where 1. light source, 2. Lens, 3. IR filter, 4. Filter, 5. Interference filter, 6. sample with/ without DPBF.

The fraction of light absorbed was calculated using equation 17 (Section 1.4.1).

$$\alpha = \frac{\sum T_{\text{filter}} (1 - T_{\text{dye}})}{\sum T_{\text{filter}}} \quad \dots 17$$

where  $\alpha$  is the fraction of the overlap integral of light for use in equation 15 and 16, section 1.4.1,  $T_{\text{filter}}$  is the transmittance of the filter and  $T_{\text{dye}}$  the transmittance of the dye (MPc). An example of the computation is shown in **Table 6**, where 0.87, 0.90 and 0.54 are the transmittance ( $T_{\text{dye}}$ ) of the dye at 640 nm, 650 and 660 nm, respectively. 0.0331, 0.238 and 0.857 are the transmittance ( $T_{\text{filter}}$ ) of the interference filter at 640, 650 and 660 nm, respectively.

**Table 6:** An illustration of the computation of  $\alpha$  coefficient.

$\lambda$ (nm)	$T_{\text{dye}}$	$1 - T_{\text{dye}}$	$T_{\text{filter}}$	$T_{\text{filter}}(1 - T_{\text{dye}})$
640	0.13	0.87	0.033	0.03
650	0.10	0.90	0.24	0.21
660	0.43	0.54	0.86	0.49
			$\Sigma T_{\text{filter}}$	$\Sigma T_{\text{filter}}(1 - T_{\text{filter}})$

From the information obtained from table,  $\alpha$  can be calculated using equation 17 (Section 1.4.1).

An ideal overlap give  $\alpha$  which has values between 0.3 and 0.9.  $\alpha$  was calculated for all solutions and then used in equation 16, Section 1.4.1 to give quantum yields of singlet oxygen.

The light intensity was measured with a power meter and was found to be  $1.5 \times 10^{17}$  photons  $\text{s}^{-1} \text{cm}^{-2}$ . The value was obtained using equation 30:

$$\Delta E = \frac{hc}{\lambda} \quad \dots 30$$

where  $h$  is Plank's constant and  $c$  the speed of light. This equation can be used to calculate the energy of light at any wavelength. Inserting the known values for  $h$  and  $c$ , results in equation 31:

$$\text{Energy at } \lambda = \frac{1.194 \times 10^5 \text{ kJ mol}^{-1}}{\lambda(\text{nm})} \quad \dots 31$$

where  $\lambda$  is the wavelength of the filter.

Singlet oxygen quantum yields were determined by irradiating a DMF solution containing the ZnPc complex with absorbance of  $\sim 1$  and DPBF ( $2 \times 10^{-3} \text{ mol. dm}^{-3}$ ), using the photolysis set-up in **Figure 2.3**. For each solution of ZnPc complex, the decrease in the concentration of DPBF was followed as a function of irradiation time by monitoring the decay of DPBF's absorbance at 417 nm.

DABCO (diazabicyclo-(2,2,2)-octane) ( $2 \times 10^{-3} \text{ mol. dm}^{-3}$ ) was used as a singlet oxygen scavenger for photobleaching studies. Photobleaching quantum yields give a measure of the photostability of the ZnPc complexes. Experiments were also performed whereby the solutions were deaerated with  $\text{N}_2$  gas or saturated with  $\text{O}_2$  in order to study the role of oxygen in the photodegradation process.

Triplet state life times and quantum yields were determined using a flash photolysis system, described in Section 2.2. Triplet state quantum yields ( $\Phi_T$ ) were calculated using a comparative method with ZnPc as a standard ( $\Phi_T \text{ ZnPc} = 0.25$ ) [69].

## 2.5 Electrochemical methods

### *Cyclic and square wave voltammetries*

For the determination of redox potentials for MPcs, a three electrode cell was employed. DMF containing  $\sim 0.5 \text{ mol. dm}^{-3}$  TBAP was used as the electrolyte. Concentration of ZnPc complexes were of the order of  $10^{-4} \text{ mol. dm}^{-3}$ . A platinum disk (3.0 mm diameter) was used as a working electrode; platinum wire auxiliary and Ag wire pseudo-reference were employed. Nitrogen was bubbled through the solution for about 15 minutes before running the cyclic or square wave voltammogram, and  $\text{N}_2$  atmosphere was maintained through voltammogram scans. The ferrocenium/ferrocene ( $\text{fc}^+/\text{fc}$ ) couple was employed as an internal standard, and potentials were referenced versus standard calomel electrode (SCE) using the reported potential of 0.46 V (vs SCE) for the  $\text{fc}^+/\text{fc}$  couple in DMF [79,80]. Prior to cyclic voltammetry scans, the platinum working electrode was polished with alumina ( $< 10 \text{ }\mu\text{m}$ ) on a Buehler felt pad, followed by washing with deionised water and rinsing with methanol and DMF.

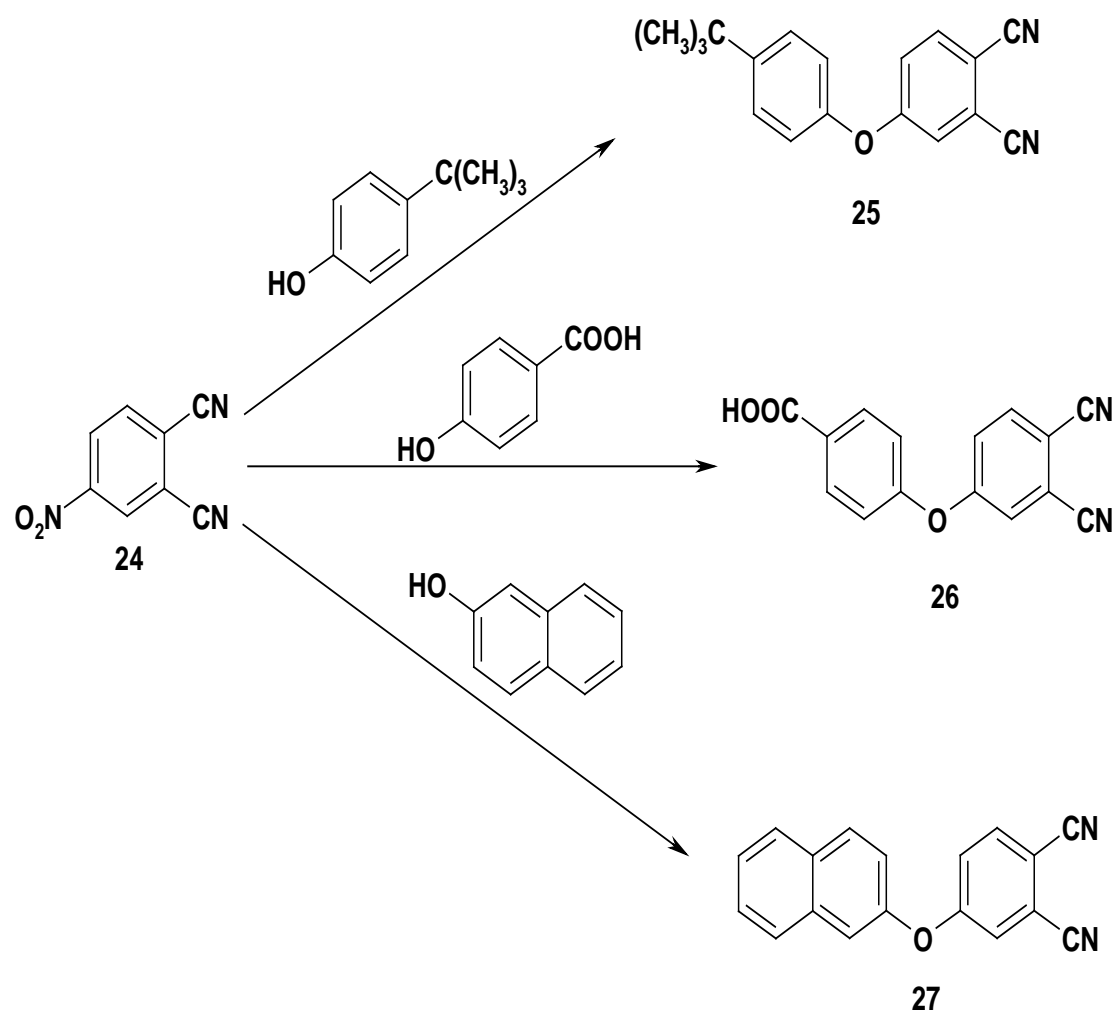
### 3. RESULTS AND DISCUSSION

#### 3.1 Characterization of phthalocyanine precursors

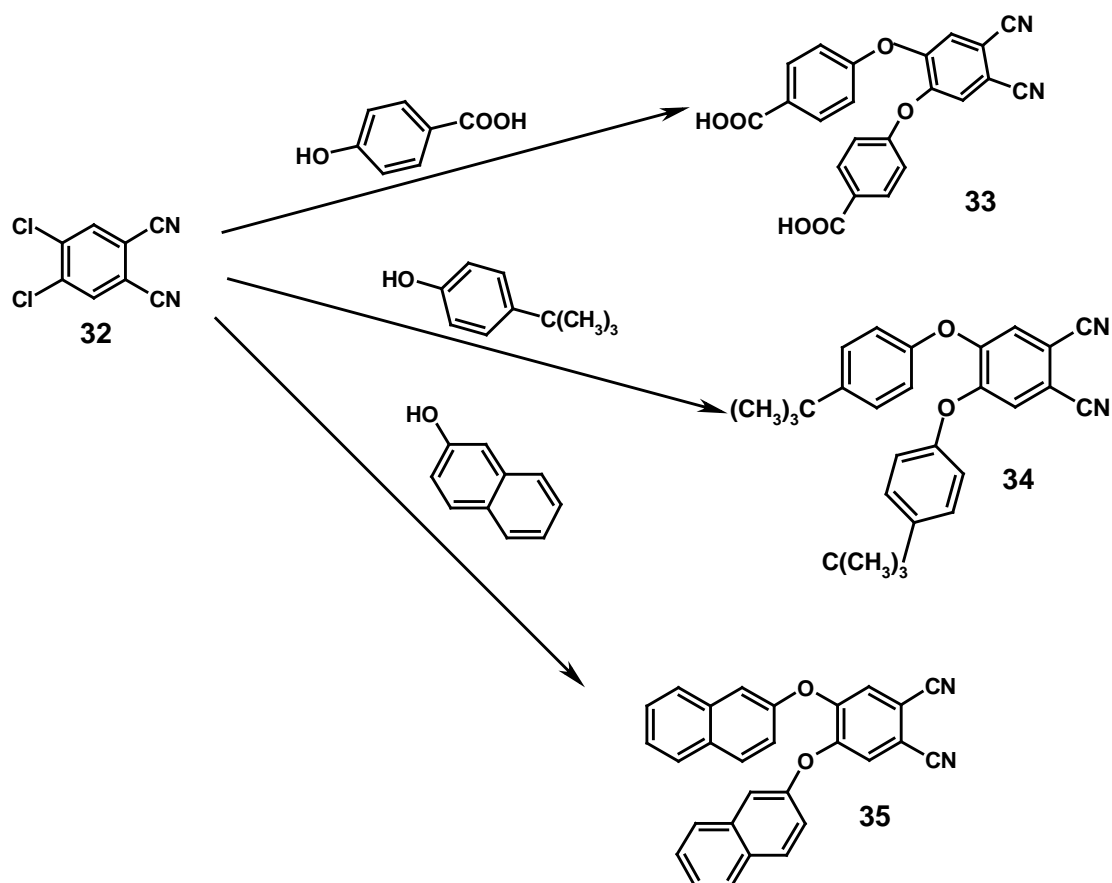
##### 3.1.1 Substituted phthalonitrile derivatization

All substituted phthalonitriles needed for this project were derived from either 4-nitrophthalonitrile or dichlorophthalonitrile. The synthesis is straightforward and can be used for synthesizing phthalonitriles with a variety of substituents. The synthetic method is known and the phthalonitriles were obtained in good yields. The reactions for nitro displacement by phenols are generally very slow. The reactions between 4-nitrophthalonitrile (**24**) and 4-*tert*-butylphenol was completed after 2 days, while the reaction of **24** with 4-hydroxy benzoic acid and 2-naphthol took 5 days.  $K_2CO_3$  was used as a base because it abstracts a proton from the -OH on the 4-hydroxybenzoic acid, 4-*tert*-butylphenol and 2-naphthol to make them nucleophiles, which then attack the 4-nitrophthalonitrile and dichlorophthalonitrile at positions 4 or 4 and 5, respectively, thus making the reaction a nucleophilic reaction. This happens at positions 4 and 5 for dichlorophthalonitriles because the Cl is a good leaving group [81]. The monosubstituted phthalonitriles: 4-(4-*tert*-butylphenoxy)benzene-1,2-dicarbonitrile (**25**), 4-carboxyphenoxy benzene-1,2-dicarbonitrile (**26**) and 4-naphthoxybenzene-1,2-dicarbonitrile (**27**) were obtained in good yields of more than 60%.

Summary of the synthesis is shown by **Scheme 3.1**. Three of the di-substituted phthalonitrile were synthesized, namely 4,5-di-(4-carboxyphenoxy)benzene-1,2-dicarbonitrile (**33**), 4,5-di-(4-tert-butylphenoxy)benzene-1,2-dicarbonitrile (**34**) and 4,5-di-(4-naphthoxy)benzene-1,2-dicarbonitrile (**35**). Summary of synthesis of di-substituted phthalonitriles is shown by **Scheme 3.2**.



**Scheme 3.1:** Summary of synthesis of monophenoxy substituted phthalonitriles.



**Scheme 3.2:** Summary of synthesis of di-phenoxy substituted phthalonitriles.

The IR spectra of all the substituted phthalonitriles showed a strong band between 2228 and 2240  $\text{cm}^{-1}$ . The frequency of these bands is characteristic of a  $\text{-C=N}$  stretch [82]. Strong bands are also found in the 1220 – 1350  $\text{cm}^{-1}$  range for all the phthalonitriles and these bands are attributed to the  $\text{C-O-C}$  bond stretches of mono and di-substituted phenoxy phthalonitriles.

Naphthalonitrile was synthesized from naphthalimide using the same method used for synthesizing 4-nitrophthalonitrile and dichlorophthalonitrile. Naphthalonitrile was obtained as a yellow compound in 46% yield.

### 3.1.2 Sub-phthalocyanine

Substituted or unsubstituted sub-phthalocyanines were prepared by the method described by Kliesch *et al.* [43] by reacting substituted or unsubstituted phthalonitrile with boron trichloride to yield a violet mixture which was purified by TLC, to give a brown sub-phthalocyanine in good yields. Tri-substituted sub-phthalocyanines were prepared using mono-substituted phthalonitriles and boron trichloride. Hexa-substituted sub-phthalocyanines were prepared from di-substituted phthalonitriles. All sub-phthalocyanines were obtained in good yields. The sub-phthalocyanines have an absorption spectrum with Q-bands between 579 and 547 nm, **Figure 3.1**.

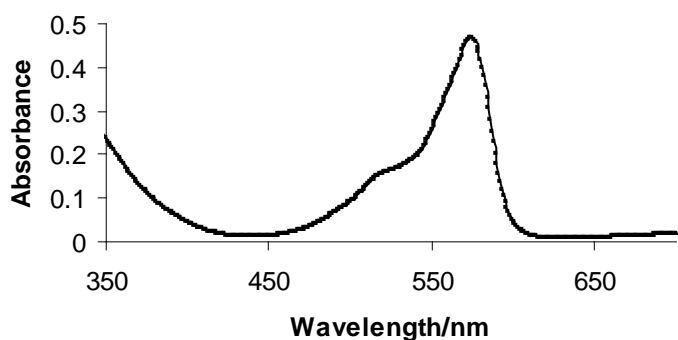


**Figure 3.1:** Electronic absorption spectra of an unsubstituted sub-phthalocyanine.

Concentration  $1 \times 10^{-5} \text{ mol dm}^{-3}$ .

## 3.2 Characterization of zinc phthalocyanine derivatives

### 3.2.1 Synthesis

Several researchers have reported on the synthesis of phthalocyanines from substituted and unsubstituted sub-phthalocyanines [22,25,51,83,84]. The sub-phthalocyanines complexes have been employed as starting materials for the

formation of unsymmetrically substituted MPc complexes by ring expansion using substituted and unsubstituted phthalonitriles. The use of sub-phthalocyanines as intermediates for the synthesis of unsymmetrically substituted phthalocyanines has gained popularity over statistical condensation of two differently substituted phthalocyanine derivatives. The later results in a complex mixture of products. However, using the reaction mixture containing phthalonitriles and boron trihalide, gives ring-halogenated sub-phthalocyanines, in addition to the desired products. Halogenated sub-phthalocyanines are difficult to separate. The sub-phthalocyanines complexes were used to prepare the unsymmetrically substituted zinc phthalocyanines according to **Scheme 2.15**, depicted in the experimental section (Section 2.3.10). The product mixture will inevitably contain halogenated Pc derivatives and the desired products were separated using thin layer chromatography (TLC).

The ZnPc derivatives (**44**, **49**) were synthesised using unsubstituted sub-phthalocyanine and ring expansion using dicyanobenzene: which was mono-substituted with tert-butylphenol (for **44**), or nitro (for **49**). For (**45**, **48** and **50**) dicyanobenzene was di-substituted with tert-butylphenol (for **45**), naphthol (for **48**) or hydroxybenzoic acid (**50**). Complexes **46**, and **51** were synthesized using sub-phthalocyanines substituted with three tert-butylphenol groups and ring expanding with unsubstituted dicyanobenzene (for **46**), or dicyanobenzene substituted with hydroxybenzoic acid (for **51**). Complex **47** was synthesized using sub-phthalocyanines substituted with six tert-butylphenol groups and ring expanding with unsubstituted dicyanobenzene (**4**). Complex **52** was synthesized from sub-naphthalocyanine (**42**) and ring expanding with dicyanobenzene. In all cases an excess of the dicyanobenzene was employed as is typical for these kinds of reactions

[51,84]. The complexes gave satisfactory spectroscopic analyses. The formation of the ZnPc derivatives was monitored using UV/vis spectroscopy, **Figure 3.2**. An expected decrease in the absorption band of the Sub-phthalocyanine in the 540 nm region and the simultaneous formation of the Q and B bands of the phthalocyanine was observed. The reaction was complete within 1 hour for complex **44** and for the other reactions the reaction time varied between 2-4 hours depending on the substituents on the phthalonitriles used for ring expansion of the sub-phthalocyanines. Much longer reaction times have been reported for these types of reactions [51].

Yields of the ZnPc derivatives were comparable or higher than those reported in the literature for the synthesis of Pcs and sub-phthalocyanines [51]. The complexes were soluble in DMF or DMSO to a varying degree. Complexes **44-48** and **51** were soluble in chloroform.

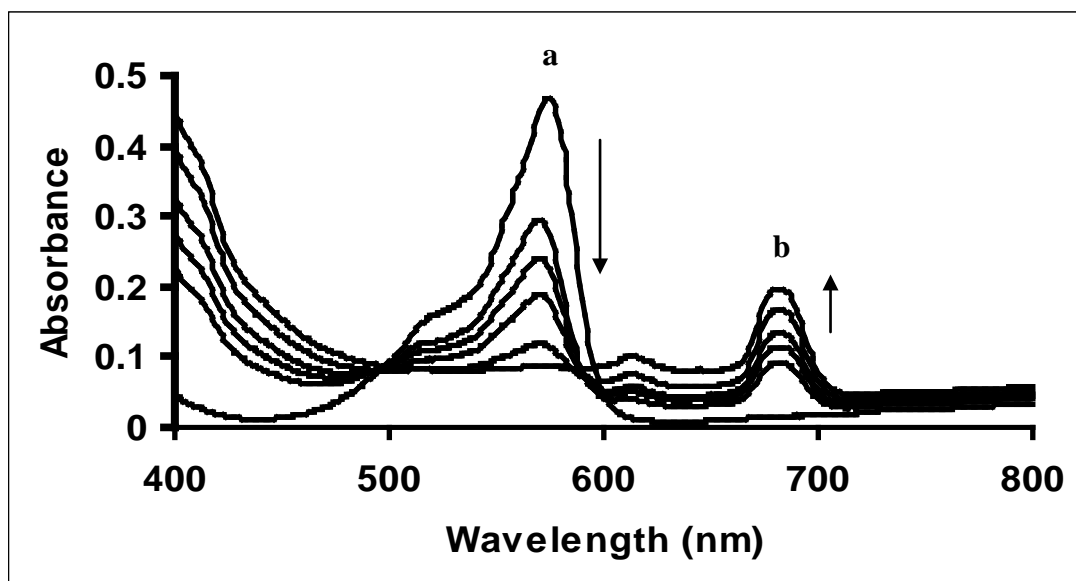


**Figure 3.2:** Changes in the UV/vis spectra observed during the formation of a ZnPc derivative from sub-phthalocyanines in a solvent mixture of DMF and chloronaphthalene. Spectra at the start (a) and end (b) of the reaction. Starting concentration of the sub-phthalocyanine was  $1 \times 10^{-5} \text{ mol dm}^{-3}$ .

### 3.2.2 Spectroscopic characterization

In general the spectra of the complexes were typical of non-aggregated species for complexes at concentrations lower than  $1 \times 10^{-5} \text{ mol dm}^{-3}$ , and Beer's law was obeyed below this concentrations, **Figure 3.3** and **3.4**.

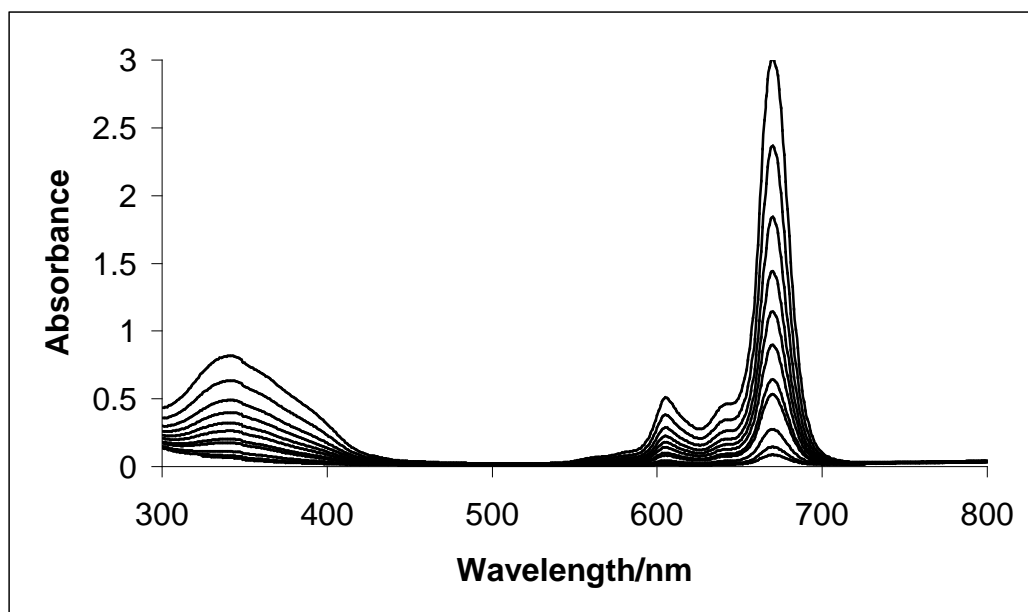


**Figure 3.3:** Decrease in the absorbance of the Q-band and the Soret band with decreasing concentration of complex **45**. Initial concentration of the complex =  $2.7 \times 10^{-5} \text{ mol.dm}^{-3}$ .

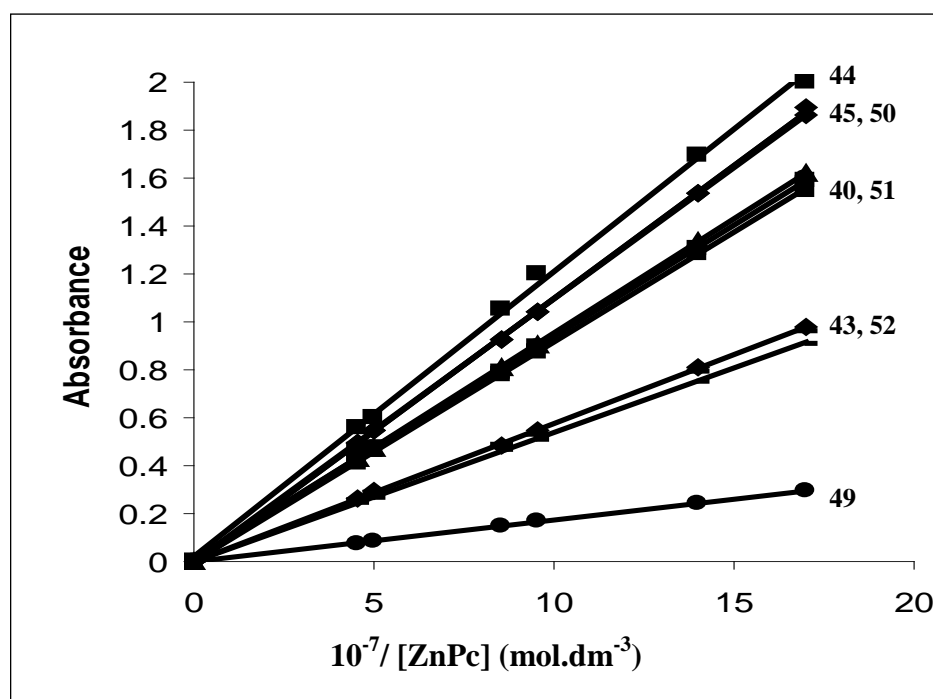


**Figure 3.4:** Beers law dependence for complexes **40**, **43-45**, **49-52** in DMF.

**Figure 3.3** shows that no new peaks were observed as the concentration of the ZnPc derivative decreased. The Q band wavelengths of the complexes ranged from 669 nm (complex **46**) to 682 nm (complex **51**) in DMF, **Table 7**. The Q band maxima for all complexes except **46** shifted to longer wavelengths compared to the unsubstituted ZnPc ( $\lambda_{\text{Q band}} = 669$  nm in DMF). It is known [85] that the Q band shifts to longer wavelengths with enlargement of the  $\pi$  conjugated system and that the shifts become less, the larger the molecules. On going from complex **43** to **47**, the bulkiness of the molecule increases as the number of tert-butylphenol groups is increased from 1 (for **44**) to 8 (for **43**). For these complexes, the wavelength of the Q band increase as follows: **45** (678 nm) > **44** (675 nm) > **47** (670 nm) ~ **43** (670 nm)  $\approx$  **46** (669 nm). Thus the Q band wavelength is shorter for the more bulky molecules (complexes **46**, **47** and **43**) and longer for less bulky molecules (complexes **44** and **45**), in agreement with literature [85].

**Table 7:** Electronic absorption data in DMF for zinc phthalocyanine complexes.

Where  $\lambda$  = wavelength in nm and  $\epsilon$  = extinction coefficient in  $\text{dm}^3 \text{mol}^{-1} \text{cm}^{-1}$ .

Compound	$\lambda_{\text{max}} (\log \epsilon)$	
	Q-bands	B-bands
43	670 (4.73), 605 (4.20)	335 (4.48)
44	675 (5.09), 609 (3.71)	348 (3.96)
45	678 (4.47), 611 (3.74)	359 (4.00)
46	669 (4.54), 604 (3.82)	335 (4.24)
47	670 (4.75), 605 (3.91)	342 (4.09)
48	670 (4.97), 605 (4.24)	335 (4.69)
49	670 (4.00), 605 (3.50)	343 (4.10)
50	671 (6.05), 606 (4.32)	354 (3.71), 284 (4.54)
51	682 (4.96), 614 (4.27)	348 (4.71)
52	672 (4.76), 607 (4.07)	344 (4.69)

The shift to longer wavelength could be due to either the destabilization of the highest occupied molecular orbital (HOMO) or the stabilization of the lowest unoccupied molecular orbital (LUMO). It has been observed that the shifting of the Q band observed on increasing the  $\pi$  system is due mainly to the destabilization of the HOMO. Lack of symmetry in phthalocyanines results in the splitting in the Q band [51]. **Figure 3.5** show spectra of some of the complexes, and no split in the Q band was observed showing that the complexes still have some symmetry.

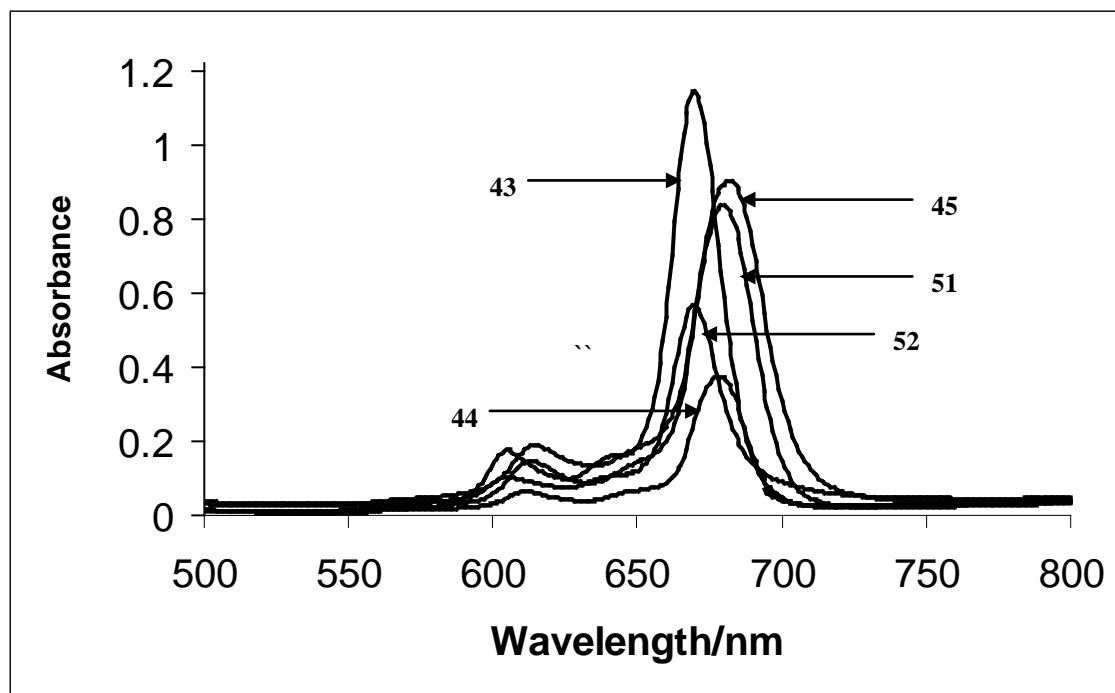


**Figure 3.5:** Electronic absorption spectra of selected complexes in DMF.

Concentration  $\sim 5 \times 10^{-6} \text{ mol.dm}^{-3}$ .

In general the IR spectra, **Table 8** of MPc complexes consists of the following bands:  $3030 \text{ cm}^{-1}$  band due to aromatic C-H stretching vibrations, the  $1670$  and  $1610 \text{ cm}^{-1}$  bands due to C-C benzene ring skeletal stretching vibrations, the  $1640 \text{ cm}^{-1}$  band due to C-N stretching vibrations, the  $1030 \text{ cm}^{-1}$  band due to C-H in-plane bending or deformation, and the  $730 \text{ cm}^{-1}$  band due to C-H out-of-plane bending vibrations.

Infrared spectra observed for the complexes are all very similar. All the complexes except **49** and **52** show a band ranging from  $1200 \text{ cm}^{-1}$  to  $1290 \text{ cm}^{-1}$ , **Table 8**, which is characteristic of a phenyl ether functionality, confirming the presence of the ether bonds. A typical IR spectra is shown by **Figure 3.6**.

**Table 8:** Infrared spectral data for zinc phthalocyanine complexes **43-52**.

Complex	IR (KBr) (cm <sup>-1</sup> )	
	Characteristic bands	Other bands
<b>43</b>	3057 $\nu$ (C-H), 2959 $\nu$ (C-H), 1607 $\nu$ (C-C), 1484 $\nu$ (C-C), 1283 (C-O-C), 1114 (C-C), 1059 $\delta$ (C-H), 886 (C-H), 728 $\pi$ (C-H)	2622, 2560, 2433, 1955, 1719, 1506, 1457, 1407, 1331, 1244, 1209, 1164, 1092, 950, 829, 794, 774, 751, 634, 540, 499, 435
<b>44</b>	3057 $\nu$ (C-H), 1607 $\nu$ (C-C), 1506 $\nu$ (C-C), 1283 (C-O-C), 1059 $\delta$ (C-H)	2959, 2622, 2560, 2433, 2230, 1955, 1719, 1484, 1456, 1407, 1331, 1244, 1163, 1114, 1092, 950, 886, 829, 794, 774, 750, 727, 634, 540, 499, 434
<b>45</b>	2964 $\nu$ (C-H), 1601 $\nu$ (C-C), 1247 (C-O-C), 726 $\pi$ (C-H)	3403, 1508, 1392, 1106, 994, 895, 831, 745, 477
<b>46</b>	2931 $\nu$ (C-H), 1625 $\nu$ (C-C), 1485 $\nu$ (C-C), 1250 (C-O-C), 1092 (C-H), 887 (C-H), 725 $\pi$ (C-H)	3385, 1709, 1331, 1185, 776, 751, 725, 467
<b>47</b>	2946 $\nu$ (C-H), 1486 $\nu$ (C-C), 1273 (C-O-C), 889 (C-H)	1699, 1409, 1332, 1091, 774, 752, 467
<b>48</b>	3054 $\nu$ (C-H), 2930 $\nu$ (C-H), 1285 (C-O-C), 1210 (C-C), 1059 $\delta$ (C-H), 887 (C-H), 721 $\pi$ (C-H)	2859, 2625, 2557, 1954, 1713, 1600, 1484, 1408, 1334, 1165, 692, 913, 809, 771, 752, 634, 541, 500, 471, 433
<b>49</b>	1652 $\nu$ (C-N), 1322 (NO <sub>2</sub> ), 1056 $\delta$ (C-H), 885 (C-H), 724 $\pi$ (C-H)	3931, 3332, 1950, 1702, 1458, 1162, 632, 577, 495, 433
<b>50</b>	3437 $\nu$ (O-H), 3050 $\nu$ (C-H), 1602 $\nu$ (C-C), 1271 (C-O-C), 889 (C-H), 745 $\pi$ (C-H)	1502, 1403, 1213, 1165, 1013, 951, 858, 982, 699, 618, 495, 433

## RESULTS AND DISCUSSION

<b>51</b>	3057 $\nu(\text{C-H})$ , 2946 $\nu(\text{C-H})$ , 1658 $\nu(\text{C-N})$ , 1499 $\nu(\text{C-C})$ , 1270 (C-O-C), 883 (C-H)	1716, 1597, 1454, 1218, 1162, 1107, 1015, 759, 690, 619, 486
<b>52</b>	3057 $\nu(\text{C-H})$ , 1440 $\nu(\text{C-C})$ , 752 $\pi(\text{C-H})$	3389, 3180, 1720, 1256, 1009, 797, 615, 468

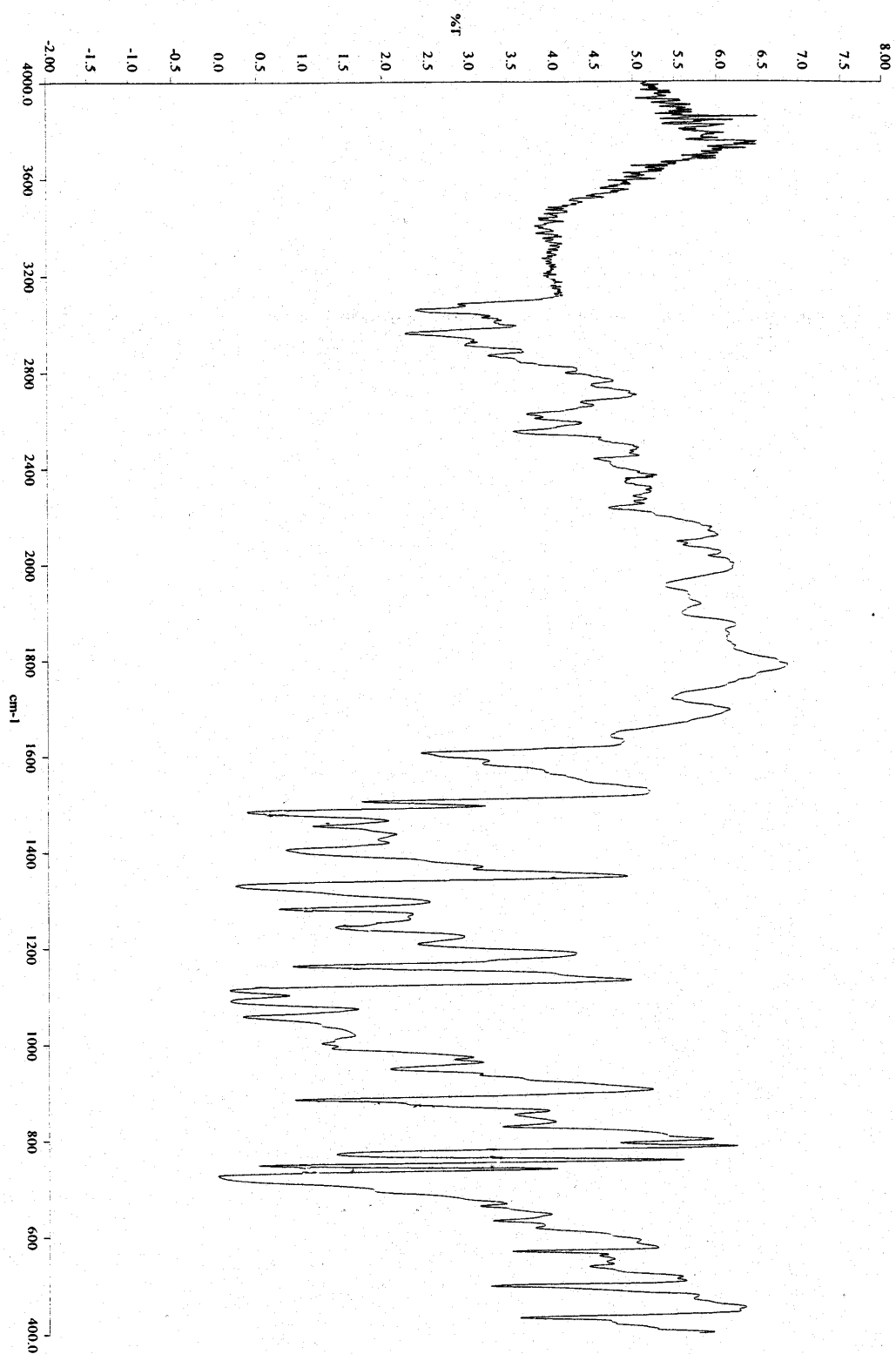
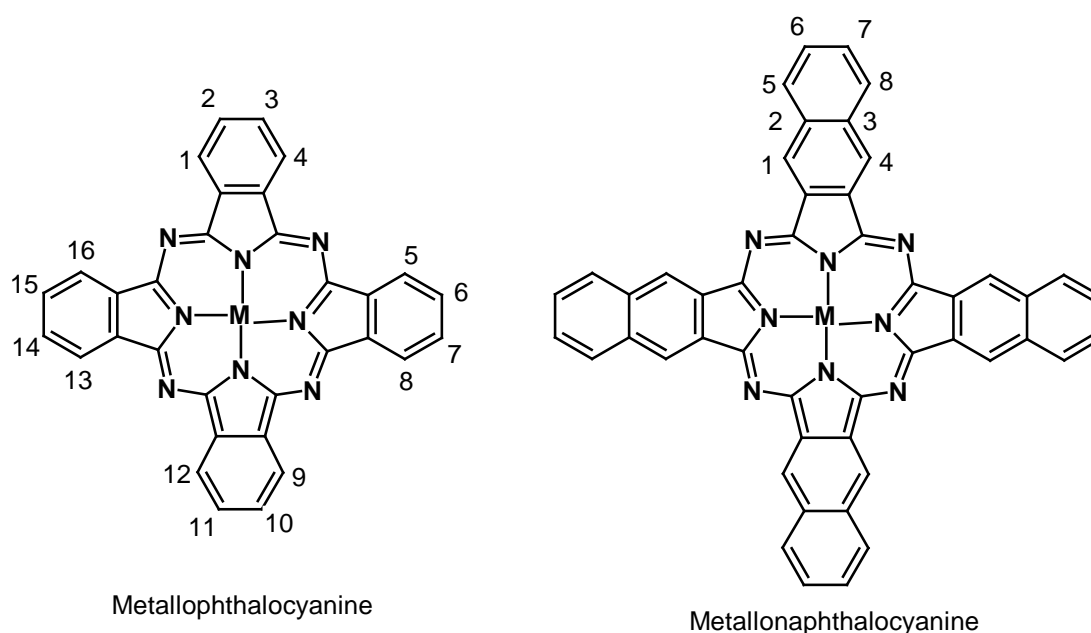


Figure 3.6: IR Spectrum of complex 44.

$^1\text{H}$  NMR spectra of the complexes were recorded in d-DMSO and the values are given in **Table 9**. Characteristic resonances due to the peripheral (1,4 positions, see **Figure 3.7** for numbering) protons of the phthalocyanines were observed as singlets ranging between 8.9 and 9.8 ppm, integrating for a total of 8 protons, for some complexes e.g. **52**, a doublet was obtained. T. J. Marks and D. R. Stororkjarkovic [47], reported ZnPc in 2%  $\text{Me}_2\text{SO}-d_6$ , to have 9.50 (8H, m) and 7.94 (8H, m). The same was observed for  $\text{PcLi}_2$  in acetone- $d_6$ . This indicates that the 1,4-Pc protons are not always observed as singlets as mostly reported in literature. The 2,3-Pc protons can also be seen as multiplets. This is due to the fact that the complexes are highly aggregated at high concentrations used for  $^1\text{H}$  NMR, thus 1-Pc and 4-Pc, 2-Pc and 3-Pc protons with the same neighbouring atoms would be different from each other as a result of different shield effects. Hence doublets which can be looked at as separate peaks for the different protons. **Figure 3.8** gives an example (for **45**) of the  $^1\text{H}$  NMR spectra for the complexes synthesized.



**Figure 3.7:** Numbering of phthalocyanines and naphthalocyanines.

2,3 protons of the phthalocyanine ring were observed at resonances ranging from 8.25 to 9.0, **Table 9**. For mono-substituted ZnPc derivatives (**44** and **49**) a singlet integrating for a total of 7 protons (2,3 protons) was observed for each complex. For di-substituted ZnPc (**48** and **50**) derivatives, singlet or doublets integrating for 6 protons were observed for 2,3 protons of each complex. Tri-substituted complex (**46**) gave multiplets integrating for (3+2) protons and for the hexa-substituted complex (**47**) a singlet integrating for 2 protons was observed as expected. Tetrasubstituted complex **51** gave a singlet for the 2,3 protons of the phthalocyanine ring, integrating for a total of 4 protons, Complex **43** is octa-substituted hence contained no 2,3 protons.

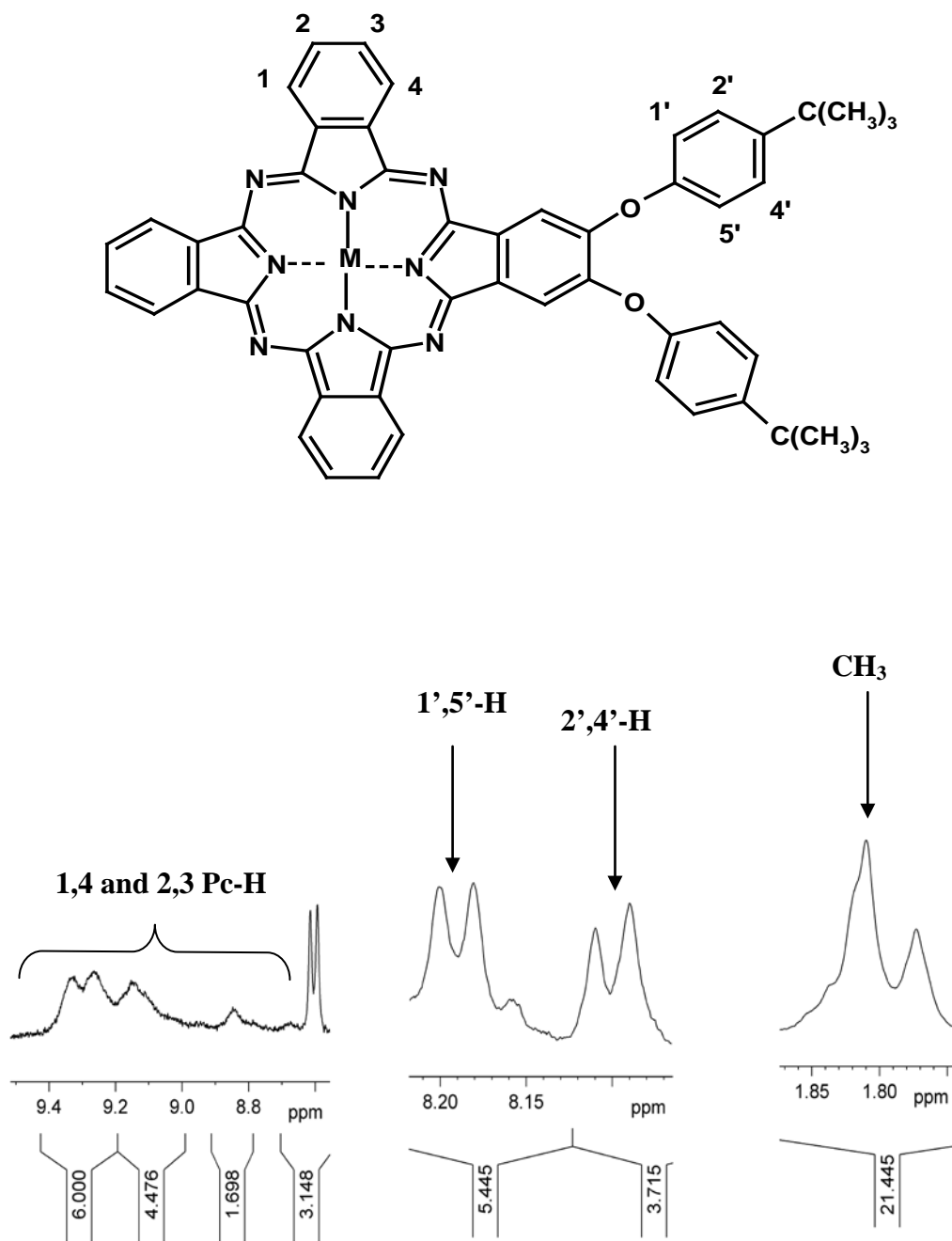


**Figure 3.8:** The  $^1\text{H}$  NMR spectra for complex 45.

The 1,4 protons of the Pc ring were observed downfield for complexes **49** (9.7 ppm) and **47** (9.8 ppm). Complex **49** contains no aromatic ring substituents, hence has no ring current effects of the benzene ring. Resonances are known to shift downfield as the ring current increases [49]. The downfield shift of complex **47** (hexa-substituted with *tert*-butylphenol) cannot be explained. Complex **49** (octa substituted with *tert* butylphenol) shows the 1,4 Pc resonances at significantly high field (9.1 ppm). Complex **52** containing naphthalene groups showed the most upfield shift of the 1,4 Pc protons (8.3 ppm).

The substituents on the phthalocyanine ring showed resonances due to the aromatic rings and these integrated correctly, **Table 9**. In the experimental section, the ring protons are denoted as 2',4'-H or 1',5'-H, and the numbering is shown in **Figure 3.8**.

**Table 9:**  $^1\text{H}$ NMR spectral data of all the complexes (**43-52**).

Complex	$^1\text{H}$ NMR		
	1,4-Pc	2,3-Pc	Ring substituents
<b>43</b>	9.50 (s, 8H)		7.5 (d, 16H, 1',5'-H), 7.0 (d, 16H, 2',4'-H), 1.2 (s, 72H, CH <sub>3</sub> )
<b>44</b>	8.90 (s, 8H)	8.85 (s, 7H)	8.10 (d, 2H, 1',5'-H), 7.40 (d, 2H, 2',4'-H), 1.30 (s, 9H, CH <sub>3</sub> )
<b>45</b>	8.54-9.40 (14H, 2,3-Pc and 1,4-Pc)		8.21-8.17 (d, 4H, 1',5'-H), 8.12-8.07 (d, 4H, 2',4'-H), 1.82-1.78 (s, 18H, CH <sub>3</sub> )
<b>46</b>	9.48 (s, 8H)	8.55 (m, 2H), 8.10 (m, 3H)	7.60 (d, 6H, 1',5'-H), 7.30 (d, 6H, 2',4'-H), 1.30 (s, 27H, CH <sub>3</sub> )
<b>47</b>	9.80 (s, 8H)	8.75 (s, 2H)	8.00 (d, 12H, 1',5'-H), 7.70 (d, 12H, 2',4'-H), 1.3 (s, 55H, CH <sub>3</sub> )
<b>48</b>	9.25 (s, 8H)	8.25 (s, 6H)	8.8-7.5 (m, 16H, naphthoxy)
<b>49</b>	9.70 (s, 8H)	8.60 (s, 7H)	
<b>50</b>	9.40-9.6 (s, 8H)	8.35 (d, 6H)	7.95 (d, 4H, 1',5'-H), 7.50 (d, 4H, 2',4'-H), 2H from COOH are not seen as their peak is too weak compared to that of the Pc ring and the phenoxy ring.
<b>51</b>	9.40 (s, 8H)	9.00 (s, 4H)	7.56 (d, 8H, 2',4'-H), 7.42 (d, 8H, 1',5'-H), 1.28 (t, 27H, CH <sub>3</sub> )

<b>52</b>	9.45 (d, 8H)		8.30 (d, 6H, 6,7-H), 7.90 (d, 6H, 5,8-H)
-----------	--------------	--	--

### 3.2.3 Voltammetry characterization

The redox properties of the ZnPc derivatives were studied using both cyclic voltammetry (CV) and Osteryoung square wave voltammetry (OSWV) in DMF containing TBAP. **Figure 3.9** shows the cyclic and square wave voltammograms for complex **44** and **Figure 3.10** the voltammograms for complex **47**. Two reduction couples labelled **II** and **III** were observed, and oxidation couple (s) (labelled as **I** or **Ia** and **Ib**) were also observed.

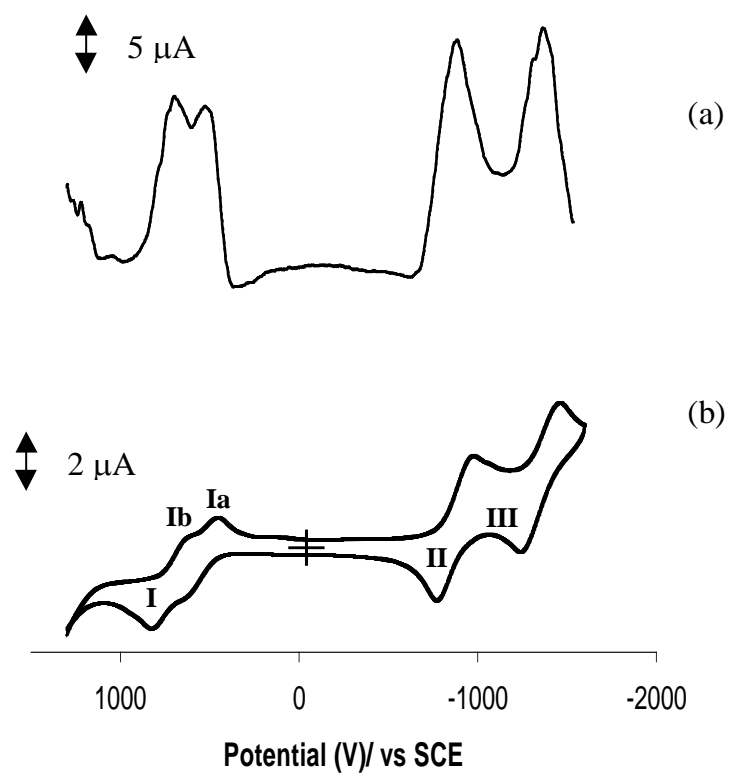


**Figure 3.9:** Osteryoung square wave voltammogram (a) and cyclic voltammogram (b) of  $1 \times 10^{-4} \text{ mol dm}^{-3}$  of complex **44** in DMF containing  $0.1 \text{ mol dm}^{-3}$  TBAP. Scan rate =  $100 \text{ mV/s}$ .

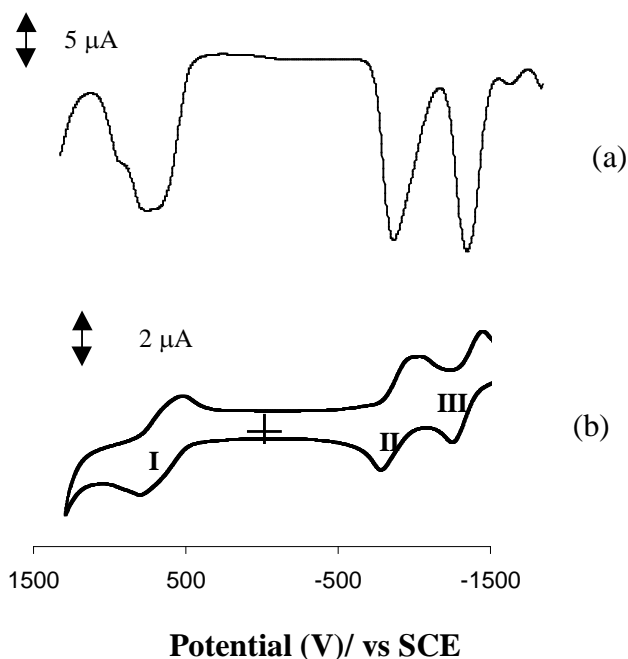


**Figure 3.10:** Osteryoung square wave voltammogram (a) and cyclic voltammogram (b) of  $1 \times 10^{-4} \text{ mol dm}^{-3}$  of complex **47** in DMF containing  $0.1 \text{ mol dm}^{-3}$  TBAP. Scan rate =  $100 \text{ mV/s}$ .

All processes are ring based since the central zinc metal is electroinactive [79,87]. Thus couples **II** and **III** are assigned to ring reduction in the ZnPc derivatives and the formation of  $\text{Pc}^{-3}/\text{Pc}^{-2}$  and  $\text{Pc}^{-4}/\text{Pc}^{-3}$ , respectively. The separation between the first and second ring reductions was found to range between 0.4 and 0.5 V in agreement with the separation reported [87] for ring based reductions in non-transition metal phthalocyanines. For complex **44**, **Figure 3.9**, two closely spaced couples (**Ia** and **Ib**) were observed for the oxidation process. For complex **47**, the splitting was more easily observed for the OSWV, **Figure 3.10**.

The cyclic voltammograms for the first scan were similar to those of the second and subsequent scans, suggesting that no complicated reactions occur following oxidation or reduction. For all couples, the cathodic to anodic peak currents ( $i_{p_c}/i_{p_a}$ ) were near unity. The peak currents increased linearly with the square root of scan rates, for scan rates ranging from 5 – 800  $\text{mVs}^{-1}$ , **Figure 3.11**, indicating that the electrode reactions are purely diffusion controlled. The potentials are listed in **Table 9**.

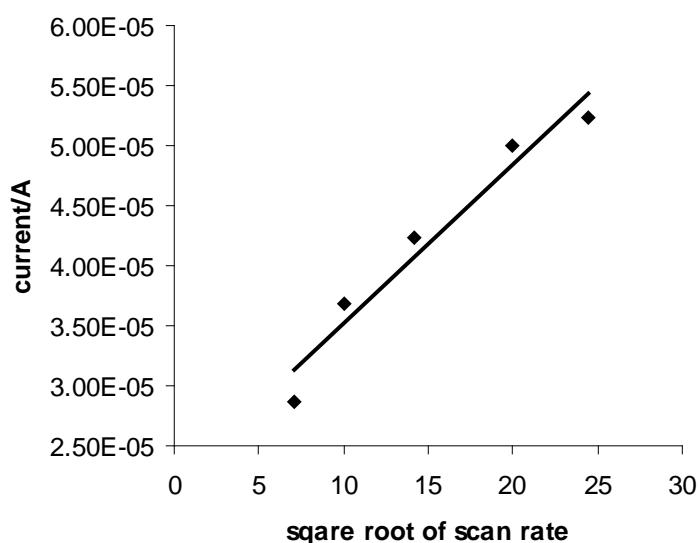


**Figure 3.11:** Plot of current vs square root of scan rate for **44**.

The splitting of the oxidation peaks was observed to varying extents for the ZnPc derivatives. The observation of two closely spaced oxidation peaks has been attributed to the presence of both the aggregated and non-aggregated substituted ZnPc complexes in solution [87]. At the concentration employed for voltammetric studies in this work ( $\sim 10^{-4}$   $\text{mol dm}^{-3}$ ), aggregation of the complexes is expected, though there was no clear broadening of the UV/vis spectra at these concentrations, **Figure 3.12**.

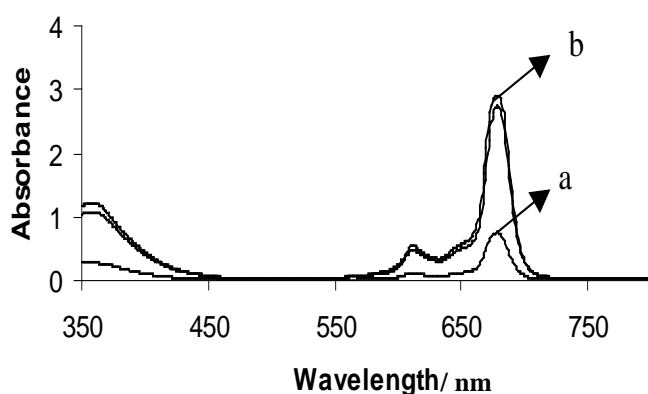


**Figure 3.12:** Spectra of Q-band with increasing concentration for complex **44**, (a) at concentration  $1 \times 10^{-6} \text{ mol. dm}^{-3}$  and (b)  $1 \times 10^{-4} \text{ mol dm}^{-3}$  in DMF.

Thus the two couples observed for the oxidation process in **Figures 3.9** and **3.10**, may be attributed to the ring oxidation of the aggregated and non-aggregated species. In **Table 9** the half-wave potentials ( $E_{1/2}$ ) for complex **44**, **46**, **47** and **43** containing increasing number of tert-butylphenol substituents are compared. The presence of electron donating methyl groups is expected to make the ring easier to oxidise. Thus it is expected that as the number of tert-butylphenol substituents increases, the ring should be more difficult to reduce and easier to oxidize. The reverse is observed in **Table 9** in that complex **43** containing a larger number of tertbutylphenoxy substituents is more difficult to oxidize. Oxidation becomes easier (difficulty in reduction) as the number of substituents decrease. This observation may suggest that steric hindrance plays an important role in the relative redox behaviour of these complexes. Considering only the oxidation of these complexes, it seems stabilization of the HOMO occurs as the number of tert-butylphenol substituents increase.

**Table 9:** Comparison of redox potentials for complexes **43,44, 46-50**. Solvent = DMF containing TBAP. Pc(-2) = phthalocyanine dianion.

Complex	No. of tert-butylphenol substituents	$E_{1/2}$ (V vs SCE)		
		I Pc <sup>-1</sup> /Pc <sup>-2</sup>	II Pc <sup>-2</sup> /Pc <sup>-3</sup>	III Pc <sup>-3</sup> /Pc <sup>-4</sup>
<b>43</b>	8	0.97	-0.68	-1.12
<b>44</b>	1	0.35 0.56	-1.08	-1.57
<b>46</b>	3	0.75	-0.82	-1.32
<b>47</b>	6	0.70	-0.84	-1.32
<b>48</b>	0	0.79	-0.90	-1.47
<b>49</b>	0	0.68	-0.97	
<b>50</b>	0	0.76	-0.82	

### 3.3 Photochemical studies

#### 3.3.1 Photobleaching

Photobleaching and singlet oxygen studies of ZnPc derivatives were determined using the details explained in the experimental section.

Photobleaching of complexes is characterised by complete disappearance of the spectra due to the degradation of the phthalocyanine ring. Photobleaching studies

were undertaken in order to determine the effects of the different substituents on the stability of the ZnPc derivatives in the presence of light.

Photobleaching studies were performed in DMSO and **Figure 3.13** shows an example of the changes in the spectra during the photobleaching process.

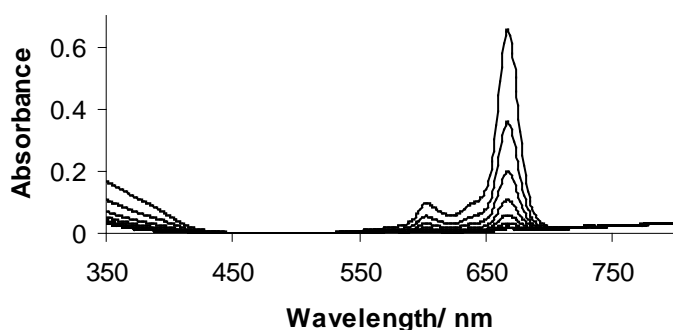


**Figure 3.13:** UV/vis spectra of **44** during the photobleaching process. The initial concentration used was  $6.8 \times 10^{-6} \text{ mol dm}^{-3}$ .

Quantum yields for photobleaching are listed in **Table 10**. Photobleaching quantum yields are in the order of  $10^{-5}$  for all the complexes. Photodecomposition of phthalocyanine complexes usually occurs through oxidative cleavage [88-91]. Comparing complexes which contain a varying number of the tert-butylphenol substituents (**43** to **47**), a low photobleaching quantum yield (hence higher stability) is observed for complex **43** which was shown to be more difficult to oxidize by electrochemical methods, hence confirming that oxidative degradation occurs for these complexes. Complex **44** was easier to oxidize electrochemically, but is relatively stable, suggesting that it is not only the oxidative mechanism which plays a

part in the photodegradation of MPc complexes,  $O_2 (^1\Delta_g)$  generated may attack the phthalocyanine ring [89]. However, the attack of  $O_2 (^1\Delta_g)$  on the Pc ring may also be affected by the shielding effect of the ring substituents [91].

Quantum yields for photobleaching increased when oxygen was bubbled to solution, confirming that oxidative degradation occurs, **Figure 3.14**. Inhibition of photobleaching processes in the presence of the singlet oxygen quencher, DABCO, is in agreement with the involvement of singlet oxygen in the degradation of the phthalocyanine macrocycle.

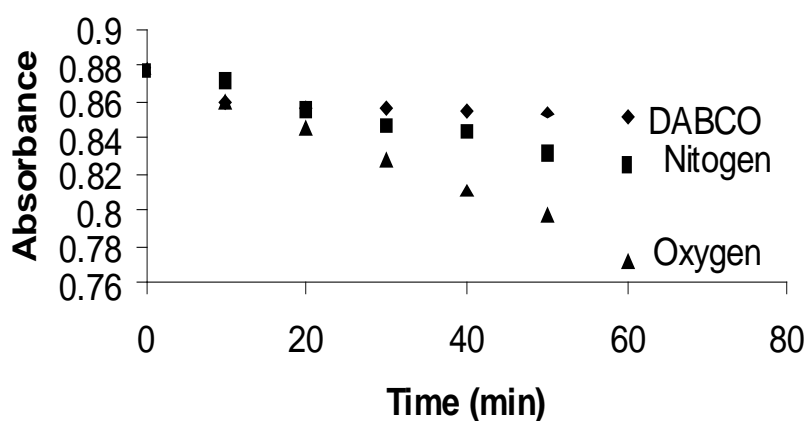


**Figure 3.14:** Kinetic curves for the photobleaching of complex **44** ( $8.5 \times 10^{-6}$  mol  $dm^{-3}$ ) in DMF conc. saturated with oxygen or nitrogen and in aerated DMF containing  $2 \times 10^{-3}$  mol  $dm^{-3}$  DABCO.

It has been shown [91,92] that the singlet oxygen interaction with the phthalocyanine results in the macrocycle destruction and the formation of the phthalimide as the product of photodegradation.

### 3.3.2 Singlet oxygen studies

**Figure 3.15** shows the spectral changes observed during the photolysis of one of the ZnPc derivatives (**44**) in the presence of DPBF for the determination of  $\Phi_{\Delta}$ . Changes in the spectra of DPBF were observed, but no spectral changes were observed for ZnPc derivative, showing that ZnPc does not degrade during the time for  $^1\text{O}_2(^1\Delta_g)$  production.

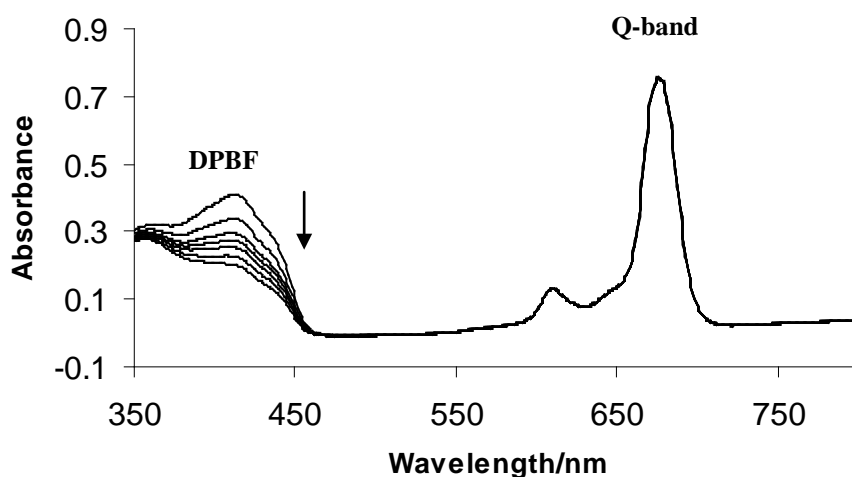


**Figure 3.15:** Spectral changes observed during photolysis of complex **49** in the presence of DPBF in DMF.  $[\text{DPBF}] = 1.5 \times 10^{-3} \text{ mol dm}^{-3}$  and  $[\text{complex } \mathbf{44}] = 7.62 \times 10^{-6} \text{ mol dm}^{-3}$ .

Quantum yields of singlet oxygen photogeneration ( $\Phi_{\Delta}$ ) of compounds **43-52** are listed in **Table 10**. These values range from 0.22 to 0.68. As **Figure 3.15** shows, no photobleaching of the complexes was observed during the determination of singlet oxygen quantum yields, since these processes occur much slower than singlet oxygen production. It is well known that aggregation of the phthalocyanine complexes results

in decreased photochemical activity due to enhanced probability of radiationless decay of excited states. The concentration employed for  $\Phi_{\Delta}$  and photobleaching studies were in the order  $10^{-6}$  mol dm<sup>-3</sup>, where aggregation is less. Comparing complexes, which contain varying number of the tert-butylphenol substituents, complexes **43-47**, complex **44** with one substituent gave the largest value of  $\Phi_{\Delta}$ . Comparing all the complexes studied the lowest  $\Phi_{\Delta}$  value was observed for complex **51**. The  $\Phi_{\Delta}$  values for the complexes synthesized in this work are within the range of  $\Phi_{\Delta}$  for complexes currently in use for PDT such as AlPc and ZnTsPc derivatives, **Table 10**.

### 3.4 Photophysical studies

**Figure 3.16** shows the triplet decay for complex **44**. Triplet life times ( $\tau_T$ ) were determined in DMSO for complexes **44**, **46** and **47** and are listed in **Table 10**. Of the three complexes, the largest  $\tau_T$  value was observed for complex **46** (240  $\mu$ s) and the lowest for **44** (114  $\mu$ s) even though the later has the highest  $\Phi_{\Delta}$  value. A direct correlation between  $\Phi_{\Delta}$  and ( $\tau_T$ ) or  $\Phi_T$  was also not evident for substituted MPc complexes reported in the literature [43]. Complex **46** contains three *tert*-butylphenoxy substituents and its  $\tau_T$  value within the range reported for other ZnPc complexes. The other two complexes **44** and **47** showed lower  $\tau_T$  values compared to the reported ZnPc complexes.

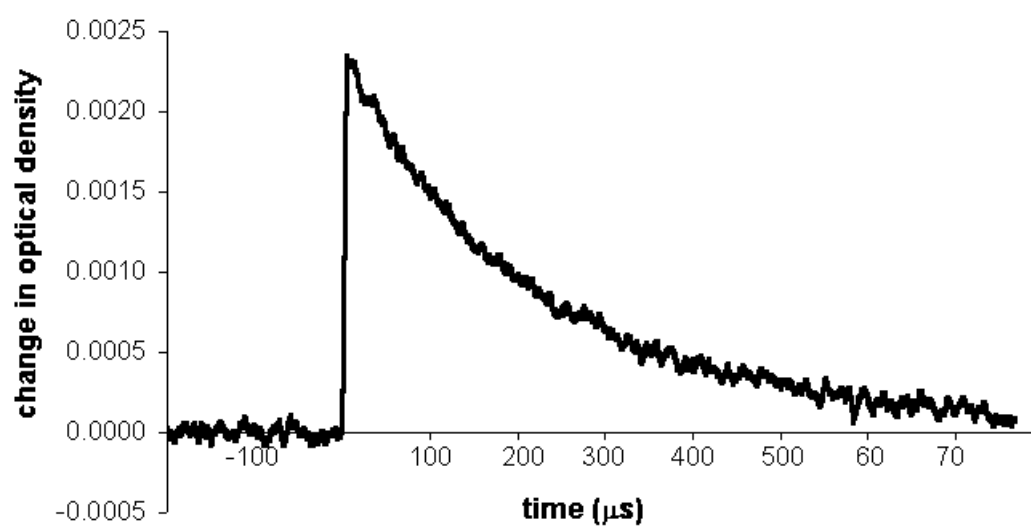


**Figure 3.16:** Triplet decay of **44** showing mono exponential decay.

**Table 11:** Quantum yields for singlet oxygen and photobleaching for the ZnPc derivatives in DMSO.

Complex	$\lambda_{Q \text{ band}}/\text{nm}$	$\Phi_{\Delta}^a$	$10^5 \Phi_{\text{photobleaching}}$
<b>43</b>	670	0.52	3.3
<b>44</b>	675	0.68 (114)	3.9
<b>45</b>	678	0.49	4.1
<b>46</b>	669	0.54 (240)	5.8
<b>47</b>	670	0.51 (129 )	6.5
<b>48</b>	670	0.43	4.1
<b>49</b>	670	0.49	3.8
<b>50</b>	671	0.40	3.7
<b>51</b>	682	0.22	3.3
<b>52</b>	672	0.32	3.0
<b>ZnPc</b>		0.55 [66]	
<b>AlTsPc</b>		0.35 [4,5]	
<b>ZnTsPc</b>		0.36 [4,5]	

<sup>a</sup> Triplet lifetimes ( $\mu\text{s}$ ) shown in round brackets for selected complexes and references in square brackets.

Fluorescence life times  $\tau_f$  ranging between 2.4 and 3.0 ns were observed for complexes **44**, **46** and **47**, **Table 11**. The  $\tau_f$  values are in the range reported for ZnPc and AlPc derivatives, except for **46**.

**Table 12:** Quantum yields of fluorescence, fluorescence lifetimes and triplet state life times for complexes **44**, **46** and **47** in DMSO.

Complex	$\tau_f$ (ns)	$\Phi_f$	$\tau_t$ ( $\mu$ s)
<b>44</b>	2.9	0.12	114
<b>46</b>	2.4	0.17	240
<b>47</b>	3.0	0.08	129
<b>ZnPc</b>	2.9	0.30	300
<b>AlTsPc</b>	2.9	0.32	245

The values of  $\tau_T$  and  $\Phi_f$  are within the range reported for complexes currently used for PDT. Thus the complexes synthesized in this work have potential for use in PDT. The complexes show intense absorption in the red region of the spectrum and the presence of phenoxy substituents on the ring improves solubility of these complexes in organic solvents like DMSO, DMF and chloroform. It has been shown that phthalocyanines with diamagnetic metal centres (e.g. Zn) exhibit larger  $\tau_T$  and  $\Phi_\Delta$  and show greater photoactivity.

### 3.5 Studies of the interaction of ZnPcS<sub>n</sub> with pyridine ligands

It is known that aggregation in phthalocyanines suppresses all photochemistry. The electronic structure of the Pc ring in the aggregated state is perturbed resulting in an alteration of the ground state and excited state properties. Broadening and splitting of the Q-band indicates the additional electronic levels of aggregates. The overlapping of energy levels leads to radiationless excited state deactivation, that compete, hence making aggregates photo-inactive. Due to enhanced radiationless degradation lifetime of aggregated excited states, triplet state quantum yields and consequently singlet oxygen quantum yields are low. Aggregation is depicted as a coplanar association of rings and is driven by enhanced van der Waals attractive forces between phthalocyanine rings. This leads to blue shifts, broadening or splitting of the Q-band in the absorption spectra and changes the excited states. The electronic spectra of [MTsPc]<sup>4-</sup> (metallotetrasulphonated phthalocyanine) complexes have well been studied [93-95]. These complexes exist as dimers in equilibrium with monomers in aqueous solutions, the spectra of [MTsPc]<sup>4-</sup> thus consists of two peaks in the Q-band region [95]. The high energy absorption band near 620 nm is associated with the dimeric species and low energy band near 670 nm is due to the monomeric species [93,95]. For ZnPcS<sub>n</sub> in water, the peak due to monomeric species is observed at 668 nm and the dimeric peak at 630 nm. The B-band peak is observed at 335 nm. As an example the absorption spectra of ZnPcS<sub>n</sub> in water is depicted in **Figure 3.17**.

In the region  $1 \times 10^{-6}$  to  $5 \times 10^{-5}$  mol dm<sup>-3</sup> Beer's law was obeyed by ZnPcS<sub>n</sub> complex in the absence of ligands. Above concentrations of  $5 \times 10^{-5}$  mol dm<sup>-3</sup> changes in the

spectra occur, that show a decrease in monomer components in solution, hence confirming aggregation.

The solubility of  $\text{ZnPcS}_n$  was found to increase with the addition of Triton-100, which is a surfactant, **Figure 3.18**. The absorption of monomeric components was also increased by the addition of a surfactant Triton x-100. The  $\text{ZnPcS}_n$  aggregates dissociate in aqueous solution in the presence Triton x-100 and the ligand. The second spectrum labelled 2 is typical of monomers, **Figure 3.18**.

It is known that zinc complexes of porphyrins co-ordinate with heterocyclic compounds like pyridine, bipyridyl, aminopyridyl. The possibility of using axial coordination in water was studied for this project. The interaction between  $\text{ZnPcS}_n$  and the ligands (pyridine, bipyridine and aminopyridyl) were followed using UV/vis spectroscopy. Therefore solutions of  $\text{ZnPcS}_n$  in water containing the compound selected for axial ligation ligation (e.g. bipyridine) were heated to 85 °C and then cooled to room temperature to obtain the complexes. As mentioned above, the electronic absorption spectrum of  $\text{ZnPcS}_n$  shows a split in the Q-band in the absence of the ligand, which is attributed to aggregation in water solution. In the presence of the ligand e.g bipyridine, the spectra of  $\text{ZnPcS}_n$  in water, **Figure 3.17**, shows an increase in the monomer components which is evident from the enhancement of the Q-band and a decrease in the band at shorter wavelengths resulting from aggregates. Similar spectroscopic changes were observed for pyridine and aminopyridyl.

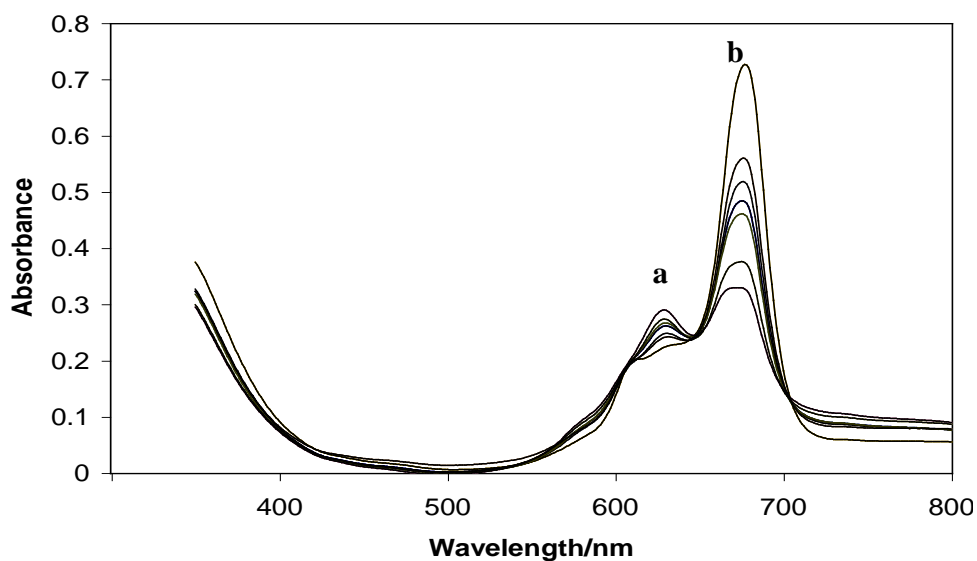


**Figure 3.17:** Electronic spectra of  $\text{ZnPcS}_n$  and axially ligated  $\text{ZnPcS}_n$  showing enhancement of the Q-band with increasing concentration of 4,4'-bipyridyl. (a) before the addition of bipyridyl and (b) is after the addition of bipyridyl. The initial concentration of  $\text{ZnPcS}_n$  used was  $8 \times 10^{-6} \text{ mol dm}^{-3}$ .

The  $\text{ZnPcS}_n$  is in the sodium salt form and thus in water solution forms  $\text{ZnPcS}_n$  anions and  $\text{Na}^+$ .

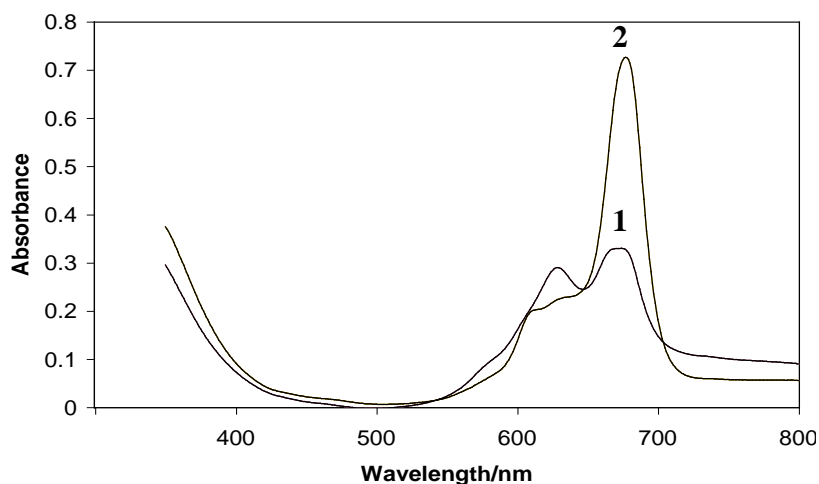


**Figure 3.18:** Absorption spectrum of (1) ZnPcS<sub>n</sub> in water and (2) in the presence of Triton x-100. [ZnPcS<sub>n</sub>]=  $8 \times 10^{-5}$  mol dm<sup>-3</sup>.

The solubility ZnPcS<sub>n</sub> was found to increase with the addition of bipyridyl axial ligand as was observed for Triton x-100. Reports have shown that pyridyl and its derivatives, axially ligate to most metallated phthalocyanines and result in increased solubility of these complexes [42]. The Q-band of the monomer component of ZnPcS<sub>n</sub> species was found to shift to higher wavelength values in the presence of Triton x-100 and increasing concentrations of bipyridyl, **Table 12**. The shift was not observed for pyridine and aminopyridyl. The variation in band position is due mainly to changes in the number of coordinated axial ligands. Thus this could mean that pyridyl and aminopyridyl are not coordinating to the central metal ion as a result no shift in the Q-band occurs. Alternatively a change in the viscosity of the medium following the addition of ligand or Triton x-100, hence a shift in the Q-band wavelength occurs.

The extinction coefficient ( $\epsilon$ ) of the monomers in the presence of Triton x-100 was calculated  $120\,000 \text{ L}\cdot\text{mol}^{-1}\cdot\text{cm}^{-1}$  at absorbance 673 nm. The  $\epsilon$  value for dimers was

calculated using equation 32, and absorbance value in the presence of Triton x-100 from **Table 12**.

**Table 12:**  $\lambda_{\max}$  (nm) and absorbance values for different concentrations of 4,4'-bipyridyl in unbuffered water.

[4,4-bipyridyl] (mol.l <sup>-1</sup> )	Q-band (monomer part) $\lambda_{\max}$ (nm)	Absorbance
0	666	0.688
0 (Triton x-100)*	673	2.03
$2.5 \times 10^{-3}$	668	0.928
$5 \times 10^{-3}$	676	0.954
$2.5 \times 10^{-2}$	678	1.461

\* No 4,4-bipyridyl was added, but  $\sim 10^{-4}$  mol.l<sup>-1</sup> Triton x-100.

$$\epsilon_m^{673} = \frac{\text{Abs} \times 2}{c \times l} \quad \dots 32$$

In equation 32 the extinction coefficient monomers is expressed as twice that of dimers, thus 2 was used since dimer goes into 2 monomers, according to equation 33.



L = pyridine, bipyridine or aminopyridyl, and L<sub>n</sub> represents the number of ligands bound to the ZnPcS<sub>n</sub> complex. The equilibrium constant K is given by equation 34:

$$K = \frac{[(L)_n ZnPcS_n]^2}{[(ZnPcS_n)_2][L]^n} \quad \dots 34$$

$$\log K = 2 \log [(L)_n ZnPcS_n] - \log [(ZnPcS_n)_2] - n \log [L] \quad \dots 35$$

$$\log K + n \log [L] = \log \frac{[(L)_n ZnPcS_n]^2}{[(ZnPcS_n)_2]} \quad \dots 36$$

So from the plot of  $\log [L]$  against  $\log [(L)_n ZnPcS_n]^2 / [(ZnPcS_n)_2]$ ,  $K$  and  $n$  were obtained, **Figure 3.19**.

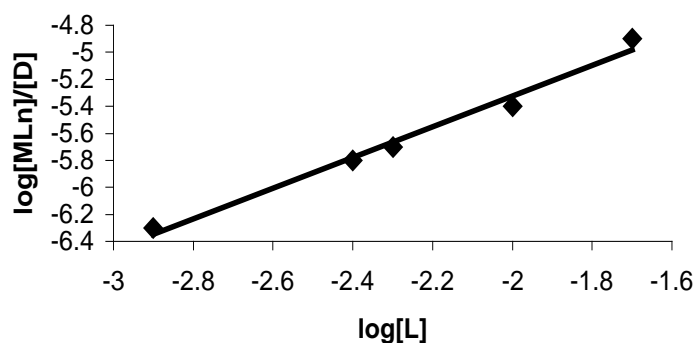


**Figure 3. 19:** A plot of  $\log [L]$  vs  $\log [MLn]/[D]$  for  $ZnPcS_n$  with 4,4'-bipyridyl as an axial ligand in water, where  $[MLn] = [(L)_n ZnPcS_n]^2$  and  $[D] = [(ZnPcS_n)_2]$ .

**Table 13:** K and n values calculated for ZnPcS<sub>n</sub> with bipyridyl, aminopyridyl and pyridine as axial ligands.

Complex	K	n
ZnPcS <sub>n</sub> + bipyridine	$8.9 \times 10^{-4}$	1
ZnPcS <sub>n</sub> + aminopyridyl	$3.0 \times 10^{-5}$	1
ZnPcS <sub>n</sub> + pyridine	$1.0 \times 10^{-4}$	1

The equilibrium constants are very low and show that binding of these ligands is not favoured.

Singlet oxygen quantum yields were determined for ZnPcS<sub>n</sub> in the presence of ligands.  $\Phi_{\Delta}$  values were determined in water using ADMA as explained in the experimental section. **Figure 3.20** shows spectral changes of (bipyr)<sub>1</sub>ZnPcS<sub>n</sub> in water and in the presence of ADMA. The concentration of ADMA decreased while that of (L)<sub>2</sub>ZnPcS<sub>n</sub> did not, showing that photobleaching does not occur during the time used for  $\Phi_{\Delta}$  studies. The  $\Phi_{\Delta}$  values, were calculated using equation 16 (Section 1.4) and are listed in **Table 14**. A considerable increase in  $\Phi_{\Delta}$  values is observed for ZnPcS<sub>n</sub> in the presence of the ligands and Triton x-100 due to the monomerization of the aggregates.

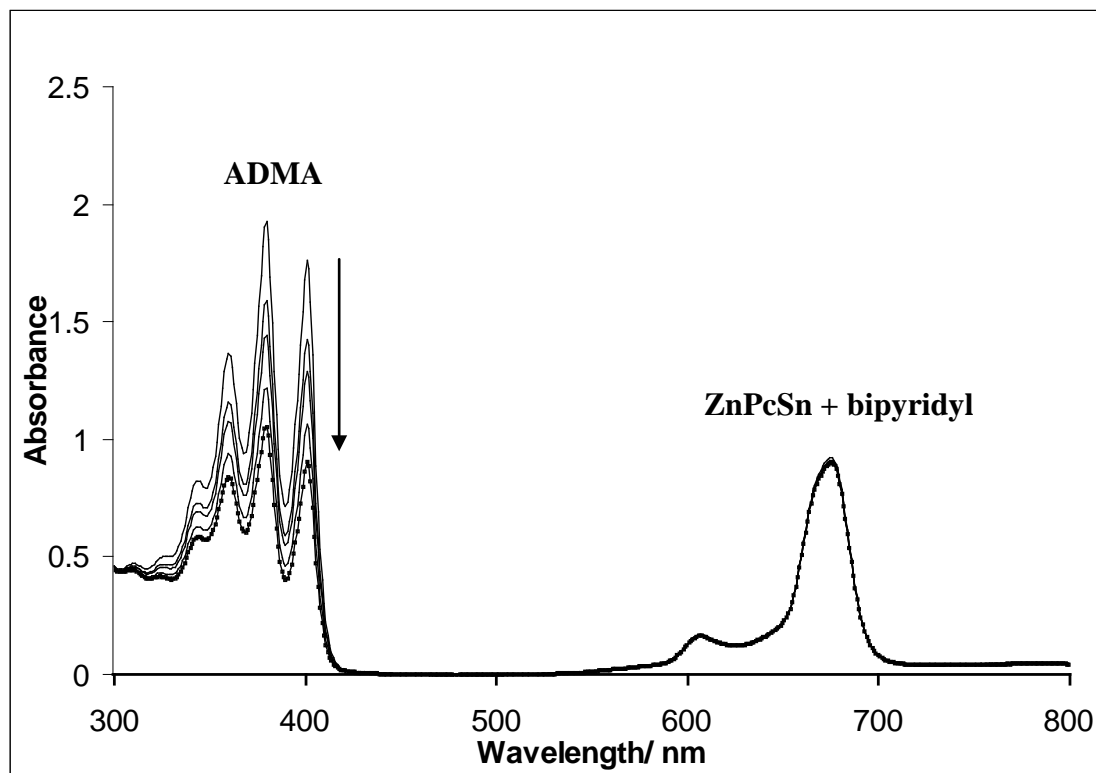


**Figure 3.20:** Electronic spectrum of  $\text{ZnPcSn}_n$  + bipyridyl in the presence of ADMA.

**Table 14:**  $\Phi_{\Delta}$  for ZnPc and AlPc derivatives in water, using ADMA as a  $\text{O}_2(^1\Delta_g)$  quencher.

Complex	$\Phi_{\Delta}$
AlPcSn	0.38 [4,5]
ZnPcSn	0.097
ZnPcSn + Triton x-100	0.82
ZnPcSn + bipyridyl	0.57
ZnPcSn + aminopyridyl	0.42

#### 4. CONCLUSIONS AND FUTURE STUDIES

It is known that axial ligation prevents stacking of Pc rings by hindering the  $\pi$ - $\pi$  interaction between Pc rings. This approach to monomerization was used since it has been successful with AlPc and SiPc complexes. For this project ZnPc was used as an example to study the possibility of using axial ligands to increase its solubility and photochemical activity. Several axial ligands were tried including pyridine, aminopyridine and 4,4'-bipyridyl. The effects of axial ligation on the photochemical activity, particularly singlet oxygen photogeneration was studied. It was found that axial ligation to ZnPcSn leads to a substantial increase to singlet oxygen quantum yields. Results show that axial coordination can be used to increase the solubility and photochemical activity of metallophthalocyanines, even though the work was terminated as a result of low equilibrium constant values obtained.

The synthesis of a range of phenoxy unsymmetrically substituted zinc phthalocyanine derivatives is described. It was found that these derivatives can be efficiently synthesized through ring expansion of sub-phthalocyanines, but require extensive cleaning procedures to get the desired product. Increasing the number of phenoxy substituents had no particular effect on the Q-band and singlet oxygen quantum yields of the zinc phthalocyanine derivatives, thus no trend was found in relation to the number of substituents on the phthalocyanine ring. The most prominent properties of the phenoxy unsymmetrically substituted zinc phthalocyanine derivatives was their enhanced solubility in most organic solvents like DMSO, DMF and acetonitrile and also their lack of aggregation in these solutions at concentrations used for their studies.

The phenoxy unsymmetrically substituted zinc phthalocyanine derivatives gave reasonable singlet oxygen quantum yield values which are comparable to those of sensitizers already in trials or in use. The photophysical data obtained for these compounds provide promising insight into whether they can be good sensitizers or not for PDT.

Voltammetric behaviour of phenoxy unsymmetrically substituted zinc phthalocyanine derivatives studied show that as the number of tertbutylphenoxy substituents increase, the complexes become more difficult to oxidize and easier to reduce. Also CV and SWV show the aggregation behaviour of these complexes at high concentrations. The complexes are relatively stable to photodegradation with quantum yields of photobleaching in the  $10^{-5}$  range. Majority of the complexes have singlet oxygen quantum yields in the 0.4 and 0.5 region, hence show promise as candidates for PDT.

Future work could include the use of other available phenoxy groups on the phthalocyanine ring, the use of other methods for synthesis, the effect of substituents on absorption into the cells during PDT. Cell studies would prove whether peripheral substituents have an effect on sensitizer uptake. Also axial ligation and unsymmetrical ring substitution could be done simultaneously and their effects on the photophysical properties of metallophthalocyanines studied.

**REFERENCES**

1. A. J. MacRobert, D. Phillips, *Chemistry and Industry*, 1 (1992) 1.
2. D. Phillips, *Pure Appl. Chem.* 67 (1995) 117.
3. D. Phillips, *Pure Appl. Chem.* 54 (1995) 126.
4. J. R. Darwent, I. McCubbin, D. Phillips, *J. Chem. Soc. Faraday Trans. 2*, 78 (1982) 347.
5. W. F. Kier, E. J. Land, A. H. MacLennan, D. J. McGarvey, T. G. Truscott, *J. Photochem. Photobiol.* 46 (1987) 587.
6. S. Dhami, D. Phillips, *J. Photochem. Photobiol. A: Chem*, 100 (1996) 77.
7. E. A. Lukyanets, *J. Porphyrins Phthalocyanines* 3 (1999) 424.
8. Xian-Fu Zhang, Hui-Jun Xu, *J. Chem. Soc. Faraday Trans.* 89 (1993) 3347.
9. N. B. McKeown, *Chemistry and Industry* 1 (Feb. 1999) 92.
10. R. Bonnet, *Chem. Soc. Rev.* 24 (1995) 19.
11. I. Rosenthal, *Photochem. Photobiol.* 54 (1991) 859.
12. N. A. Kutznesova, O. L. Kaliya, *Russ. Chem. Rev.* 42 (1998) 424.
13. E. Lukyanets, *J. Phorphyrins Phthalocyanines* 3 (1998) 424.
14. R.W. Boyle, J. E. Lier, *Synthesis* (1995) 1079.
15. I. Rosenthal, E. Ben-Hur in *Phthalocyanines: Properties and Applications*, Eds, C. C Leznoff and A. B. P Lever, Vol. 1, VCH, 1989: New York Ch. 6.
16. M. Ambroz, A. Beeby, J. MacRoberts, M. S. Simpson, R. K. Svenson, D. Phillips, *J. Photochem. Photobiol.* 9 (1991) 87.
17. L.R. Milgram in *Colours of life*, Oxford University Press, 1977, Oxford, 1<sup>st</sup> Ed.
18. V. Iliev, V. Alexiev, L. Bilyarska, *J. Mol. Catal. A. Chem.* 137 (1999) 15.
19. P.C. Martin, M. Gouterman, B.V. Pepich, G.E. Renzeoni, D.C. Schindele,

- Inorg. Chem. 30 (1991) 3305.
20. N. L. Oleinick, A. R. Antunez, M. E. Clay, B. D. Rihter, M. E. Kenney, Photochem. Photobiol. 54 (1993) 242.
21. R.W. Boyle, D. Dolphin, Photochem. Photobiol. 64 (1996) 469.
22. M. Geyer, F. Plenzig, J. Rausechnabel, M. Hanach, B. del Rey, A. Sastre, T. Torres, Synthesis (1996) 1139.
23. K. Lang, D.M. Wagnerova, J. Brodilova, J. Photochem. Photobiol. A: Chem 72 (1993) 9.
24. P. Margaron, R. Langlois, J. E. van Lier, S. Gaspard, J. Photochem. Photobiol. B: Biol. 14 (1992) 187.
25. H. Ali, S.K. Sim, J.E. van Lier, J. Chem. Research (S) (1999) 496.
26. N. Kobayashi, R. Kondo, S.-I. Nakajima, T. Osa, J. Am. Chem. Soc. 112 (1990) 9640.
27. C.G. Claessens, T. Torres, Chem. Eur. J. 6 (2000) 2168.
28. S. Nalwa, J.S. Shirk in Phthalocyanines: Properties and Applications, Eds, C.C. Leznoff, A.B.P. Lever, Vol. 4, VCH, 1999: New York Ch. 4.
29. K. Hanabusa, H. Shirai in Phthalocyanines: Properties and Applications, Eds., C.C. Leznoff, A.B.P. Lever, Vol. 2, VCH, 1993: New York, Ch. 4.
30. J. Simon, P. Bassoul in Phthalocyanines: Properties and Applications, Eds., C.C. Leznoff, A.B.P. Lever, Vol. 2, VCH, 1993: New York, Ch. 5.
31. N.B. McKeown in Phthalocyanine Materials: Synthesis, Structure and Function, Cambridge University Press, 1998.
32. A. Meller, A. Osko, Monatsh. Chem. 103 (1972) 150.
33. M. Geyer, F. Plenzig, J. Rausechnabel, M. Hanach, B. del Rey, A. Sastre, T. Torres, Synthesis (1996) 1139.

34. L. Milgrom, S. MacRobert, *Chemistry in Britain*, May 1998.
35. S.B. Brown, T. G. Truscott, *Chemistry in Britain* (1993) 956.
36. N. B. McKeow, *Chemistry and Industry* (1999) 513.
37. Y. H. Tse, P. Janda, H. Lam, J. Zang, W. J. Pietro, A. B. P. Lever, *Anal. Chem.* 67 (1995) 981.
38. W. Spiller, H. Kliesch, D. Whorle, S. Hackbarth, B. Roder, G. Schnurpfeil, *J. Porphyrins Phthalocyanines* 4 (2000) 147.
39. S. Chatterjee, T. S. Srivastava, *J. Porphyrins Phthalocyanines* 3 (1999) 424.
40. J. M. Roberts, *J. Chem. Soc.* (1936) 1195.
41. R. P. Linstead, A. R. Lowe, *J. Chem. Soc.* (1934) 1022.
42. J. Metz, O. Schneider, Hanack, *Inorg. Chem.* 23 (1984) 1065.
43. H. Kliesch, A. Weitemeyer, S. Muller, D. Wohrle, *Liebigs. Ann.* (1995) 1272.
44. R. P. Linstead, *J. Chem. Soc.* (1934), 1016.
45. D. Wohrle, G. Schnurpfeil, G. Knothe, *Dye and Pigments*, 18 (1992) 97.
46. S. Oliver, T. D. Smith, *Heterocycles* 22 (1984) 2049.
47. T. J. Marks, D. R. Stojakovic, *Inorg. Chem.* (1978) 1695.
48. E. A. Cuellar, T. J. Marks, *Inorg. Chem.* 20 (1981) 3766.
49. K. Kuninobu, I. Tsutomu, H. Makoto, *Inorg. Chim. Acta* 196 (1992) 127.
50. S. Nonell, N. Rubio, B. del Rey, T. Torres, *J. Chem. Soc., Perkin Trans. 2* (2000) 1091.
51. N. Kobayashi, T. Ishizaki, K. Ishii, H. Konami, *J. Am. Chem. Soc.* 121 (1999) 9096.
52. C. C. Leznoff, P. I. Svirskaya, B. Khouw, R. L. Cerney, P. Seymour, A. B. P.

- Lever, J. *Org. Chem.* 57 (1991) 82.
53. R. Bonnett, in *Chemical aspects of Photodynamic Therapy*, 1<sup>st</sup> Ed, Gordon and Breach Science 2000.
54. S. W. Oliever, T. D. Smith, *J. Chem. Soc., Perkin Trans. 2* (1987) 1549.
55. M. Maree, T. Nyokong, *J. Chem. Research (S)* (2001) 68.
56. J. H. Weber, D. H. Busch, *Inorg. Chem.* 4 (1965) 472.
57. R. W. Boyle, J. E. van Lier, *Syn. lett.* (1993) 375.
58. O.V. Dolotova, N. I. Bundina, O. L. Kaliya, E. A. Lukyates, *J. Porphyrins Phthalocyanines*, 1 (1997) 356.
59. W. Kobel, M. Hanack, *Inorg. Chem.* 25 (1986) 103.
60. M. J. Stillman, T. Nyokong in C. C. Leznoff and A. B. P. Lever (ed) *Phthalocyanines: Properties and applications*, VCH, Vol 1, Ch. 6, 1989.
61. A. B. P. Lever, S. R. Pickens, P. C. Minor, S. Licoccia, B. S. Ramaswamy, K. Mangal, *J. Am. Chem. Soc.* 103 (1981), 6800.
62. W. A. Nevin, M. R. Hempstead, W. Liu, C. C. Leznoff, A. B. P. Lever, *Inorg. Chem.* 26 (1987), 540.
63. A. W. Dale, *Trans. Faraday Soc.* 65 (1969), 311.
64. A. Gilbert, J. Baggot in *Essentials of molecular Photochemistry*, Blackwell Science Ltd. Oxford, 1991.
65. J. R. Darwent, I. McCubbin, D. Phillips, *J. Chem. Soc. Faraday Trans 2* (1982) 78.
66. S. M. Bishop, A. Beeby, A. W. Parker, M. S. C. Foley, D. Phillips, *J. Photochem. Photobiol.* 90 (1995) 39.
67. R. Bensasson, C. R. Goldschmidt, E. Land, T. G. Truscott, *Photochem. Photobiol.*, 28 (1978) 277.

68. J. C. Dalton, N. J. Turro, *Mol. Photochem.* 2 (1970) 133.
69. J. A. Lacey, D. Phillips, L. R. Milgrom, G. Yahroglu, R. D. Rees, *Photochem. Photobiol.* 67 (1998) 97.
70. P. Jacques, A. M. Braun, *Helv. Chim. Acta* 64 (1981) 1800.
71. A. J. Bard, L. R. Faulkner in *Electrochemical methods: Fundamentals and Applications*, John Wiley & Sons, New York, 1980, 1<sup>st</sup> edn.
72. P. T. Kissinger, W. R. Heineman, *Laboratory Techniques in Electrochemistry*, Marcel and Dekker, New York, , 1996, 3<sup>rd</sup> edn.
73. C. M. A. Brett, A. O. Brett in *Electrochemistry: Principles, methods and applications*, Oxford University Press, New York, , 1993, 1<sup>st</sup> edn.
74. J. Wang in *Analytical Electrochemistry*, VCH Publishers, New York, 1994, 1<sup>st</sup> edn.
75. T. Nyokong, *S. Afr. J. Chem.* 48 (1995), 23.
76. M. D. Maree, T. Nyokong, *J. Porphyrins Phthalocyanines* 5 (2001) 555.
77. D. Wohrle, M. Eskes, K. Shigehara, A. Yamaha, *Synthesis* (1993) 194.
78. A. Weitermeyer, H. Kliesch, D. Wohrle, *J. Org. Chem.* 60 (1995) 4900.
79. M. Sekota, T. Nyokong, *Polyhedron* 15 (1996) 2901.
80. T. Nyokong, *J. Chem. Soc. Dalton Trans.* (1994) 1359.
81. McMurray, *Organic Chemistry* (4<sup>th</sup> ed.), Brooks/Cole, Oxford, 1996.
82. K. Nakamoto in *Infrared and Raman Spectra of Inorganic and coordination compounds*, John Wiley & Sons, New York, 1978 3<sup>rd</sup> edn.
83. J. R. Stock, R. J. Putecek, W. S. Durfee, B. C. Noll, *Tetrahedron Lett.* 40 (1999) 9096.
84. G. Schmid, M. Sommerrauer, M. Hanack in: *Phthalocyanines in Properties and Applications*, Vol. 3. C. C. Leznoff, A. B. P. Lever (eds), VCH, 1999

- New York, Ch.1.
85. N. Kobayashi, H. Konami in *Phthalocyanines: Properties and Applications*, vol. 3. C. C. Leznoff, A. B. P. Lever (eds), VCH, New York, 1999, Ch. 9.
  86. T. J. P. Mafatle, MSc Thesis, Rhodes University, 1998.
  87. A. B. P. Lever, E. R. Milaeva, G. Speier in: *Phthalocyanines: Properties and Applications*, vol. 3. C. C. Leznoff, A. B. P. Lever (eds), VCH, New York, 1999, Ch. 1.
  88. M. D. Maree, N. Kuznetsova, T. Nyokong, *J. Photochem. Photobiol. A: Chem.* 140 (2001), 117.
  89. S. E. Maree, T. Nyokong, *J. Porphyrins Phthalocyanines* 5 (2001) 782.
  90. I. Seotsanyana-Mokhosi, N. Kuznetsova, T. Nyokong, *J. Photochem. Photobiol. A: Chem.*, 140 (2001), 215.
  91. G. Winter, H. Heckmann, P. Hisch, W. Eberhardt, M. Hanack, L. Lürer, H. J. Egelhaaf, D. Oelkrug, *J. Am. Chem. Soc.* 120 (1998) 11663.
  92. G. Schnurpfeil, A. Sobbi, W. Spiller, H. Klicsh, D. Wöhrle, *J. Porphyrins Phthalocyanines* 1 (1997) 159.
  93. L. C. Gruen, R. J. Blagrove, *Aust. J. Chem.* 26 (1973) 319.
  94. E. W. Abel, J. M. Pratt, R. Whelan, *J. Chem. Soc., Dalton Trans.* (1976) 509.
  95. J. Oni, T. Nyokong, *Polyhedron* 19 (2000) 1355.